Synthetic gauge potentials and analogue gravity in Bose-Einstein condensates

Salvatore Butera

Submitted for the Degree of Doctor of Philosophy

Heriot-Watt University

School of Engineering and Physical Sciences

August 2017

Abstract

In this thesis multi-component, spinorial cold atomic gases are studied. We investigate first the new perspectives introduced by nonlinear, that is density dependent, synthetic gauge fields in atomic Bose-Einstein condensate. Such fields stem from a collisionally induced detuning in combination with synthetic magnetism arising from the light-atom coupling. The effective mean field dynamics of the condensate shows the appearance of an exotic nonlinearity which is proportional to the current in the system. It introduces a chirality, whose effects on the stability and dynamical properties of the rotating state of a condensate is investigated. We show that by properly shaping the profile and the magnitude of the light-matter interaction parameters, it may happen that the rotating state is energetically favorable compared to the corresponding non-rotating one. Furthermore, we analyze the effects of the nonlinear field on the dynamics of a vortex in a condensate. We obtain the equation of motion for the vortex core, showing the appearance of an extra force which is explicitly depending on the number of particles that are in the system.

Furthermore, we consider the implications of the same type of density-dependent fields in the context of analogue gravity. We show that they provide an extra degree-of-freedom that can be exploited in order to design effective non-trivial spacetimes experienced by phonons.

In the framework of analogue models of gravity, we finally discuss the perspectives of two-dimensional systems, and address the problem of the black hole lasing effect in the spin modes of the system. By developing a Gross-Pitaevskii theory for the problem, we prove the onset of the lasing instability, and the phenomenon of mode conversion at the horizons. To this aim we consider both homogeneous and harmonically trapped condensates.

Acknowledgments

Life is about people. Mostly about people. And every period of our lives bring new encounters, and possibly friendships. Whether they are people we just meet once, or they become part of our life. Or even people who come in our lives without a reason, by accident, and in a moment. We might not see them anymore, but we keep them forever in our memories. Each of them teaches us something. Borrowing a few words from Coldplay "each has been sent as guide".

In these lines I would like to thank you all. Whether you have been or you are still part of my life. All of you that I have had the pleasure to meet during my PhD. All of you that life brought so close to me and then pushed away. I will keep you with me, in my heart, and I hope I will see you again.

My first and most important thanks go to my supervisor, Patrik. I would like to thank him for his patience, kindness and guidance throughout the course of my PhD. I thank him for his support and all his encouragement. For having always been there whenever I needed.

A special thanks goes to Iacopo, whom I consider my co-supervisor. Thanks for inviting me in his group in Trento, for his kindness and guidance. Because the few months we spent together during the past two years have been extremely exciting. Thanks for his support, and for having shared many of his ideas with me. I hope we will be able to carry out our projects in the near future.

I would like to thank all the people at the BEC Center in Trento as well. Thanks to all the staff for the invitation to spend this amazing period there, and to all the postdocs and students for welcoming me in the group. We had a great time

together. It has been exciting from the scientific point of view, and at the same time I had the chance to build true friendships. I would like to thank in particular Grazia. I will remember our chats during the coffee and strawberry breaks. Thanks for her wonderful "babà", which I am sure I will have the chance to have again in the future. Thanks to Matteo and Marco, because of their friendship and all the fun we had together, and thanks of course to Giulia.

Many thanks go to Fabio, my second supervisor. For all the coffees and the interesting discussions we had together. For his esteem and all his support.

I cannot not say thanks to Roberto, once more. Because despite the distance between us nothing has changed and never will change. Because between us is not just a sincere friendship, but even more. Thanks for the unconditional support he has always given me during these twenty-five years.

Many thanks to Loraine, because she has always been so nice and friendly to me. Thanks for all the nice chats we had together and because she has always tried to cheer me up whenever I was not in a good mood.

Thanks to Roberto and Lucia, because it all started with a master thesis, and it ended up in a true friendship. Because they have always been there to help me whenever I needed. In work as well as in life. Thanks also to Federico, for the high consideration he has on me, and because it is always nice to meet and chat about our lives and projects.

Thanks to Manuel, the postdoc of the group. I will remember all the valuable suggestions you gave me during these years.

Last but not least I would like to recognize the support I have received from the Scottish Doctoral Training Centre in Condensed Matter Physics. I would like to thank all the management team, and in particular Prof. Ian Galbraith, Dr. Chris Hooley and Dr. Julie Massey for their hard work and the special attention they have always given to the needs of all of us students.

Thank you all,

Giulio

Contents

List of Publications

In the following are reported all the publications which resulted from the PhD activity. Papers on which the thesis is based are listed separately.

Thesis based Publications

1. Butera S., Öhberg P., Carusotto I., Black hole Laser in spinorial Bose-Einstein condensates, *Phys. Rev. A*, **96**, 013611, (2017).

2. Butera S., Valiente M., Öhberg P., Vortex dynamics in superfluids governed by an interacting gauge theory, *New Journal of Physics*, **18**, 085001, (2016).

3. Butera S., Valiente M., Öhberg P., Quantized vortices in interacting gauge theories, *Journal of Physics B: Atomic, Molecular and Optical Physics*, **49**, 015304, (2016).

Other Publications

1. Armata F., Kim M. S., Butera S., Passante R., Rizzuto L., Nonequilibrium dressing in a cavity with a movable reflecting mirror, *Phys. Rev. D*, **96**, 045007, (2017).

2. Armata F., Butera S., Fiscelli G., Incardone R., Notararigo, V., Palacino, R., Passante R., Rizzuto L., Spagnolo S., Effect of boundaries on vacuum field fluctuations and radiation-mediated interactions between atoms, *J. Phys. Conf. Ser.*, **880,**, 012064, (2017).

3. Bartolo N., Butera S., Lattuca M., Passante R., Rizzuto L., Spagnolo S.,

Vacuum Casimir energy densities and field divergences at boundaries, *J. Phys.: Condens. Matter*, **27**, 214015, (2015).

4. Butera S., Di Paola M., Mellin transform approach for the solution of coupled systems of fractional differential equations, *Communications in Nonlinear Science and Numerical Simulation*, **20**, 32-38, (2015).

5. Butera S., Di Paola M., A physically based connection between fractional calculus and fractal geometry, *Annals of Physics*, **350**, 146-158, (2014).

6. Butera S., Di Paola M., Fractional differential equations solved by using Mellin transform, *Communications in Nonlinear Science and Numerical Simulation*, **19**, 2220-2227, (2014).

Chapter 1 Introduction

Artificial gauge fields [1, 2] and analogue models for gravity [3, 4] are both implementations of the seminal idea of *quantum simulators* introduced by Feynman in 1982 [5]. The aim is to use experimentally accessible physical systems in order to emulate the dynamics of other systems of interest, whose investigation is out of current analytic, computational or experimental capabilities.

Ultracold neutral atomic systems, such as Bose-Einstein condensates or degenerate Fermi gases, provide a remarkably flexible experimental playground for this perspective. The great ability in tuning the physical parameters governing the dynamics of such systems, such as confining potentials, particle density, dimensionality, and even the interactions between atoms, allows to experimentally simulate a number of phenomena characteristic of condensed matter systems [6–13].

The implementation of effective (artificial), static (that is not affected by the atomic degrees of freedoms) orbital magnetism for neutral atoms, and more in general of non-abelian gauge potentials, enlarges the perspectives of the field, allowing for the investigation of a plethora of intriguing phenomena at the quantum level, such as the quantum Hall effect or Rashba-type spin orbit coupling (SOC). Beside fundamental reasons, the interest in synthetic gauge fields relies on practical motivations. Orbital magnetism and SOC, are for example strictly related to the existence of topological states of matter [14, 15]. The interest in such exotic states relies on their topological properties, which makes them robust against external perturbations, such as finite temperature effects or noise, and thus relevant for future technological applications in particular in the context of quantum computation. Here we seek for physical systems with the necessary properties in order to build error-free quantum computers [75]. An example of these topological states are the conducting edge states appearing in

a topological insulator [14, 15], which are responsible for the quantized conductance which characterizes the integer quantum Hall effect [77, 78]. Such edge states may also be useful in order to investigate anyons [14, 16], which are exotic excitations of a system, satisfying neither bosonic nor fermionic statistics, which have been predicted to appear in quantum Hall liquids [16] and topological superfluids [14].

The ultimate goal of the research on artificial gauge fields is to emulate fully dynamical gauge theories, with the purpose of addressing a number of still open questions in different areas of physics, ranging from condensed-matter, where they appear as effective field theories, to the much higher energy scales of particle physics, where the gauge fields describe the fundamental interactions of nature. A number of proposals have been suggested to engineer dynamical fields with cold atoms systems [17–22], but the complexity involved has unfortunately prevented their experimental implementation so far.

One approach in this direction has been done in the context of synthetic magnetism with neutral atoms [23]. Here the authors show, by exploiting collisional induced detuning, how nonlinear synthetic magnetic fields arise in the adiabatic dynamics of the atoms, whose internal states are coherently coupled by a laser. These nonlinear effective fields do not reproduce a truly dynamical gauge field, but their explicit particle density dependence provides a local back-reaction effect between matter (the atoms) and the (effective) fields, which gives rise to new interesting physics, opening up novel perspectives in quantum simulation.

Analogue models for gravity and quantum field theory in general, represent another concrete realization of Feynman's proposal, which allows us to emulate the physics of quantum fields in curved spacetime. In this discipline physical systems are sought, whose underlying dynamics is not governed by Einstein's equations, but where an effective, generally curved, spacetime emerges in the dynamics of the elementary excitations of the system.

The quantum field theory in curved spacetime, i.e. the theory of semi-classical interaction between gravity and matter fields [24, 25], can thus be experimentally investigated in physical systems characterized by energies far below the energies

pertaining cosmological scale systems, and attainable in ordinary laboratories. As a consequence, effects such as Hawking radiation, the process by which black holes evaporate by emitting thermal radiation and proposed by Hawking [26, 27], or cosmological particle creation [28–32] are no longer unattainable experimentally.

The work presented in this thesis concerns the two implementations of the quantum simulator program discussed above, and in particular regards synthetic magnetism and analogue gravity with Bose-Einstein condensates (BECs). Accordingly, the thesis is divided into two parts, after a first introduction to the theory of weakly interacting Bose gases and the implementation of synthetic magnetism with neutral atoms, which are discussed in Chapters 2 and 3, respectively. The work is summarized as follows:

Rotating BECs and nonlinear synthetic magnetism – This part of the thesis investigates the novel physics introduced by nonlinear synthetic fields [23], giving particular emphasis to the stability and dynamical properties of a rotating condensate. In Chapter 4 we envisage a situation in which the explicit density dependence of the effective vector and scalar potentials acting on the atoms, makes it energetically favorable for the condensate to rotate rather than staying in its static state. We will see in particular that the induced vorticity increases with the particle density. In Chapter 5 we develop a minimal model which describes the dynamics of a vortex state in a condensate, whose atoms are subjected to a nonlinear gauge potential. We show that, other than the usual Magnus force, which originates from the relative motion between the vortex and the condensate bulk, another force appears acting on the vortex core because of the presence of the vector potential. What differentiates the present situation from the standard case, in which an ordinary (that is non density dependent) vector potential acts on the system, is that the nonlinear nature of the synthetic potential makes the magnitude of this force depending on the number of particles that are in the system.

Analogue gravity with coherently coupled two-component condensates – The second part of the thesis is devoted to the topic of analogue models for gravity in coherently coupled two-component atomic BECs. In Chapter 6 we investigate the effects of the nonlinear synthetic potentials in the context of BEC based analogue models for

gravity. We show that the nonlinear potentials provide an extra degree-of-freedom that can be exploited to implement non-trivial effective spacetime configurations for the elementary excitations of the systems. This endows the effective spacetime with new features, enriching the physics that can be investigated. Chapter 7 introduces the so-called black hole laser effect [33], and is preparatory in the perspective of the original work discussed in Chap. 8. Working in the classical limit, we show how the lasing mechanism in *spin* modes rather than in the *density* modes of the condensate can be created. We point out several promising advantages of this setup with respect to standard single-component systems, especially regarding the investigation of the spontaneous Hawking radiation.

Part I – Background

Chapter 2 Bose-Einstein Condensates

The aim of this chapter is to give a brief overview on the theory of Bose-Einstein condensation in weakly-interacting atomic gases and, at the same time, define the notation, the basic concepts and physical quantities that will be used in the rest of the thesis. To this aim we refer to the standard literature on the topic [34–38]. We start the chapter by introducing in Sec. 2.1 the Bogoliubov theory for a weakly-interacting Bose gas at zero temperature. In Sec. 2.2 we introduce small amplitude excitations in the system, developing the analysis within the (classical) Gross-Pitaevskii theory for a BEC, and discuss their quantum-mechanical interpretation. These concepts will be useful in the second part of the thesis, in Chapter 6-8, where the topic of analogue gravity models in BECs is discussed. In Sec. 2.3 we treat the problem of a rotating condensate, and its stability properties. The results of this section represent a theoretical background for the work presented in the first part of the thesis, which includes Chapters 4 and 5, where we discuss the effects of nonlinear synthetic potentials on the stability and dynamics of a vortex state, respectively.

2.1 Weakly-interacting Bose gas at zero temperature

The origin of Bose-Einstein condensation dates back to Bose's work on the statistics of photons [39] in 1924, and the subsequent extension by Einstein of these concepts to the case of a gas of non-interacting massive bosons [40]. We do not give here any historical introduction of the path leading to condensation, but refer for example to the E. A. Cornell and C. E. Wieman Nobel lecture [41] to this aim. Together with W. Ketterle, they were the first who observed, in 1995, the phenomenon of Bose-Einstein condensation in rubidium [42] and sodium [43] vapours. In the same year, experimental evidence of condensate with lithium was also observed [44].

2.1.1 Bogoliubov approximation

By *dilute* system it is commonly meant a system at very low density. To understand the order of magnitudes we are speaking about, note that typical values achieved in state-of-the-art cold-atoms experiments are in the range $10^{12}-10^{15}$ atoms/cm^3, while densities of the order 10^{19} atoms/cm^3 and 10^{22} atoms/cm^3 characterize respectively air at room temperature and atmospheric pressure, and liquid and solid phases. The reasons for investigating such rarefied systems are many: i) For sufficiently low densities, the average distance $d = n^{-1/3}$ (with n the particle density) between atoms is much larger than the range r_0 of the interatomic forces, defined as the distance beyond which the interaction between particles is negligible. Under these conditions the probability of finding three or more particles interacting simultaneously is extremely low, and the physics of the system is governed, to a good approximation, by pairwise interactions only. This prevents or at least attenuates molecule formation, which is a three-body process, and the consequent losses of atoms from the system, ensuring a sufficiently long life-time for a condensate in actual experiments. ii) Because of the large separation between particles, the wavefunction of the relative motion of colliding atoms can be approximated by its asymptotic form. This ensures that the collisions and all the properties of the system can be expressed in terms of the so-called scattering amplitude (see the review [45], the lectures [46–49] and standard textbook such as [50] for further details).

Working with such rarefied gases, the value attained by the critical temperature for condensation is of the order of 100 nK in typical cold-atoms experiments [36, 37, 51, 52]. At such temperatures, the atoms move so slowly that their De-Broglie thermal wavelenght $\Lambda_T \equiv \sqrt{2\pi\hbar^2/mk_BT}$ is much larger than the range r_0 of the interatomic potential. In terms of the typical wavevector of the relative motion of the atoms $k \sim 1/\Lambda_T$, this condition can be expressed as

$$kr_0 \ll 1. \tag{2.1}$$

For such low values of the momenta, the interactions between atoms are governed by the s-wave channel. The scattering amplitude and the effects of interactions on the physical properties of the system can be described in terms of a single parameter,

which is the s-wave scattering length denoted by a [46–50]. This parameter, together with the atomic density, enters into the condition defining a nearly ideal, that is weakly interacting gas for which

$$na^3 \ll 1. \tag{2.2}$$

This condition needs to be satisfied in order to apply the Bogoliubov theory of dilute gases here discussed, which represents the zero order approximation of the many-body problem with respect to the perturbative parameter na^3 [36, 53].

The study of the physics of a dilute system composed by N bosons, pair-wise interacting via the potential $V(\mathbf{r})$ and confined by the external potential $V_{\text{ext}}(\mathbf{r})$, starts from the many-body Hamiltonian that is given, in the second quantization formalism, by [34–36]

$$\hat{H} = \int d\mathbf{r} \left[\hat{\Psi}^\dagger(\mathbf{r}) \left(-\frac{\hbar^2}{2m}\boldsymbol{\nabla}^2 + V_{\text{ext}}(\mathbf{r}) \right) \hat{\Psi}(\mathbf{r}) \right] + \frac{1}{2} \int d\mathbf{r} d\mathbf{r}' \left[\hat{\Psi}^\dagger(\mathbf{r}) \hat{\Psi}^\dagger(\mathbf{r}') V(\mathbf{r}-\mathbf{r}') \hat{\Psi}(\mathbf{r}') \hat{\Psi}(\mathbf{r}) \right]. \tag{2.3}$$

The boson field operators $\hat{\Psi}(\mathbf{r})$ and $\hat{\Psi}^\dagger(\mathbf{r})$ annihilates and creates respectively a particle at position $\mathbf{r}$, and satisfy the commutation rules

$$\left[\hat{\Psi}(\mathbf{r}), \hat{\Psi}^\dagger(\mathbf{r}') \right] = \delta\left(\mathbf{r}-\mathbf{r}'\right), \qquad \left[\hat{\Psi}(\mathbf{r}), \hat{\Psi}(\mathbf{r}') \right] = 0. \tag{2.4}$$

In Eq. (2.3), the first integral is the single-particle Hamiltonian, while the second accounts for the two-body interaction between particles. By using the commutation law (2.4), the time evolution of the field operator $\hat{\Psi}\left(\mathbf{r}, t\right)$, in the Heisenberg picture, reads

$$\begin{aligned} i\hbar \frac{\partial}{\partial t} \hat{\Psi}\left(\mathbf{r}, t\right) &= \left[\hat{\Psi}, \hat{H} \right] \\ &= \left[-\frac{\hbar^2}{2m}\boldsymbol{\nabla}^2 + V_{\text{ext}}(\mathbf{r}) + \int d\mathbf{r}' \hat{\Psi}^\dagger(\mathbf{r}', t) V(\mathbf{r}'-\mathbf{r}) \hat{\Psi}(\mathbf{r}', t) \right] \hat{\Psi}(\mathbf{r}, t), \end{aligned} \tag{2.5}$$

which represents the Schrödinger equation for the many-body problem. In order to avoid solving the full problem, a mean field approach may be pursued when dealing with weakly interacting systems, which was originally formulated by Bogoliubov [53]. In order to illustrate the theory, we expand the field operator in the basis of the Hilbert space composed by the single-particle wavefunctions $\{\psi_i(\mathbf{r})\}$, in the form:

$\hat{\Psi}(\mathbf{r}) = \sum_i \psi_i(\mathbf{r})\,\hat{a}_i$, where $\hat{a}_i$ are the operators annihilating a particle in the state $\psi_i(\mathbf{r})$. These operators, together with their Hermitian conjugates $\hat{a}_i^\dagger$, are defined in terms of their action on the states of the Fock space $|\{n_j\}\rangle$ [50], through the relations

$$\hat{a}_j|n_0, n_1, ..., n_j, ...\rangle = \sqrt{n_j}|n_0, n_1, ..., n_j - 1, ...\rangle, \tag{2.6a}$$

$$\hat{a}_j^\dagger|n_0, n_1, ..., n_j, ...\rangle = \sqrt{n_j + 1}|n_0, n_1, ..., n_j + 1, ...\rangle, \tag{2.6b}$$

where n_j is the occupancy of the jth single-particle states, and eigenvalue of the number operator $\hat{n}_j = \hat{a}_j^\dagger\hat{a}_j$. In order to satisfy the relations in Eq. (2.4), the annihilation and creation operators have to obey the commutation rules

$$\left[\hat{a}_i, \hat{a}_j^\dagger\right] = \delta_{ij}, \qquad [\hat{a}_i, \hat{a}_j] = 0. \tag{2.7}$$

Below the critical temperature condensation takes place, resulting in a macroscopic occupation of the single-particle ground state, where by macroscopic we mean of the order of the total number of particles. Indicating by N_0 the number of condensed atoms this means that, in the thermodynamic limit, $N_0 \gg 1$. In this limit, states of the system with N_0 and $N_0 \pm 1 \approx N_0$ correspond essentially to the same physical configuration so that, following Eqs. (2.6a) and (2.6b), the operators $\hat{a}_0$ and $\hat{a}_0^\dagger$ can be treated as c-numbers, with value $\hat{a}_0 = \hat{a}_0^\dagger \sim \sqrt{N_0}$. From another point of view, this classical approximation for the ground state operators can be justified by noting that the commutators in Eq. (2.7) are c-numbers, and thus bounded, with norm $\left\|\left[\hat{a}_i, \hat{a}_i^\dagger\right]\right\| = 1$. Conversely, the operators $\hat{a}_i$ and their Hermitian conjugates $\hat{a}_i^\dagger$ are unbounded. For $N_0 \gg 1$, we have

$$\frac{\|\left[\hat{a}_0, \hat{a}_0^\dagger\right]|n_0\rangle\|}{\|\hat{a}_0|n_0\rangle\|} = \frac{1}{N_0} \approx 0, \tag{2.8}$$

from which we infer that the norm of the commutator in Eq. (2.7) is negligibly small compared to (loosely speaking) the norm of the operators themselves, and can be neglected. In some sense, this is the same idea as the classical limit of electromagnetism according to which, when the number of photons is large, the corpuscular nature of the radiation is no longer appreciable, in favour of its undulatory description.

According to these ideas, we can make the Bogoliubov ansatz and treat the macroscopic component $\psi_0(\mathbf{r})\hat{a}_0$ of the field operator as a classical field [53], and write

$$\hat{\Psi}(\mathbf{r}) = \Psi_0(\mathbf{r}) + \delta\hat{\Psi}(\mathbf{r}), \tag{2.9}$$

where $\Psi_0(\mathbf{r}) \equiv \sqrt{N_0}\psi_0(\mathbf{r})$ has the physical meaning of an *order parameter* for the system and is usually referred to as *wave function* of the condensate, while $\delta\hat{\Psi}(\mathbf{r}) = \sum_{i\neq 0}\psi_i(\mathbf{r})\,\hat{a}_i$ is the *depletion* of the condensate. If the system is weakly interacting and for temperatures well below the condensation temperature, quantum and thermal depletion of the condensate is small, and the excited component $\delta\hat{\Psi}(\mathbf{r})$ can be neglected compared to $\Psi_0(\mathbf{r})$. This is equivalent to assuming that all the particles are condensed in the ground state, so that $N_0 = N$. A closed equation for the order parameter can be derived in such conditions, which is the zeroth order approximation to Eq. (2.5).

2.1.2 Gross-Pitaevskii equation

It is important to stress that, when we speak about a weakly interacting system in a dilute gas context, we do not mean that the interactions between atoms are weak, but that the condition (2.2) is satisfied. These interactions are actually strong when the mutual distance between the two atoms is close to the range r_0 of the potential. Because of this reason, the direct substitution of the field operator $\hat{\Psi}(\mathbf{r},t)$ with the condensate wavefunction $\Psi_0(\mathbf{r},t)$ into Eq. (2.5) would lead to an inconsistency, since the latter does not contain any information about the short distance correlations between the atoms due to their interaction. In order to overcome this difficulty we can use an effective potential $V_{\text{eff}}(\mathbf{r})$ in Eq. (2.5) instead of the bare $V(\mathbf{r})$, which includes these correlations into its definition. In other words, we need a $V_{\text{eff}}(\mathbf{r})$ having the property of correctly describing the effective interaction between the long-wavelength degrees of freedom of the system, when the short-wavelength ones have been *integrated out* [35]. Since at low temperatures the condition (2.1) is satisfied, the scattering between two particles is dominated by the s-wave contribution, and the effects of collisions can be described in terms of a single parameter, which is the scattering length a. This quantity fully describes the scattering at low energies, and encodes the effects of the short-range correlations. The expression of the scattering

length in the first Born approximation

$$a_{\mathrm{B}} = \frac{m}{4\pi\hbar^2}\int d\mathbf{r}\, V(\mathbf{r}), \tag{2.10}$$

suggests that the exact low-energy scattering behaviour can be obtained by using an effective interaction potential, having the property

$$\int d\mathbf{r}\, V_{\mathrm{eff}}(\mathbf{r}) = \frac{4\pi\hbar^2 a}{m} \equiv g. \tag{2.11}$$

The contact potential

$$V_{\mathrm{eff}}(\mathbf{r}) = g\,\delta(\mathbf{r}) \tag{2.12}$$

satisfies this property, and its use is formally justified by the theory of scattering in the low energy limit $k \to 0$ [35, 46, 54]. By substituting the effective potential defined above into Eq. (2.5), we can safely replace the field operator $\hat{\Psi}(\mathbf{r}, t)$ with the order parameter $\Psi_0(\mathbf{r}, t)$, obtaining the Gross-Pitaevskii (GP) equation [55–58]

$$i\hbar\frac{\partial}{\partial t}\Psi_0(\mathbf{r}, t) = \left(-\frac{\hbar^2}{2m}\boldsymbol{\nabla}^2 + V_{\mathrm{ext}} + g|\Psi_0|^2\right)\Psi_0(\mathbf{r}, t). \tag{2.13}$$

Upon the same substitutions into the Hamiltonian operator (2.3), we get the energy of the system in the form of the functional operator

$$E\left[\Psi_0, \Psi_0^*\right] = \int d\mathbf{r}\left(\frac{\hbar^2}{2m}|\boldsymbol{\nabla}\Psi_0|^2 + V_{\mathrm{ext}}|\Psi_0|^2 + \frac{g}{2}|\Psi_0|^4\right). \tag{2.14}$$

This energy is conserved, that is $dE/dt = 0$, if Ψ_0 is a solution of the GP Eq. (2.13). The latter can be alternatively derived by imposing the stationarity condition, with respect to variations in Ψ_0^*, to the action $\mathcal{S}$ defined as

$$\mathcal{S} = \int dt d\mathbf{r}\, \mathcal{L}, \tag{2.15}$$

with the Lagrangian density

$$\mathcal{L} = -i\hbar\Psi_0^*\frac{\partial\Psi_0}{\partial t} + \left(\frac{\hbar^2}{2m}|\boldsymbol{\nabla}\Psi_0|^2 + V_{\mathrm{ext}}|\Psi_0|^2 + \frac{g}{2}|\Psi_0|^4\right). \tag{2.16}$$

2.1.3 Hydrodynamic formalism

The unitary evolution of the condensed component of the system, described by the GP equation, guarantees the conservation of the total number of particles. In the Eulerian formalism, this conservation law takes the form of the continuity equation

$$\frac{dN}{dt} = \frac{\partial n}{\partial t} + \boldsymbol{\nabla} \cdot \mathbf{j} = 0, \tag{2.17}$$

where $n(\mathbf{r}) = |\Psi_0(\mathbf{r})|^2$ is the particle density in the condensate and

$$\mathbf{j}(\mathbf{r}, t) = -\frac{i\hbar}{2m} \left(\Psi_0^* \boldsymbol{\nabla} \Psi_0 - \Psi_0 \boldsymbol{\nabla} \Psi_0^* \right), \tag{2.18}$$

is the current density. By using the Madelung representation for the order parameter $\Psi_0(\mathbf{r}, t) = \sqrt{n}\, e^{iS}$, where $S(\mathbf{r}, t)$ is the phase of the condensate wavefunction, the latter can be explicitly written in terms of the superfluid velocity field $\mathbf{v} = (\hbar/m)\boldsymbol{\nabla} S$, as $\mathbf{j} = n\mathbf{v}$. This velocity is irrotational as every field which originates from a potential flow, so that $\boldsymbol{\nabla} \times \mathbf{v} = 0$ [59–61]. The continuity equation (2.17), together with the equation for the phase

$$\hbar \frac{\partial S}{\partial t} + \left(\frac{1}{2} m \mathbf{v}^2 + V_{\text{ext}} + gn - \frac{\hbar^2}{2m\sqrt{n}} \boldsymbol{\nabla}^2 \sqrt{n} \right) = 0, \tag{2.19}$$

which can be obtained by substituting the Madelung expression given above for the order parameter into the GP equation (2.13), provide a closed set of coupled equations equivalent to the original GP equation. It is interesting to note that Eq. (2.19), once written as an equation for $\mathbf{v}$ instead of S, resembles the Euler hydrodynamic equation for the flow of a classical inviscid fluid, except for the appearance of the last term. This term, known as the *quantum pressure*, has no classical analogue and represents a purely quantum effect. As well as the term $m\mathbf{v}^2/2$, which represents the kinetic energy of the particles flowing in the condensate, it originates from the kinetic energy contribution $(\hbar^2/2m)|\boldsymbol{\nabla}\Psi_0|^2$ to the energy density (2.16). It accounts for a sort of *zero-point* motion which does not give rise to any particle current, but describes forces originating from an inhomogeneous density profile of the condensate.

2.1.4 Thomas-Fermi limit

A stationary solution of the GP equation is obtained by inserting into Eq. (2.13) the order parameter in the form $\Psi_0(\mathbf{r},t) = \Psi_0(\mathbf{r})e^{-i\mu t/\hbar}$, with μ the chemical potential of the system. This expression comes directly from the definition of the order parameter as the matrix element of the field operator $\hat{\Psi}(\mathbf{r})$ between the ground states of the system with N and $N-1$ particles [62–64]:

$$\Psi(\mathbf{r},t) = \left\langle N-1 \middle| \hat{\Psi}(\mathbf{r}) \middle| N \right\rangle = \Psi_0(\mathbf{r})\, e^{-i(E_N - E_{N-1})t/\hbar}, \tag{2.20}$$

where E_N and E_{N-1} are the corresponding energies. In the thermodynamic limit, we have: $E_N - E_{N-1} \approx \partial E/\partial N \equiv \mu$. This substitution leads to the time-independent GP equation for the spatial profile of the order parameter [55–57]

$$\left(-\frac{\hbar^2}{2m}\boldsymbol{\nabla}^2 + V_{\text{ext}} + g|\Psi_0(\mathbf{r})|^2\right)\Psi_0(\mathbf{r}) = \mu\Psi_0(\mathbf{r}). \tag{2.21}$$

An alternative way to derive the same equation is by imposing the stationary condition to the energy functional (2.14) with respect to variation in $\Psi_0^*(\mathbf{r})$, constrained by the normalization condition $N = \int d\mathbf{r}|\Psi_0(\mathbf{r})|^2$. This corresponds to extremizing the grand-canonical energy functional

$$E'\left[\Psi_0, \Psi_0^*\right] = E\left[\Psi_0, \Psi_0^*\right] - \mu \int d\mathbf{r}|\Psi_0(\mathbf{r})|^2, \tag{2.22}$$

in which the chemical potential takes the role of a Lagrange multiplier, whose value is determined by the normalization condition.

When the spatial variations of the density in the condensate occur on length scales much larger than the so-called *healing length* $\xi \equiv \hbar/\left(2mgn\right)^{1/2}$, the mean field interaction represents the main contribution to the energy of the system, and the quantum pressure in the hydrodynamic equations (2.19) or, which is equivalent, the kinetic term in Eq. (2.21), may be neglected. This condition defines the Thomas-Fermi (TF) limit, and the ground state of the system can be approximated as [65]

$$n\left(\mathbf{r}\right) = \begin{cases} \left[\mu - V\left(\mathbf{r}\right)\right]/g, & \text{if} \quad V\left(\mathbf{r}\right) < \mu, \\ 0 & \text{otherwise.} \end{cases} \tag{2.23}$$

In the experimentally relevant case of harmonic trapping

$$V_{\text{ext}}(\mathbf{r}) = \frac{1}{2}m\left(\omega_x^2 x^2 + \omega_y^2 y^2 + \omega_z^2 z^2\right), \tag{2.24}$$

the spatial extension of the cloud in the three directions is given in this limit by the TF radii

$$R_i = \sqrt{\frac{2\mu}{m\omega_i^2}}, \qquad i = x, y, z, \tag{2.25}$$

with the chemical potential taking the value

$$\mu = \frac{15^{2/5}}{2}\left(\frac{Na}{a_{\text{ho}}}\right)^{2/5}\hbar\omega_{\text{ho}}. \tag{2.26}$$

In Eq. (2.26), $a_{\text{ho}} = \sqrt{\hbar/m\omega_{\text{ho}}}$ is the characteristic length of the harmonic oscillator associated with the geometric average $\omega_{\text{ho}} \equiv (\omega_x\omega_y\omega_z)^{1/3}$ of the frequencies of the trap in the three directions. Taking as average extension of the cloud $R_{\text{ho}} \equiv (R_x R_y R_z)^{1/3} = 15^{1/5}\,(Na/a_{\text{ho}})^{1/5}\,a_{\text{ho}}$, the condition of applicability of the TF approximation can be inferred from the ratio

$$\frac{R_{\text{ho}}}{\xi} = \frac{2\mu}{\hbar\omega_{\text{ho}}} = \left(15\frac{Na}{a_{\text{ho}}}\right)^{2/5}, \tag{2.27}$$

which shows the key role played by the TF parameter Na/a_{ho}. More precisely, the TF approximation is justified when the interaction energy E_{int} of the system is dominating compared to the kinetic energy E_{kin} [36]. An estimate of the relative weight can be obtained considering the atoms in the ground state of the harmonic oscillator, for which $E_{\text{int}} = gN\bar{n} = (4\pi\hbar^2/m)\,(aN^2/a_{\text{ho}}^3)$ with $\bar{n} \equiv N/a_{\text{ho}}^3$ the average density in the cloud, and $E_{\text{kin}} = N\hbar\omega_{\text{ho}} = (\hbar^2/m)\,(N/a_{\text{ho}}^2)$. Given these results, we obtain

$$\frac{E_{\text{int}}}{E_{\text{kin}}} \approx \frac{Na}{a_{\text{ho}}}. \tag{2.28}$$

Since typical values of the ratio a/a_{ho} are of the order 10^{-3} in state-of-the-art experiments (see [36] and references therein), a number of particles of the order of 10^5 is usually sufficient in order to have $Na/a_{\text{ho}} \gg 1$ and safely apply the TF approximation.

2.2 Elementary excitations

2.2.1 Small amplitude fluctuations

We introduce here the theory of small amplitude fluctuations in a BEC, defined as small time and space perturbation of the order parameter with respect to a stationary background configuration. Although a fully quantum mechanical approach is feasible [53, 55, 56, 66], we develop the following arguments based on the classical Gross-Pitaevskii theory, as described in the previous section. This procedure leads to the same spectrum and eigenmodes for the fluctuations field, which can be quantized a posteriori, as we show in Sec. 2.2.2. Within this formalism, the occurrence of small fluctuations in the system can be taken into account by writing the order parameter in the form

$$\Psi_0(\mathbf{r},t) = \left[\Psi_0(\mathbf{r}) + \delta\Psi_0(\mathbf{r},t)\right] e^{-i\mu t/\hbar}. \tag{2.29}$$

Here Ψ_0 is the condensed background state, on top of which the small fluctuations $\delta\Psi_0$ occur. Since we consider stationary background configurations, frequencies are conserved, and we look for solutions of the type [55, 56]:

$$\delta\Psi_0(\mathbf{r},t) = \sum_i \left[u_i(\mathbf{r})e^{-i\omega_i t} + v_i^*(\mathbf{r})e^{i\omega_i t}\right], \tag{2.30}$$

where $u_i(\mathbf{r})$ and $v_i(\mathbf{r})$ are functions that give the spatial profile of the modes, and ω_i are the corresponding frequencies. By substituting Eq. (2.29) and Eq. (2.30) into Eq. (2.13) and collecting terms evolving in time as $e^{-i\omega_i t}$ and $e^{i\omega_i t}$, we obtain the so-called Bogoliubov-de Gennes equations [55, 56]

$$\hbar\omega_i\, u_i(\mathbf{r}) = \left(\hat{H}_0 - \mu + 2gn(\mathbf{r})\right) u_i(\mathbf{r}) + g\Psi_0^2(\mathbf{r})\, v_i(\mathbf{r}), \tag{2.31}$$

$$-\hbar\omega_i\, v_i(\mathbf{r}) = \left(\hat{H}_0 - \mu + 2gn(\mathbf{r})\right) v_i(\mathbf{r}) + g\Psi_0^{*2}(\mathbf{r})\, u_i(\mathbf{r}), \tag{2.32}$$

where $\hat{H}_0 \equiv -(\hbar^2/2m)\,\boldsymbol{\nabla}^2 + V_{\text{ext}}$ is the non-interacting single-particle Hamiltonian. By collecting the solutions in the vectorial notation $\mathbf{W}_i \equiv (u_i,\, v_i)$, the set of equations (2.31) and (2.32) can be written in the compact form [35]

$$(\boldsymbol{\sigma}_z\mathbf{M})\,\mathbf{W}_i = \hbar\omega_i\mathbf{W}_i, \tag{2.33}$$

where $\boldsymbol{\sigma}_z = \mathrm{diag}\,(1,-1)$ and

$$\mathbf{M} = \begin{pmatrix} \left[\hat{H}_0 - \mu + 2gn\,(\mathbf{r})\right] & g\Psi_0^2\,(\mathbf{r}) \\ g\Psi_0^{*2}\,(\mathbf{r}) & \left[\hat{H}_0 - \mu + 2gn\,(\mathbf{r})\right] \end{pmatrix}. \tag{2.34}$$

The operator $(\boldsymbol{\sigma}_z\mathbf{M})$ is η-pseudo-Hermitian [67–69], that is a Hermitian linear automorphism η exists in the Hilbert space, such that

$$(\boldsymbol{\sigma}_z\mathbf{M})^\dagger = \eta\,(\boldsymbol{\sigma}_z\mathbf{M})\,\eta^{-1}. \tag{2.35}$$

In the present case $\eta \equiv \boldsymbol{\sigma}_z$. Because of this property, its eigenvalues are real or come in complex conjugate pairs with the same multiplicity [67–69]. The appearance in general of non-real solutions of Eq. (2.33) can also be justified because of the fact that the operator $(\boldsymbol{\sigma}_z\mathbf{M})$ is self-adjoint (or loosely speaking Hermitian) with respect to the *not* positive definite inner product

$$\begin{aligned} \langle \mathbf{A}, \mathbf{B} \rangle_{\sigma_z} &\equiv \int d\mathbf{r}\, \mathbf{A}^\dagger\,(\mathbf{r})\, \boldsymbol{\sigma}_z \mathbf{B}\,(\mathbf{r}) \\ &= \sum_{k=1,2} \int d\mathbf{r}\, A_k^*\,(\mathbf{r})\, (\boldsymbol{\sigma}_z\mathbf{B})_k\,(\mathbf{r}) \\ &= \int d\mathbf{r}\, (A_1^* B_1 - A_2^* B_2), \end{aligned} \tag{2.36}$$

where we defined $\mathbf{A} = (A_1, A_2)^T$ and $\mathbf{B} = (B_1, B_2)^T$. This means that the spectral theorem [70] cannot be applied in this case (see [24], p. 228), and complex frequency eigenvalues of Eq. (2.33) may exist. The Hermicity of the operator guarantees that these eigenvalues appear in complex conjugated pairs.

By opportunely combining Eqs. (2.31) and (2.32), we see that the solutions of Eq. (2.33) satisfy the following orthogonality condition

$$\left(\omega_i - \omega_j^*\right) \langle \mathbf{W}_i, \mathbf{W}_j \rangle_{\sigma_z} = 0, \tag{2.37}$$

which shows that real frequency solutions are orthogonal to each other as defined in Eq. (2.36). For reasons that will be justified in Sec. 2.2.2, where we treat the quantization of the small amplitude fluctuations, we normalize these solutions as

$$\langle \mathbf{W}_i, \mathbf{W}_i \rangle_{\sigma_z} = \int d\mathbf{r}\, \left(|u_i|^2 - |v_i|^2\right) = 1. \tag{2.38}$$

Complex frequency solutions have vanishing norm according to Eq. (2.37). When this happens, we are in the presence of a dynamical instability of the system. From the inspection of Eqs. (2.31) and (2.32) it results that, for any solution (u_i, v_i) with frequency ω_i, the other solution (v_i^*, u_i^*) with frequency $-\omega_i$ and opposite norm exists. From a physical point of view, solutions with opposite frequency represent the same physical oscillation, as can be inferred from Eq. (2.30).

The eigensystem in Eqs. (2.31) and (2.32) can be solved exactly for a uniform system, in which case $V_{\text{ext}} = 0$ for example, and the ground state takes the simple form $\Psi_0(\mathbf{r}) = \sqrt{n_0}$, where n_0 is the particle density. Because of the translational invariance, the normal modes take the form of plane waves $u_{\mathbf{k}}(\mathbf{r}) = u_k e^{i\mathbf{k}\cdot\mathbf{r}}$ and $v_{\mathbf{k}}(\mathbf{r}) = v_k e^{i\mathbf{k}\cdot\mathbf{r}}$, with u_k, v_k constants to be determined. In this case the chemical potential takes the value $\mu = gn_0$, and the Eqs. (2.31) and (2.32) reduce to the set of equations

$$\begin{aligned} \hbar\omega_i\, u_k &= \frac{\hbar^2 k^2}{2m} u_k + gn_0(u_k + v_k), \\ -\hbar\omega_i\, v_k &= \frac{\hbar^2 k^2}{2m} v_k + gn_0(u_k + v_k), \end{aligned} \tag{2.39}$$

with $k = |\mathbf{k}|$. They admit a non-trivial solution if the determinant of the coefficients vanishes, and lead to the Bogoliubov spectrum [53]

$$(\hbar\omega)^2 = \left(\frac{\hbar^2 k^2}{2m}\right)^2 + \frac{\hbar^2 k^2}{m}\, gn_0 \equiv (\epsilon_k)^2 . \tag{2.40}$$

Considering the positive frequency solution $\hbar\omega = \epsilon_k$ we get the following relations between the coefficients

$$v_k = -\frac{gn_0}{\epsilon_k + \xi_k} u_k, \tag{2.41}$$

where $\xi_k \equiv \hbar^2 k^2/2m + gn$. By posing the normalization $|u_k|^2 - |v_k|^2 = 1$ and choosing without loss of generality u_k, and v_k to be real, we finally find [35]

$$u_k^2 = \frac{1}{2}\left(\frac{\xi_k}{\epsilon_k} + 1\right), \qquad v_k^2 = \frac{1}{2}\left(\frac{\xi_k}{\epsilon_k} - 1\right). \tag{2.42}$$

The nature of these excitations can be understood by a close inspection of the Bogoliubov spectrum and the behaviour of the coefficients u_k and v_k as a function of k. Identifying with $\mathbf{p} = \hbar\mathbf{k}$ the momentum of the elementary excitations in the system, the Bogoliubov dispersion law takes for small momenta $p \ll mc$, the

phonon-like form $\epsilon_p = c\,p$, where $c = \sqrt{gn/m}$ defines the speed of sound and $p = |\mathbf{p}|$. This shows that the Bogoliubov theory for weakly interacting Bose gases predicts that the long wavelength excitations behave as sound waves propagating in the condensate. The divergence of the coefficients $u_p, v_p \to \sqrt{mc/2p}$ that appear in this limit, is a consequence of this interpretation. For small wavevectors we see that they attain the same value, maximizing in this way the mixing between positive and negative frequency modes. This dramatically modifies the free particle nature of the excitations, that behave as collective fluctuations of the system in this case, as sound waves are. In the opposite limit $p \gg mc$ instead, the spectrum approaches the free particle law

$$\epsilon_p = \frac{p^2}{2m} + gn, \tag{2.43}$$

and the mixing between positive and negative frequency solutions is negligible: $|v| \ll |u| \approx 1$. The transition between the two regime takes place for $p \sim mc$, that is for wavelengths of the order of the healing length.

2.2.2 Quantum interpretation

The classical theory of small amplitude oscillations developed above admits a very natural quantum interpretation in terms of elementary excitations of the system [34]. In order to quantize the theory we work in the Heisenberg representation and write the field operator as

$$\hat{\Psi}\left(\mathbf{r},t\right) = \left(\Psi_0\left(\mathbf{r}\right) + \delta\hat{\Psi}\left(\mathbf{r},t\right)\right) e^{-i\mu t/\hbar}, \tag{2.44}$$

which is equivalent to Eq. (2.29) but with the perturbative term being this time an operator. The grand canonical Hamiltonian is defined as $\hat{H}' = \hat{H} - \mu\hat{N}$, where $\hat{H}$ is given by (2.3), with the effective potential $V_{\text{eff}} = g\delta(\mathbf{r})$ replacing the bare interaction potential, so that

$$\hat{H} = \int \left[d\mathbf{r}\, \hat{\Psi}^\dagger \left(-\frac{\hbar^2}{2m}\boldsymbol{\nabla}^2 + V_{\text{ext}}(\mathbf{r}) \right) \hat{\Psi} \right] + \frac{g}{2}\int d\mathbf{r}\, \hat{\Psi}^\dagger\hat{\Psi}^\dagger\hat{\Psi}\hat{\Psi} \tag{2.45}$$

and $\hat{N} \equiv \int d\mathbf{r}\hat{\Psi}^\dagger\hat{\Psi}$. It can be expanded around the equilibrium configuration in the form $\hat{H}' = E_0' + \hat{H}^{(2)}$, where the zero order term is the value of the grand canonical energy (2.22) at the equilibrium, while the second order term $\hat{H}^{(2)}$ is the

contribution due to the excitations. The term linear in the perturbation vanishes at equilibrium since Ψ_0 is the solution of the time-independent GP equation and thus extremizes the grand canonical potential. By using the Heisenberg equation describing the time evolution of $\delta\hat{\Psi}(\mathbf{r},t)$, which is obtained upon substitution of Eq. (2.44) into Eq. (2.5) (with V_{eff} instead of V) and retaining only terms linear in $\delta\Psi(\mathbf{r},t)$, the Hamiltonian for the excited component can be recast in the form:

$$\hat{H}^{(2)} = \frac{i\hbar}{2}\int d\mathbf{r}\left[\delta\hat{\Psi}^{\dagger}\left(\frac{\partial}{\partial t}\delta\hat{\Psi}\right) - \left(\frac{\partial}{\partial t}\delta\hat{\Psi}^{\dagger}\right)\delta\hat{\Psi}\right]. \tag{2.46}$$

The connection with the classical Bogoliubov theory developed in the previous section is made by taking solutions for $\delta\hat{\Psi}$ in the form

$$\delta\hat{\Psi}(\mathbf{r},t) = \sum_i \left[u_i(\mathbf{r})\,\hat{b}_i\,e^{-i\omega_i t} + v_i^*(\mathbf{r})\,\hat{b}_i^{\dagger}\,e^{i\omega_i t}\right], \tag{2.47}$$

where $u_i(\mathbf{r})$, $v_i(\mathbf{r})$ are solutions of Eqs. (2.31) and (2.32), ω_i is the frequency, and the operators $\hat{b}_i$ and $\hat{b}_i^{\dagger}$ annihilate and create particles in the ith mode, and satisfy the Bose commutation rule $\left[\hat{b}_i,\hat{b}_j^{\dagger}\right] = \delta_{ij}$, with all others commutators vanishing. By substituting the expression (2.47) into Eq. (2.46), and exploiting the orthogonality (2.37) between solutions with different energies, the Hamiltonian operator for the excitations takes the form:

$$\hat{H}^{(2)} = \sum_i \int d\mathbf{r}\,\hbar\omega_i\left(|u_i|^2 - |v_i|^2\right)\hat{b}_i^{\dagger}\hat{b}_i, \tag{2.48}$$

where the zero-point contribution due to the non-commutativity of the $\hat{b}_i$ and $\hat{b}_i^{\dagger}$ operators has been omitted. The Eq. (2.48) justifies the choice made in Eq. (2.38) for the normalization of the u_i and v_i solutions, from which follows that Eq. (2.48) takes the form of the Hamiltonian of a system of independent particles and the quantization procedure is concluded.

2.3 Rotating condensates

2.3.1 Uniform system

In this section we give a brief overview of the physics of rotating condensates, with special attention to the stability properties. What follows represents a theoretical

background, in the perspective of the original work discussed in Chapters 4 and 5. The following arguments have been originally developed in [55–57], and reviewed in [71–74].

As first theoretically predicted by Onsager [75] and Feynman [59], and experimentally verified by Vinen working with superfluid helium [76–81], a superfluid rotates through the nucleation of vortices with quantized value of circulation. This is a purely quantum phenomenon, due to the restriction imposed to the condensate wave function to be single-valued, which dramatically differs from the behaviour of a classical fluid, which gains instead angular momentum by rotating as a rigid body. Subsequent experiments [82, 83] revealed the appearance of the same physics in atomic condensates, and showed the occurrence of the characteristic triangular lattice structure [84], known as Abrikosov lattice.

The simplest solution of the GP equation (2.21) describing a rotating condensate is given by an axial-symmetric vortex line, which is mathematically represented by the order parameter [55–57]

$$\Psi_0(\mathbf{r}) = f(r_\perp, z)\, e^{i\ell\varphi}. \tag{2.49}$$

Here we assumed the axis of the vortex line to be in the z direction, and introduced the polar coordinates $r_\perp$, φ, while ℓ is an integer that ensures the single-valuedness of the wavefunction, whose physical meaning is illustrated in the following. By using the definition given in Sec. 2.1.3, we see that the velocity field induced by such a solution is purely azimuthal and equal to

$$\mathbf{v}(\mathbf{r}) = \frac{\ell}{2\pi}\frac{\boldsymbol{\kappa}\times\mathbf{r}}{r^2}, \tag{2.50}$$

where we defined $\boldsymbol{\kappa} = \kappa\,\hat{z}$, with $\kappa \equiv h/m$ ($h = 2\pi\hbar$). The physical meaning of κ can be deduced from the circulation Γ of the velocity field along a line C surrounding the axis of the vortex line, which reads

$$\Gamma \equiv \oint_C \mathbf{v}\cdot d\mathbf{l} = \ell\kappa. \tag{2.51}$$

Inspection of Eq. (2.51) reveals that the circulation is quantized, and κ has the

meaning of a circulation quantum. The velocity field in Eq. (2.50) is irrotational everywhere, except at the vortex line at $r_\perp = 0$, where the phase of the condensate wavefunction is singular. The vorticity of the system is then localized along the vortex line and, with the aid of the Stokes' theorem [85] (according to which $\oint_C \mathbf{v} \cdot d\mathbf{l} = \int_S (\boldsymbol{\nabla} \times \mathbf{v}) \cdot d\mathbf{S}$, with S a surface having the contour C as boundary), one obtains

$$\boldsymbol{\nabla} \times \mathbf{v} = \ell\kappa\, \delta^{(2)}(\mathbf{r}_\perp)\, \hat{z}, \tag{2.52}$$

where $\delta^{(2)}(\mathbf{r}_\perp)$ is the two-dimensional Dirac delta function in the plane orthogonal to the vortex line.

The energy of the vortex is obtained by evaluating the energy functional (2.14) with the order parameter given in Eq. (2.49), and takes the form

$$E = \int d\mathbf{r} \left\{ \frac{\hbar^2}{2m} \left[\left(\frac{\partial f}{\partial r_\perp} \right)^2 + \left(\frac{\partial f}{\partial z} \right)^2 \right] + \frac{\hbar^2}{2m} \frac{\ell^2}{r_\perp^2} f^2 + V_{\rm ext}(\mathbf{r}) f^2 + \frac{g}{2} f^4 \right\}. \tag{2.53}$$

It is larger compared to the case of a non-rotating state, because of the extra contribution to the kinetic energy due to the azimuthal flow and the density variations close to the vortex core, where the particle density vanishes because of the centrifugal barrier. In order to evaluate it explicitly, we need first to determine the radial profile f of the order parameter.

The equation for the amplitude $f\,(r_\perp, z)$ is derived by minimizing the grand-canonical energy $E' = E - \mu N$, with E given in Eq. (2.53) and $N = \int d\mathbf{r}\, f^2$, or by inserting the order parameter (2.49) directly into the GP equation (2.21), obtaining:

$$-\frac{\hbar^2}{2m} \left[\frac{1}{r_\perp} \frac{\partial}{\partial r_\perp} \left(r_\perp \frac{\partial f}{\partial r_\perp} \right) + \frac{\partial^2 f}{\partial z^2} \right] + \frac{\hbar^2 \ell^2}{2m r_\perp^2} f + V_{\rm ext}\,(\mathbf{r})\, f + g f^3 = \mu f. \tag{2.54}$$

Considering the uniform system, it is useful to identify two limit regimes of the solution, relative to the regions far and close to the vortex line respectively. In the far region, the centrifugal potential barrier $\hbar^2\ell^2/2mr_\perp^2$ vanishes, and the system approaches the uniform state with density $n_0 = \mu/g \equiv f_0^2$. On the other hand, in the region close to the vortex line, f goes to zero as $f \sim r_\perp^{|\ell|}$, as an effect of the centrifugal barrier [50]. By comparing the centrifugal potential with the interatomic interaction energy, we see that the cross-over between the two regimes occurs at

distances from the vortex line of the order $\sim |\ell|\xi$, which defines the size of the vortex core. The exact profile of the particle density is the solution of Eq. (2.54) that, in the dimensionless variables $\chi \equiv f/f_0$ and $x = r_\perp/\xi$, reads

$$\frac{1}{x}\frac{d}{dx}\left(x\frac{d\chi}{dx}\right) + \left(1 - \frac{\ell^2}{x^2}\right)\chi - \chi^3 = 0. \tag{2.55}$$

Once we solve Eq. (2.55), for example numerically or by a variational calculation [34, 35, 86], we are in the position to address the calculation for the energy of the rotating condensate. We are interested in particular in the excess of energy compared to the uniform state of the system with the same number of particles. In order to calculate such energy difference, we assume the condensate confined in a cylindrical vessel of radius $R \gg |\ell|\xi$, whose energy ϵ per unit length along the vortex line has the form:

$$\epsilon = \int_0^R dr_\perp\, 2\pi r_\perp \left[\frac{\hbar^2}{2m}\left(\frac{df}{dr_\perp}\right)^2 + \frac{\hbar^2\ell^2}{2m}\frac{f^2}{r_\perp^2} + \frac{g}{2}f^4\right]. \tag{2.56}$$

We need to subtract from Eq. (2.56) the energy $\epsilon_0 = (n^2 g/2)\pi R^2$ relative to the same system in the uniform state, with $n = \nu/\pi R^2$ and ν the number of particles per unit length contained in the vessel. The value of ν is given by

$$\nu = \int_0^R dr_\perp 2\pi r_\perp f^2 = \pi R^2 f_0^2 - \int_0^R dr_\perp 2\pi r_\perp \left(f_0^2 - f^2\right), \tag{2.57}$$

where we added and substracted the value pertaining the uniform state in the last equation. Given Eq. (2.57), the energy per unit length of the uniform system can be readily calculated:

$$\begin{aligned}\epsilon_0 &= \frac{g}{2}n^2\pi R^2 \\ &= \frac{\pi}{2}R^2 g f_0^4 - g f_0^2 \int_0^R dr_\perp 2\pi r_\perp \left(f_0^2 - f^2\right),\end{aligned} \tag{2.58}$$

where terms of order $(\xi/R)^2$ have been neglected, as we work under the assumption $R \gg \xi$. The excess of energy ϵ_v associated with the presence of a vortex is the difference between Eqs. (2.56) and (2.58) and is equal to

$$\epsilon_v = \int_0^{R_\perp} 2\pi r_\perp dr_\perp \left[\frac{\hbar^2}{2m}\left(\frac{df}{dr_\perp}\right)^2 + \frac{\hbar^2\ell^2}{2m}\frac{f^2}{r_\perp^2} + \frac{g}{2}\left(f_0^2 - f^2\right)^2\right]. \tag{2.59}$$

Since the particle density attains a constant value far from the vortex line, the kinetic energy associated to the azimuthal flow diverges logarithmically, and represents the

major contribution to the vortex energy. In such a regime, $f \simeq f_0 = \sqrt{n_0}$, and the energy per unit length in the case of a single quantized vortex ($\ell = 1$) is approximately equal to $\epsilon_v \approx (\pi\hbar^2/m)n_0 \ln(R/\xi)$. Taking into account the contributions due to the other terms, a more accurate result has been obtained by evaluating the energy functional (2.59) with a numerical solution of the Eq. (2.55) for the amplitude of the order parameter. This gives [34, 35, 87]

$$\epsilon_v = \pi\frac{\hbar^2}{m}n_0 \ln\left(1.464\frac{R}{\xi}\right). \tag{2.60}$$

Analogous result holds true for vortices with multiple quanta of circulation. In such a case, by following the same reasoning as above, the vortex energy takes the form $\epsilon_v^\ell \approx (\pi\hbar^2\ell^2/m)n_0 \ln(R/|\ell|\xi)$ [34, 35]. This shows that, in a uniform condensate, configurations involving more vortices with a single quantum of circulation are energetically favoured over states with vortices with multiple quanta of circulation.

2.3.2 Harmonically trapped system

Using the results of the previous section, we here estimate the energy of a vortex in a harmonically trapped condensate. To this aim we first consider the simpler two-dimensional system composed by a cylindrical cloud confined in a rotationally invariant harmonic potential $V_{\rm ext} = m\omega_\perp^2 r_\perp^2/2$ with respect to the vortex axis. We assume the number of particles is high enough that the corresponding non-rotating state of the system is accurately described within the TF approximation introduced in Sec. 2.1.4. In this limit, the extension of the cloud is much larger compared to the size of the vortex core ξ_0 at the center of the cloud, and results

$$\frac{\xi_0}{R_\perp} = \frac{\hbar\omega_\perp}{2\mu} \ll 1, \tag{2.61}$$

where $R_\perp = \sqrt{2\mu/m\omega_\perp^2}$ is the TF radius. The excess energy due to the presence of the vortex can be conveniently estimated by splitting the calculation in two regions, separated by an intermediate radius ρ satisfying the relation $\xi_0 \ll \rho \ll R$. Working in the TF limit, the particle density varies smoothly in space and, in the inner region, it can be considered uniform and equal to the value $n(0)$ attained by the non-rotating condensate at the center of the trap. The contribution to the energy relative to this region is then given by the results in Eq. (2.60) for the uniform

system, provided we substitute $n \to n(0)$ and $R \to \rho$. By contrast, in the outer region the density profile is not affected by the presence of the vortex, and the main contribution to the vortex energy is due to the azimuthal kinetic energy. Combining these two contributions, we have the excess energy per unit length [35, 87]

$$\begin{aligned}\epsilon_v &= \pi n(0)\frac{\hbar^2}{m}\ln\left(1.464\frac{\rho}{\xi_0}\right) + \int_\rho^{R_\perp} dr_\perp\, 2\pi r_\perp \frac{\hbar^2}{2m}\frac{n(r_\perp)}{r_\perp^2} \\ &= \pi n(0)\frac{\hbar^2}{m}\left[\ln\left(1.464\frac{R_\perp}{\xi_0}\right) - \frac{1}{2}\right] \\ &= \pi n(0)\frac{\hbar^2}{m}\ln\left(0.888\frac{R_\perp}{\xi_0}\right),\end{aligned} \tag{2.62}$$

where we evaluated the integral using the TF profile for the density $n(r_\perp) = n(0)\,(1 - r_\perp^2/R_\perp^2)$. The results obtained above for the effectively two dimensional system can be extended to the fully three-dimensional case. By neglecting the kinetic energy due to the spatial variations of the order parameter in the z direction, again justified since we work in the TF limit, the energy of the vortex can be estimated by integrating the contribution of each infinitesimal slide of the cloud as $E = \int_{-R_z}^{R_z} dz\, \epsilon_v(z)$, where R_z is the transverse extension of the cloud defined as in Eq. (2.25). Given the TF particle density $n(r_\perp, z) = n(0)\,(1 - r_\perp^2/R^2 - z^2/R_z^2)$, the z-dependent radial extension of the condensate $R_\perp(z) = R_\perp\,(1 - z^2/R_z^2)^{1/2}$ and core size $\xi(z) = \xi_0\,[n(0,0)/n(0,z)]^{1/2}$, the energy of the vortex reads [35, 87]

$$\begin{aligned}E_v &= \frac{\pi\hbar^2}{m}\int_{-R_z}^{R_z} dz\, n(0,z)\ln\left[0.888\frac{R_\perp(z)}{\xi(z)}\right] \\ &= \frac{4\pi n(0)}{3}\frac{\hbar^2}{m}R_z\ln\left(0.671\frac{R_\perp}{\xi_0}\right).\end{aligned} \tag{2.63}$$

Note that the procedure leading to the energy in Eq. (2.63) is based on the hypothesis that $R(z) \gg \xi(z)$, a condition that is less and less satisfied for $|z| \to R_z$. However, the estimate based on this simplifying assumption turns out to be in good agreement with numerical results obtained for large number of particles [35, 88].

Eq. (2.63) can be generalized to the case of an off-axis vortex displaced by $r_\perp = b$ from the minimum of the harmonic potential, as [35, 89, 90]

$$E(b) \simeq E\left(1 - \frac{b}{R}\right)^{3/2}. \tag{2.64}$$

This result can be derived by evaluating the integral in Eq. (2.63) in the more

generic form

$$E = \frac{\pi\hbar^2}{m}\int_{-R_z(b)}^{R_z(b)} dz\, n(b,z)\ln\left(\frac{R_\perp(z)}{\xi(b,z)}\right), \tag{2.65}$$

with $R_z(b) = R_z\left(1 - b^2/R_\perp^2\right)^{1/2}$ the vertical heigth of the cloud at the radial position $r_\perp = b$, and $\xi(b,z) = \xi_0\sqrt{n(0,0)/n(b,z)}$ the healing length at the point $r_\perp = b$ and z. This result shows that the configuration with the vortex in the center of the trap is unstable with respect to small displacements of the vortex line from the axis of symmetry of the trapping potential. As a consequence, the vortex would leave the cloud in the presence of a dissipative mechanism that removes angular momentum from the condensate, transferring the vortex towards its lower energy states. Such a mechanism could be provided by the interaction between the vortex and the thermal cloud for example [91]. Rotating traps, however, can stabilize a vortex state. In order to show how that is possible, it is convenient to move to the reference frame co-rotating with the external potential, where the Hamiltonian does not depend on time. According to the Galilean transformations, the energy E' of the system in the frame rotating with angular velocity $\mathbf{\Omega}$, can be expressed in terms of the energy E and of the angular momentum $\mathbf{L}$ in the non-rotating frame as $E' = E - \mathbf{\Omega}\cdot\mathbf{L}$ [92]. This relation shows that, in the rotating frame, states of the system with projection of the angular momentum in the direction of the rotations different from zero can be stabilized. Indicating by E_s the energy and by L_s the relevant component of the angular momentum, such a state becomes energetically favorable with respect to the ground state of the system with energy E_0, when the rotational velocity exceeds the critical value

$$\Omega_{\rm cr} = \frac{E_s - E_0}{L_s}. \tag{2.66}$$

This stability criterion can be applied to a vortex state, for which we calculated the excess energy $E_v \equiv E_s - E_0$ in Eq. (2.64) for the case of a harmonically trapped cloud, when the vortex line is displaced with respect to the axes of symmetry of the potential. What is left to do is to calculate the angular momentum, which is equal

to

$$\begin{aligned} L_v \equiv \langle L_z \rangle &= \int d\mathbf{r}\, \Psi_0(\mathbf{r})^\dagger L_z \Psi_0(\mathbf{r}) = \\ &= \int_{-R_z(b)}^{R_z(b)} dz \int_b^{R_\perp(z)} 2\pi r_\perp n(r_\perp, z)\, dr_\perp \\ &= \hbar N \left(1 - \frac{b^2}{R^2}\right)^{5/2}, \end{aligned} \tag{2.67}$$

where we used the order parameter $\Psi_0 = \sqrt{n(r_\perp, z)} e^{i\varphi}$, with $n(r_\perp, z)$ the TF density profile introduced above, and the definition of the angular momentum operator in polar coordinates $L_z = -i\hbar \frac{\partial}{\partial \varphi}$. Eq.(2.67) shows that, although the circulation around the vortex is quantized, the angular momentum per particle is not, as it decreases by increasing the distance of the vortex line from the center of the trap. Combining Eqs. (2.64) and (2.67), the energy of the vortex in the rotating frame takes the form [34, 35, 89, 90]

$$\begin{aligned} E_v' &= E_v - \Omega L_v \\ & E \left(1 - \frac{b^2}{R^2}\right)^{3/2} - \hbar N \Omega \left(1 - \frac{b^2}{R^2}\right)^{5/2}. \end{aligned} \tag{2.68}$$

Eq. (2.68) shows that a rotation of the system lowers the energy of a vortex state in the co-rotating reference frame. At the critical value $\Omega_{\rm cr}$, the energy is zero, and eventually becomes negative for higher values of the angular velocity. Under these conditions, the vortex state becomes a globally stable solution.

For the simpler case of an axial symmetric ($b = 0$), harmonically trapped, cylindrical system, Eq. (2.68) reduces to

$$\epsilon_v' = \epsilon - \hbar\nu\Omega, \tag{2.69}$$

where ϵ_v is given by Eq. (2.62) and

$$\nu = \int d^2\mathbf{r}\, n(r_\perp) = \frac{\pi}{2} n(0) R_\perp^2, \tag{2.70}$$

is the number of particles per unit length. Here we used the TF density profile $n(r_\perp) = n(0)\,(1 - r_\perp^2/R_\perp^2)$. The critical angular velocity in such a case is thus equal to

$$\Omega_{\rm cr} = \frac{\epsilon_v}{\hbar\nu} = \frac{2\hbar}{m R_\perp^2} \log\left(0.888 \frac{R_\perp}{\xi_0}\right). \tag{2.71}$$

Chapter 3 Artificial magnetism

The concept of *artificial gauge fields*, and in particular *synthetic magnetism*, is a concrete implementation of the idea of *quantum simulators*, first conceived by Feynman in 1982 [5]. Tha aim is to exploit the universality of the laws of quantum mechanics to use a controllable system in order to reproduce the physics of other systems of interest, whose experimental investigation is out of the technological capabilities.

Within this framework, the way by which orbital magnetism is simulated can be understood in terms of the so called Aharonov-Bohm effect [93, 94], according to which the wavefunction of a charged particles gains a phase factor when it travels around a closed path pierced by a non-zero magnetic flux. Following this picture, magnetism can be simulated with neutral atoms by inducing geometrical phases such as the Berry phase [95], that arise when the Hamiltonian of a quantum system depends on one or more parameters that adiabatically change in time. Assuming the atoms move slowly enough, a Berry connection [95] appears in the physical space, when the Hamiltonian of the atoms parametrically depends on the position, which plays the role of an effective vector potential. The emergence of such effective dynamics has been first pointed out in [96, 97], by coupling the center-of-mass motion of the atoms to their internal dynamics, via opportunely designed space-dependent light-matter interaction. Because of the high level of controllability reached in state-of-the-art experiments, successive works proposed the implementation of non-trivial synthetic electric and magnetic fields in cold atoms systems [98–102]. Based on these theoretical proposals, synthetic magnetism were experimentally realized at NIST [103–105], working with cold atoms in the bulk geometry described above, which is the configuration that will be used in the rest of the thesis, and reviewed in the present chapter. It is however worth mentioning that lattice geometries have also been widely used to the same aim (see [1, 2, 106, 107] and references therein).

We start the chapter by introducing in Sec. 3.1 the general concept of geometric (Berry) phase and show how they emerge in quantum mechanics. We use these concepts in Sec. 3.2, in which we set the formalism for geometric potentials in the physical space, where they can be seen as effective vector and scalar potentials. In Sec. 3.3 we address the practical implementation of this with cold atoms, considering two-level and Λ-level internal configurations. We finally show in Sec. 3.5, how these arguments can be generalized to take into account the interparticle interactions, leading to nonlinear (that is density dependent) synthetic magnetic and electric potentials.

3.1 Berry phase

Let us consider a system whose dynamics is described by the Hamiltonian $\hat{H}(\boldsymbol{\lambda})$, parametrically depending on one or more quantities here collectively denoted as $\boldsymbol{\lambda}$. The stationary states $|\psi_n(\boldsymbol{\lambda})\rangle$ of the system, which we assume form a discrete set, and the corresponding energies $E_n(\boldsymbol{\lambda})$, are defined by

$$\hat{H}(\boldsymbol{\lambda})\,|\psi_n(\boldsymbol{\lambda})\rangle = E_n(\boldsymbol{\lambda})\,|\psi_n(\boldsymbol{\lambda})\rangle. \tag{3.1}$$

For each value of $\boldsymbol{\lambda}$, the set $\{|\psi_n(\boldsymbol{\lambda})\rangle\}$ is assumed to form an orthonormal basis for the Hilbert space, so that the generic state of the system can be expanded as $|\psi\rangle = \sum_n c_n|\psi_n(\boldsymbol{\lambda})\rangle$.

We consider the system initially prepared in the state $|\psi_i(\boldsymbol{\lambda})\rangle$ that is, at $t = 0$, $c_i = 1$ and $c_n = 0$ if $n \neq i$, and assume to vary the value of $\boldsymbol{\lambda}$ along a closed contour $\mathcal{C}$ in the parameters' space. If such variation occurs in the time interval $t = [0, T]$, this means that $\boldsymbol{\lambda}(T) = \boldsymbol{\lambda}(0)$. In the hypothesis that the time evolution of the parameters is slow enough, the adiabatic theorem holds true [108] and, to first approximation, the state of the system remains proportional to the original eigenstate at all the times. In these assumptions, the final state of the system at $t = T$ is still equal to $|\psi_i(\boldsymbol{\lambda})\rangle$, up to a phase factor. To show this result, we use the adiabatic assumption and write the state of the system at the generic time instant t as $|\psi(t)\rangle = c_i(t)|\psi_i(\boldsymbol{\lambda}(t))\rangle$, where $c_i(t)$ is a phase factor to be determined. The reduced dynamics of the system

is obtained by projecting the Schrödinger equation

$$i\hbar\frac{d|\psi(t)\rangle}{dt} = \hat{H}\left(\boldsymbol{\lambda}(t)\right)|\psi(t)\rangle, \tag{3.2}$$

onto the subspace of the Hilbert space spanned by $|\psi_i\left(\boldsymbol{\lambda}(t)\right)\rangle$, and results in the equation

$$i\hbar\dot{c}_i = \Big(E_i(t) - i\hbar\dot{\boldsymbol{\lambda}}\cdot\mathbf{A}_i(\boldsymbol{\lambda})\Big)\,c_i, \tag{3.3}$$

where we defined $\mathbf{A}_i(\boldsymbol{\lambda}) = i\hbar\langle\psi_i(\boldsymbol{\lambda})|\boldsymbol{\nabla}\psi_i(\boldsymbol{\lambda})\rangle$, and we denoted time derivatives by dotted symbols. This equation can be integrated, yielding

$$c_i(T) = e^{-i\int_0^T E_i(t)dt/\hbar}e^{i\gamma_i[\mathcal{C}]}c_i(0). \tag{3.4}$$

The first term in Eq. (3.4) is the usual dynamical phase factor that appears also in time-independent problems, while the second term represents an extra phase factor, providing the *geometric* phase [95, 107]

$$\gamma_i[\mathcal{C}] = \frac{1}{\hbar}\oint_{\mathcal{C}}\mathbf{A}_i(\boldsymbol{\lambda})\cdot d\boldsymbol{\lambda}. \tag{3.5}$$

The name "geometric" is ascribed to the fact that such a phase shift is given by the contour integral of $\mathbf{A}_i(\boldsymbol{\lambda})$ along the path $\mathcal{C}$ in the parameter space, whose value only depends on the trajectory followed by $\boldsymbol{\lambda}(t)$ and is independent on how such a contour is traversed (provided T is large enough compared to the other relevant energy scales involved, and the adiabatic approximation can be applied).

Eq. (3.5) is the central result of this section. It clearly shows that $\mathbf{A}_i(\boldsymbol{\lambda})$ can be interpreted as equivalent of an electromagnetic vector potential acting in the parameter space, and the geometrical phase shift as an analogue Aharonov-Bohm effect. Because of this reason, $\mathbf{A}_i(\boldsymbol{\lambda})$ is usually referred to as a *Berry connection*, and $\mathbf{B}_i(\boldsymbol{\lambda}) \equiv \boldsymbol{\nabla}\times\mathbf{A}_i$, which represents the corresponding magnetic field in the parameter space, takes the name of *Berry curvature*.

From this it is clear how synthetic magnetism can arise in a quantum system. What is needed is to make the Hamiltonian in Eq. (3.1) parametrically dependent on the position, that is, making the identification $\boldsymbol{\lambda} \equiv \mathbf{r}$. How this prescription can be implemented with cold atoms is the topic of the next two sections.

3.2 Synthetic magnetic fields

3.2.1 General formalism

Synthetic magnetic fields acting on neutral atoms emerge by for instance coupling the centre of mass motion of the particles to their internal degrees of freedom [96, 97], in turn coupled between each other by a laser field [109–111]. This can be achieved by making the light-matter interaction parameters space-dependent. We will see in the following sections that, within the rotating-wave approximation [109–111], the internal dynamics of the particles interacting with an electromagnetic field can be described by a time-independent Hamiltonian, hereafter labelled $\hat{H}_{\text{int}}(\mathbf{r})$, so that the Hamiltonian for a particle of mass M takes the general form

$$\hat{H} = \left(\frac{\hat{\mathbf{p}}^2}{2M} + V_{\text{ext}}(\mathbf{r}) \right) \otimes \mathbb{I} + \hat{H}_{\text{int}}(\mathbf{r}), \tag{3.6}$$

where $\hat{\mathbf{p}} \equiv -i\hbar\boldsymbol{\nabla}$ is the quantum momentum operator of the particle, $V_{\text{ext}}(\mathbf{r})$ accounts for possible external potentials, and $\mathbb{I}$ is the identity operator for the internal Hilbert space.

Retracing the reasoning illustrated in the previous section, we define the eigenstates of the atom *dressed* by the interaction with the field, and the relative energies, as

$$\hat{H}_{\text{int}}(\mathbf{r})|\psi_n(\mathbf{r})\rangle = E_n(\mathbf{r})|\psi_n(\mathbf{r})\rangle, \tag{3.7}$$

both parametrically depending on the position in general. As done in Sec. 3.1, we consider the particle initially prepared in one of its dressed states, and suppose it moves slowly enough that the adiabatic approximation can be safely applied (more details on the validity of this condition are discussed in the following). Within these assumptions the atom remains in the same internal state at all time. Analogously to what was done in the previous section, the reduced dynamics of the atom is obtained by projecting the Schrödinger equation

$$\begin{aligned} i\hbar \frac{d|\psi(\mathbf{r},t)\rangle}{dt} &= \hat{H}|\psi(\mathbf{r},t)\rangle \\ &= \left[\left(\frac{\hat{\mathbf{p}}^2}{2M} + V_{\text{ext}}(\mathbf{r}) \right) \otimes \mathbb{I} + \hat{H}_{\text{int}}(\mathbf{r}) \right] |\psi(\mathbf{r},t)\rangle, \end{aligned} \tag{3.8}$$

onto the subspace of the Hilbert space spanned by the initial, say $|\psi_i(\mathbf{r})\rangle$, dressed

state. In this procedure, a crucial role is played by the kinetic term of the atomic center-of-mass motion, from which geometric vector and scalar potentials arise. The effective dynamics of the particles can be derived by considering first the action of the momentum operator on the full state $|\psi(\mathbf{r},t)\rangle = \sum_n \psi_n(\mathbf{r},t)|\psi_n(\mathbf{r})\rangle$. Since the dressed states explicitly depend on the position, we have

$$\hat{\mathbf{p}}|\psi(\mathbf{r},t)\rangle = \sum_{m,n} \left[\left(\delta_{m,n}\hat{\mathbf{p}} + \mathbf{A}_{m,n}(\mathbf{r})\right)\psi_n(\mathbf{r},t)\right]|\psi_m(\mathbf{r})\rangle, \tag{3.9}$$

where we used the completeness relation $\sum_m |\psi_m(\mathbf{r})\rangle\langle\psi_m(\mathbf{r})| = \mathbb{I}$, and we defined $\mathbf{A}_{m,n}(\mathbf{r}) \equiv \langle\psi_m(\mathbf{r})|\,\hat{\mathbf{p}}\,|\psi_n(\mathbf{r})\rangle$. By using Eq. (3.9), and neglecting all the amplitudes $\psi_n(\mathbf{r},t)$ with $n \neq i$ (because of the adiabatic assumption of the atomic motion), the projection of the kinetic term onto the initial $|\psi_i(\mathbf{r})\rangle$ direction, takes the form [1, 2, 107]

$$\left\langle \psi_i(\mathbf{r}) \right| \frac{\hat{\mathbf{p}}^2}{2M} \left| \psi(\mathbf{r},t) \right\rangle = \left[\frac{\left(\hat{\mathbf{p}} - \mathbf{A}_i(\mathbf{r})\right)^2}{2M} + W_i(\mathbf{r})\right]\psi_i(\mathbf{r},t) \tag{3.10}$$

with

$$\mathbf{A}_i(\mathbf{r}) = -\langle\psi_i|\,\hat{\mathbf{p}}\,|\psi_i\rangle\,, \tag{3.11a}$$

$$W_i(\mathbf{r}) = \sum_{n\neq i} \frac{|\langle\psi_n|\,\hat{\mathbf{p}}\,|\psi_i\rangle|^2}{2M}. \tag{3.11b}$$

Comparison with the definition given in Sec. 3.1 shows that $\mathbf{A}_i(\mathbf{r})$ has the structure of a Berry connection in the physical space and represents the sought effective magnetic vector potential. In addition, the Eq. (3.10) shows that the atom, during its adiabatic evolution, feels the action of the effective scalar potential $W_i(\mathbf{r})$. The reduced dynamics is thus described by the following equation for the time evolution of the probability amplitude $\psi_i(\mathbf{r},t)$

$$i\hbar\frac{\partial\psi_i}{\partial t} = \left[\frac{\left(\hat{\mathbf{p}} - \mathbf{A}_i\left(\mathbf{r}\right)\right)^2}{2M} + E_i\left(\mathbf{r}\right) + W_i\left(\mathbf{r}\right)\right]\psi_i\left(\mathbf{r},t\right), \tag{3.12}$$

that has the form of the Schrödinger equation for a particle with unit charge, moving in the magnetic field $\mathbf{B}_i \equiv \boldsymbol{\nabla}\times\mathbf{A}_i$, associated with the vector potential $\mathbf{A}_i(\mathbf{r})$ and subject to a potential that is the combination of $W_i\left(\mathbf{r}\right)$ and the space-dependent energy $E_i\left(\mathbf{r}\right)$ of the dressed state.

3.2.2 Validity of the adiabatic approximation

In this section we give a deeper insight into the validity of the adiabatic approximation, on which the above arguments rely. By following [112], we show that the condition required for its applicability is that the characteristic time scale of the center-of-mass motion need to be sufficiently large compared to the time scales set by all the relevant atomic Bohr frequencies.

To this aim, we work in the semi-classical approximation, according to which the centre-of-mass motion is treated classically, while quantum mechanics is still used to describe the internal dynamics. Starting with an atom initially at rest in the $|\psi_i\rangle$ internal dressed state, we say that it is adiabatically set in motion with the final velocity $\mathbf{v}$, if the population Π_n of the other states $|\psi_n\rangle$, with $n \neq i$, is $\Pi_n \ll 1$ at the end of the process. In order to find under which conditions this requirement is fulfilled, we suppose that the atom is uniformly accelerated to the final velocity $\mathbf{v}$ in the time T, with the velocity taking instantaneously the value $\mathbf{v}(t) = \mathbf{v}\, t/T$ for $0 \leq t \leq T$. Given the general expression $|\psi\rangle = \sum_n \psi_n(t)|\psi_n\left(\mathbf{r}(t)\right)\rangle$ for the internal state of the atom, the time evolution is obtained from the Schrödinger equation $i\hbar|\dot{\psi}\rangle = \hat{H}_{\rm int}|\psi\rangle$, considering the relation $|\dot{\psi}\rangle = \sum_n \Big[\dot{\psi}_n|\psi_n\rangle + \psi_n \mathbf{v}\cdot|\boldsymbol{\nabla}\psi_n\rangle\Big]$. The equation of motion for the amplitudes $\psi_j(t)$ takes the form

$$\frac{d\psi_j}{dt} = -i\omega_j\psi_j - \sum_n \left(\psi_n \mathbf{v}\cdot\langle\psi_j|\boldsymbol{\nabla}\psi_n\rangle\right), \tag{3.13}$$

with $\hbar\omega_j = E_j$. To zeroth order in $\mathbf{v}$, the internal state of the atom is not coupled with the center-of-mass motion, and all ψ_j's are zero except ψ_i, which evolves as $\psi_i(t) = \exp(-i\omega_i t)$. To first order, Eq. (3.13) can be solved, by noting that the general solution of the differential equation $\dot{y}+P(t)y = Q(t)$ can be written as $y(t) = \xi(t)\exp(-\int dt' P(t'))$, with $\xi(t) = \xi(0)+\int_0^t dt'\left[Q(t')\exp\left(\int_0^t dt' P(t')\right)\right]$. In our case, $P = i\omega_j$, $Q(t) = -\mathbf{v}\cdot\langle\psi_j|\boldsymbol{\nabla}\psi_i\rangle(t/T)\exp\left(-i\omega_i t\right)$ and, assuming $T(\omega_j-\omega_i) \gg 1$, we get for $j \neq i$

$$\begin{aligned}\psi_j(T) &= -\mathbf{v}\cdot\langle\psi_j|\boldsymbol{\nabla}\psi_i\rangle e^{-i\omega_j T}\int_0^T dt\, e^{i(\omega_j-\omega_i)t}\frac{t}{T} \\ &\approx i\frac{\mathbf{v}\cdot\langle\psi_j|\boldsymbol{\nabla}\psi_i\rangle}{\omega_j-\omega_i}e^{-i\omega_i T}.\end{aligned} \tag{3.14}$$

The populations of the internal atomic states with $j \neq i$, at the end of the acceleration, are thus equal to

$$\Pi_j(T) = |\psi_j(T)|^2 \approx \left| \frac{\mathbf{v} \cdot \langle \psi_j | \boldsymbol{\nabla} \psi_i \rangle}{\omega_j - \omega_i} \right|^2 = \left| \frac{\langle \psi_j | \dot{\psi}_i \rangle}{\omega_j - \omega_i} \right|^2 , \tag{3.15}$$

which shows that the condition for the validity of the adiabatic approximation ($\Pi_j \ll 1$) is that the angular velocity of $|\psi_i\rangle$, induced by the center-of-mass motion, is much smaller than all the relevant transition frequencies [108].

3.3 Practical implementations

We consider here the implementation of the formalism developed in Sec. 3.2, to the case of a neutral atom interacting with an external laser field. We start with the simplest possible scheme, which consists of a close to resonance monochromatic laser beam with frequency ω_f shone on an atom, whose internal dynamics can be restricted to a single relevant transition between a ground $|g\rangle$ and an excited $|e\rangle$ state, with characteristic frequency ω_0. The dressed states in this simple *two-level* model for the atom are defined as a linear combination of the ground and the excited states. We see in the following that, in order to have a sizeable synthetic magnetic field, the relative weights of the two states in this combination need to be of the same order. This poses severe limitations on the experimental feasibility of this configuration, which could be used provided the radiative lifetime of the excited atomic state is long enough compared to the other relevant experimental time scales. In this scenario the spontaneous emission from the excited state is negligible during the duration of the experiment. This is a realistic assumption working with alkali-earth atoms (such as Strontium) or Ytterbium, for which lifetimes of the order of seconds and even of tens of seconds are achievable [113]. The limitations of the two-level scheme can be circumvented, by using more complex internal atomic structures. The idea in this case is to take advantage of eventual degeneracies of the electronic ground level, and work with dressed states which are linear combinations of the the ground sublevels only. This allows to exploit a wider class of atomic species, like the alkali-metal atoms which are mostly used in state-of-the-art cold atoms experiments.

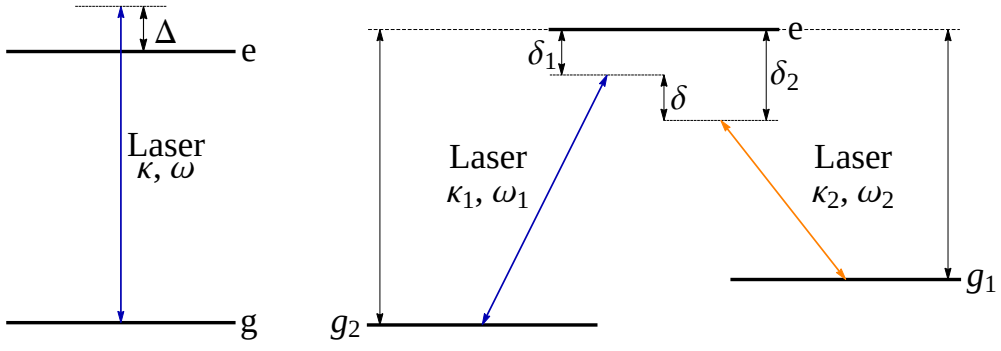

(a) (b)

Figure 3.1: Atomic internal states configurations. (a) Two-level scheme. (b) Λ-level scheme.

We start this section with the description of the two-level scheme in Sec. 3.3.1, since it is the simplest configuration useful in order to generate synthetic gauge fields [1, 2, 107]. We extend the arguments in Sec. 3.3.2, introducing the three-level atom in the Λ-configuration [1, 2].

3.3.1 Two-level atomic model

Let us consider a two-level atom, with transition frequency ω_0 between the ground $|g\rangle$ and the excited $|e\rangle$ states. In the dipole interaction approximation $\hat{H}_{\rm dip} = -\hat{\mathbf{d}}\cdot\mathbf{E}$ [109, 110], with $\hat{\mathbf{d}}$ the dipole operator of the atom, the Hamiltonian describing the semi-classical interaction with the electromagnetic field $\mathbf{E} = \left(\mathbf{E}_0 e^{-i\omega_f t} + \text{c.c.}\right)/2$, reads [109, 110]

$$\hat{H}'_{\rm int} = \hat{H}_{\rm at} + \hat{H}_{\rm dip}, \tag{3.16}$$

with

$$\hat{H}_{\rm at} = \frac{\hbar\omega_0}{2}|e\rangle\langle e| - \frac{\hbar\omega_0}{2}|g\rangle\langle g|, \tag{3.17a}$$

$$\hat{H}_{\rm dip} = \frac{\hbar}{2}\left(\kappa e^{-i\omega_f t} + \tilde{\kappa} e^{i\omega_f t}\right)|e\rangle\langle g| + \text{c.c.}\ . \tag{3.17b}$$

In Eq. (3.17b), we defined the Rabi frequency $\kappa \equiv -\mathbf{d}_{eg}\cdot\mathbf{E}_0/\hbar$ and $\tilde{\kappa} \equiv -\mathbf{d}_{eg}\cdot\mathbf{E}_0^*/\hbar$, with $\mathbf{d}_{ij} = \langle i|\,\mathbf{d}\,|j\rangle$ $(i,j = g,e)$. In the nearly resonant condition $\omega_f \approx \omega_0$, we make the *rotating-wave* approximation (RWA) [109, 110], according to which the terms in the Hamiltonian which are rapidly oscillating (that are the ones evolving in time as $e^{\pm i\left(\omega_0+\omega_f\right)}$ in the interaction picture) can be averaged to zero. In this approximation,

the atom-light interaction takes the form:

$$\hat{H}_{\rm dip}^{\rm RWA} = \frac{\hbar}{2}\left(\kappa e^{-i\omega_f t}|e\rangle\langle g| + \kappa^* e^{i\omega_f t}|g\rangle\langle e|\right), \tag{3.18}$$

and the Hamiltonian describing the internal dynamics of the atom reads

$$\hat{H'}_{\rm int}^{\rm RWA} = \hat{H}_{\rm at} + \hat{H}_{\rm dip}^{\rm RWA}. \tag{3.19}$$

The time dependence in Eq.(3.19) can be removed by the unitary transformation $U = e^{i\omega_f t/2}|e\rangle\langle e| + e^{-i\omega_f t/2}|g\rangle\langle g|$, obtaining

$$\begin{aligned}\hat{H}_{\rm int} &= \hat{U}\hat{H'}^{\rm RWA}\hat{U}^\dagger - i\hbar\hat{U}\frac{\partial\hat{U}^\dagger}{\partial t} \\ &= \frac{\hbar}{2}\left(\Delta|e\rangle\langle e| - \Delta|g\rangle\langle g| + \kappa|e\rangle\langle g| + \kappa^*|g\rangle\langle e|\right)\end{aligned} \tag{3.20}$$

or, in matrix form:

$$H_{\rm int} = \frac{\hbar}{2}\begin{pmatrix}\Delta & \kappa \\ \kappa^* & -\Delta\end{pmatrix}. \tag{3.21}$$

Here $\Delta = \omega_0 - \omega_f$ is the *detuning* of the coupling field from the atomic transition.

It is useful to rewrite the atom-light interaction operator in Eq. (3.21), by introducing the generalized Rabi frequency Ω_r and the mixing angle θ, which are defined as

$$\Omega_r = \sqrt{|\kappa|^2 + \Delta^2}, \qquad \cos\theta = \frac{\Delta}{\Omega_r}, \qquad \sin\theta = \frac{|\kappa|}{\Omega_r}. \tag{3.22}$$

In terms of these quantities, and of the phase ϕ of the electric field, entering into the definition of the Rabi frequency $\kappa = |\kappa|e^{-i\phi}$, Eq. (3.21) takes the form

$$H_{\rm int} = \frac{\hbar\Omega_r}{2}\begin{pmatrix}\cos\theta & e^{-i\phi}\sin\theta \\ e^{i\phi}\sin\theta & -\cos\theta\end{pmatrix}. \tag{3.23}$$

The eigenstates $\{|+\rangle, |-\rangle\}$ of Eq. (3.23) are the internal states of the two-level atom dressed by the interaction with the light field, and have the form

$$|+\rangle = \begin{pmatrix}\cos(\theta/2) \\ e^{i\phi}\sin(\theta/2)\end{pmatrix}, \qquad |-\rangle = \begin{pmatrix}-e^{-i\phi}\sin(\theta/2) \\ \cos(\theta/2)\end{pmatrix}, \tag{3.24}$$

with eigenvalues $\hbar\Omega_r/2$ and $-\hbar\Omega_r/2$ respectively. The Eqs. (3.11a) and (3.11b), evaluated for dressed states $|\pm\rangle$ defined above, yield the following expressions for

the vector and the scalar potentials [1, 2, 107]

$$\mathbf{A}_{\pm} = -\frac{\hbar}{2}\left(1 \mp \cos\theta\right)\boldsymbol{\nabla}\phi, \tag{3.25}$$

$$W_{\pm} = \frac{\hbar^2}{8M}\left[\left(\boldsymbol{\nabla}\theta\right)^2 + \sin^2\theta\left(\boldsymbol{\nabla}\phi\right)^2\right], \tag{3.26}$$

from which the following synthetic magnetic field is obtained

$$\mathbf{B}_{\pm} = \pm\frac{\hbar}{2}\boldsymbol{\nabla}(\cos\theta) \times \boldsymbol{\nabla}\phi. \tag{3.27}$$

Eq. (3.27) shows that a nonzero value for the magnetic field occurs when both the mixing angle θ and the phase of the light field vary in space with non collinear gradients. A spatial dependence for the former can be obtained by either modulating in space the Rabi frequency κ, by choosing an appropriate space profile for the laser intensity, or by varying in space the detuning Δ. This can be accomplished for example by exploiting a space-dependent Zeeman shift of hyperfine levels of the atoms, induced by an inhomogeneous magnetic field [102–104].

3.3.2 Λ-level atomic model

Let us consider a three-level atom, whose relevant internal states are disposed according to the Λ-scheme depicted in Fig. 3.1(b). It is characterized by a two-fold ground subspace, whose states $|g_1\rangle$ and $|g_2\rangle$ are coupled to an excited state $|e\rangle$ by two laser beams, respectively of angular frequencies ω_{f_1} and ω_{f_2}. In the rotating wave approximation, the internal dynamics of the atoms is described by the Hamiltonian

$$\begin{aligned} H'^{\mathrm{RWA}}_{\mathrm{int}} = {} & \hbar\omega_e|e\rangle\langle e| + \hbar\omega_{g_2}|g_2\rangle\langle g_2| \\ & + \frac{\hbar}{2}\left(\kappa_1 e^{-i\omega_{f_1}t}|e\rangle\langle g_1| + \kappa_2 e^{-i\omega_{f_2}t}|e\rangle\langle g_2| + H.c.\right), \end{aligned} \tag{3.28}$$

in which we set the energy of $|g_1\rangle$ equal to zero, and we indicated the Rabi frequencies of the $g_1 - e$ and $g_2 - e$ transitions as κ_1 and κ_2 respectively. We define the detuning of the laser beams with respect to these atomic transitions as $\delta_1 = \omega_e - \omega_{f_1}$ and $\delta_2 = \omega_e - \omega_{g_2} - \omega_{f_2}$, together with their average value $\Delta = (\delta_1 + \delta_2)/2$ and difference $\delta = \delta_1 - \delta_2$. The latter quantity physically represents the detuning of the two-photon (Raman) transition between $|g_1\rangle$ and $|g_2\rangle$. This Hamiltonian can be written in a

time-independent form by applying the unitary transformation

$$\hat{U} = e^{i(\omega_e - \Delta)t}|e\rangle\langle e| + e^{i\delta t/2}|g_1\rangle\langle g_1| + e^{i(\omega_{g_2} - \delta/2)t}|g_2\rangle\langle g_2|. \tag{3.29}$$

In matrix notation, it finally reads as [1]

$$H_{\text{int}} = \frac{\hbar}{2}\begin{pmatrix} -\delta & \kappa_1^* & 0 \\ \kappa_1 & 2\Delta & \kappa_2 \\ 0 & \kappa_2^* & \delta \end{pmatrix}, \tag{3.30}$$

with the basis chosen as $\{|g_1\rangle, |e\rangle, |g_2\rangle\}$. In the case of a perfectly resonant Raman excitation $\delta = 0$, with the lasers symmetrically tuned respect to the $g_1 - e$ and $g_2 - e$ transitions (i.e. $\Delta = 0$), a zero energy dressed state of the atom exists called *dark state*, given by the superposition of the ground states [114]

$$|D\rangle = \left(\kappa_2|g_1\rangle - \kappa_1|g_2\rangle\right)/\kappa, \tag{3.31}$$

with $\kappa = \sqrt{|\kappa_1|^2 + |\kappa_2|^2}$. The other two dressed states have energies $\pm\hbar\kappa/2$ and take the form [114]

$$|\pm\rangle = \left(|B\rangle \pm |e\rangle\right)/\sqrt{2}, \tag{3.32}$$

where $|B\rangle = \left(\kappa_1^*|g_1\rangle + \kappa_2^*|g_2\rangle\right)/\kappa$ is the so-called *bright* state. Considering the atom initially prepared in the $|D\rangle$ state, its adiabatic evolution leads to synthetic vector and scalar potentials having the form $\mathbf{A} = i\hbar\langle D|\boldsymbol{\nabla} D\rangle$ and $W = \hbar^2\left|\langle B|\boldsymbol{\nabla} D\rangle\right|^2/2M$. By comparing the expression of the dark state in Eq. (3.31) with (for example) the $|+\rangle$ state in Eq.(3.24), an analogy between the system here considered and the two-level configuration of the atom can be identified. This analogy can be made explicit by the following identifications between the parameters of the Raman coupling and the mixing angle θ and the laser phase ϕ that characterize the two-level configuration

$$\sqrt{\zeta} \equiv \left|\frac{\kappa_1}{\kappa_2}\right| = -\tan\left(\frac{\theta}{2}\right), \qquad \phi_1 - \phi_2 = \phi. \tag{3.33}$$

The effective magnetic field resulting from the vector potential defined above takes the form [1, 115, 116]

$$\mathbf{B} = \hbar\frac{\boldsymbol{\nabla}\phi \times \boldsymbol{\nabla}\zeta}{(1+\zeta)^2}. \tag{3.34}$$

We thus showed that synthetic vector potentials appear in the projected dynamics of the three-level atom onto its dark state. As this state belongs to the ground

manifold of the internal Hilbert space of the atom, the setup does not suffer of issues related to spontaneous decay of atoms.

It is worth mentioning that a different implementation of synthetic magnetism is also feasible with the Λ-level scheme, which is different from the one presented above. As shown in Capter 8, in the case of a far detuned coupling between the ground and the excited states, the latter can be formally eliminated from the dynamics of the system, which effectively reduces to a two-level problem in the ground subspace. The dressed states of the atom $|\pm\rangle$ introduced in Sec. 3.3.1 are thus combinations of the ground states in this case, and spontaneous atomic decay related issues are avoided.

3.3.3 Experimental overview

We here give a brief overview of the experiments which first led to the observation of synthetic potentials acting on neutral atoms, in the continuum configuration discussed in the previous sections [103, 104]. The setup used is depicted in Fig. 3.2, and is described in the following. It is based on a non-homogeneous detuning for optical Raman transitions between different atomic ground sublevels.

The system is composed of Rb^{87} atoms, prepared in the $F = 1$ hyperfine submanifold, with the Zeeman states $|m_F\rangle$ (with $m_F = 0, \pm 1$) coupled via quasi-resonant Raman (that is two-photon) transitions. An additional, spatially dependent, magnetic field is applied, in order to resolve the degeneracy of the hyperfine levels, splitting the states with $m_F = \pm 1$ with respect to the $m_F = 0$ state. The Raman transitions are driven by two laser beams, respectively with wave vectors $\mathbf{k_1}$ and $\mathbf{k_2}$, which couple states differing in $\Delta m_F = \pm 1$. Since the single photon detuning Δ of the coupling lasers, with respect to the excited state manifold involved in the transition, is much larger compared to the amplitude of the Rabi frequencies $|\kappa_1|$ and $|\kappa_2|$, the excited states of the atoms can be adiabatically eliminated from the dynamics of the system, as discussed in Sec. 8.2.1 of Chap. 8. The effective Hamiltonian, describing the ground submanifold dynamics takes thus the form of Eq. (3.30), with $\Delta = 0$, and κ_1^* and κ_2 replaced by $\kappa \equiv \kappa_1 \kappa_2^* = |\kappa| e^{i\phi}$, with $\phi = \mathbf{k}_d \cdot \mathbf{r}$

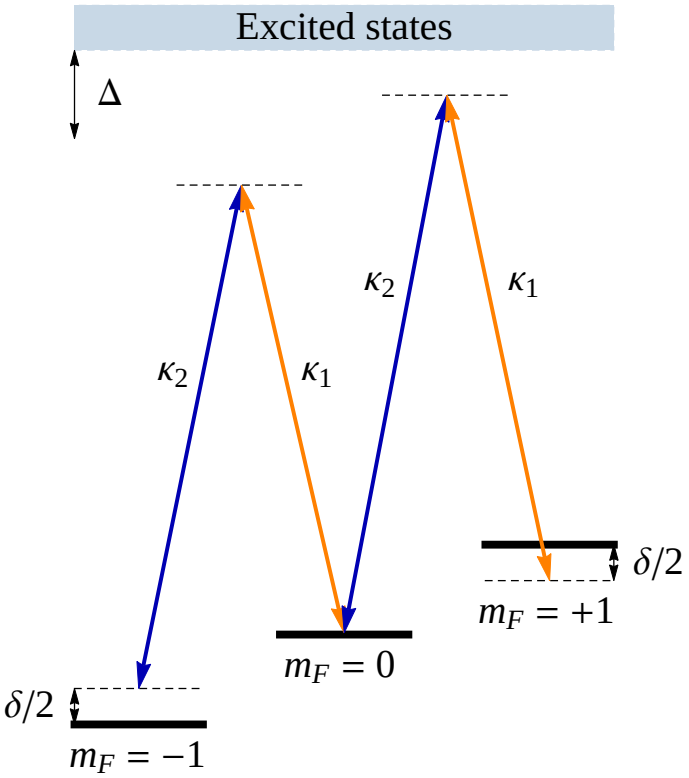

Figure 3.2: Experimental configurations used in [103, 104], and discussed in the text. Note that the frequencies in the picture are not to scale, as $\Delta \gg \delta$ and $\Delta \ll E_e - E_g$ in practice (with E_e and E_g the excited and ground manifold energies).

and $\mathbf{k}_d = \mathbf{k}_1 - \mathbf{k}_2$.

Focusing on the lower energy dressed state

$$|\chi\rangle = e^{i\phi}\cos^2\frac{\theta}{2}|-1\rangle - \frac{\sin\theta}{\sqrt{2}}|0\rangle + e^{-i\phi}\sin^2\frac{\theta}{2}|+1\rangle, \tag{3.35}$$

with $\tan\theta = \sqrt{2}|\kappa|/\delta$, the vector potential takes the form

$$\mathbf{A} = \mathbf{i}\hbar\langle\chi|\boldsymbol{\nabla}\chi\rangle = -\hbar\mathbf{k_d}\cos\theta. \tag{3.36}$$

Eq. (3.36) shows that, as discussed in the previous sections, a non-trivial magnetic field can be created by modulating in space the amplitude of the Rabi frequencies κ_i (with $i = 1, 2$), or using a non-homogeneous Raman detuning δ. In [104], the authors obtained an effective magnetic field acting on the atoms, by using the latter configurations.

3.4 Lattice configuration

As mentioned in the introduction of this chapter, another important branch of the current research on artificial gauge fields is devoted to the study of magnetic effects on charged particles in spatially periodic potentials. The reasons for the interest in studying magnetic phenomena in such a configuration are many. Spatially periodic potentials naturally arise in condensed matter systems, as is the case for example for electrons in the periodic lattice of crystals. The richness of the physics of these systems, compared to the continuum case, is due to the existence of two competing fundamental length scales in the problem, which are the the lattice period a, and the magnetic length $\ell_{\mathrm{mag}} = \sqrt{\hbar/qB}$ (q is here the charge of the particle), which characterizes the cyclotron orbit of a charged particle immersed in the magnetic field B. The ratio between these two length scales can be written in terms of the magnetic flux through the unit cell of the lattice $\Phi = \int_{\mathrm{cell}} \mathbf{B} \cdot d\mathbf{S} = Ba^2$, and the flux quantum $\Phi_0 \equiv h/q$ (with $h = 2\pi\hbar$) as

$$\frac{a^2}{\ell_{\mathrm{mag}}^2} = \frac{qBa^2}{\hbar} = 2\pi\frac{\Phi}{\Phi_0}. \tag{3.37}$$

As long as $\Phi \ll \Phi_0$, the length of the cyclotron orbit is much larger than the lattice spacing, and particles effectively see the periodic potential as a uniform medium. Nothing relevant thus changes in this case, compared to magnetism in free space. On the other hand, when $\Phi \sim \Phi_0$, the competition between the two length scales is at the origin of interesting effects, such as the fractal structure of the single-particle energy spectrum, known in literature as Hofstadter butterfly [117]. Because of the recent technical advances in manipulating cold atoms in optical lattices, discrete systems are well suited for reaching this limit, and thus promising in order to study the quantum Hall physics, and related effects such as the quantization of the conductivity or the topological properties of the energy bands.

3.4.1 General Formalism

We briefly illustrate in the following the general formalism used in order to study magnetism in discrete systems (see [1, 2, 107] for a more detailed review). For simplicity, we consider the case of a two-dimensional square lattice, and limit the

following discussion to the physics of a single band. Assuming particles are able to hop via tunneling into the nearest neighbour lattice sites, with J the corresponding tunnel amplitude, the single-particle dynamics in the absence of magnetic field can be conveniently modelled by the tight-binding Hamiltonian (Hubbard model)

$$\hat{H} = -J \sum_{j,l} \left(|j+1, l\rangle\langle j, l| + |j, l+1\rangle\langle j, l| \right) + \text{h.c.}. \tag{3.38}$$

In Eq. (3.38) we indicated by $|j, l\rangle$ (with $j, l \in \mathbb{Z}$) the state of a particle localized on the lattice site at the position $\mathbf{r} = a\,(j\mathbf{u}_x + l\mathbf{u}_y)$.

As noticed in the previous sections, the effect of a vector potential on the wave function of a charged particle is encoded in the Aharonov-Bohm phase it gains travelling from two different positions, respectively $\mathbf{r}$ and $\mathbf{r}'$, which is equal to

$$\phi\left(\mathbf{r} \to \mathbf{r}'\right) = \frac{q}{\hbar} \int_{\mathbf{r}}^{\mathbf{r}'} \mathbf{A}(\mathbf{r}) \cdot d\mathbf{r}. \tag{3.39}$$

In light of Eq. (3.39), the Hamiltonian in Eq. (3.38) can be generalized in order to take into account the presence of a magnetic field, by assigning a complex term to the tunneling matrix elements. This procedure, that is the substitution of a real hopping amplitude with a complex one, is known in literature as *Peierls substitution* [118, 119], and leads to the single-particle Hamiltonian of the form (Hofstadter model)

$$\hat{H} = -J \sum_{j,l} \left(e^{i\phi_{j,l\to j+1,l}} |j+1, l\rangle\langle j, l| + e^{i\phi_{j,l\to j,l+1}} |j, l+1\rangle\langle j, l| \right) + \text{h.c.}. \tag{3.40}$$

The effect of a magnetic field results thus in the net phase accumulated by a particle traversing the unit cell of the lattice, hereafter called the *plaquette*. Such a phase is given by the sum of the phases gained by the particle, travelling along each side of the unit cell:

$$\frac{q}{\hbar}\Phi_{j,l} = \phi_{j,l\to j+1,l} + \phi_{j+1,l\to j+1,l+1} + \phi_{j+1,l+1\to j,l+1} + \phi_{j,l+1\to j,l}, \tag{3.41}$$

where $\Phi_{j,l}$ is the flux of the magnetic field through the plaquette having the site (j, l) in its lower left corner. The gauge freedom related to the choice of the vector potential in the continuum case is recovered in the discrete system. As the only

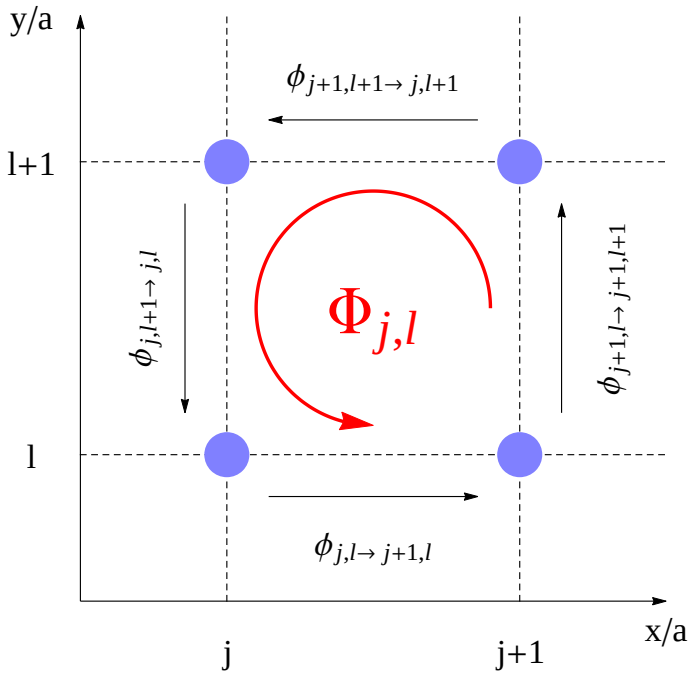

Figure 3.3: Phase accumulated by a particle travelling around the unit cell of a square lattice, in the presence of a non-zero magnetic flux.

gauge invariant quantity is the flux through the plaquette $\Phi_{i,j}$, an infinite number of choices for the phases in Eq. (3.40) (or in Eq. (3.41)) exist, which leads to the same flux per plaquette. These equivalent gauge choices are related to each other by a simple redefinition of the phase of the $|j,l\rangle$ states.

3.4.2 Experimental overview

There are many ways by which complex hopping amplitudes can be engineered in the context of cold atoms in the periodic potential of optical lattices. Such potentials generate a periodic array of trapping sites, linked between each other by quantum tunneling, which arise from the interference pattern of several off-resonant lasers [120, 121]. We list in what follows few of these techniques, and refer the interested reader to the comprehensive reviews [1, 2] for more details.

Rotating system - The simplest technique consists in rotating the lattice [122, 123], and has already been discussed in Chap. 2, in the context of a continuum condensate.

Shaking modulation - Another technique makes use of time-dependent optical po-

tentials, resulting in a rapid shaking of the lattice. By making the period of the temporal modulation of the potential much smaller than the other time scales of the problem, it is possible to separate the dynamics of an effective, time-independent Hamiltonian from the micro-motion induced by the rapid shaking [124–126]. It can be shown [127, 128] that the effective long time scale dynamics of the system shows the appearance of generally complex tunnel amplitudes between lattice sites. This techniques has been implemented experimentally both in one-dimensional [128, 129], and two-dimensional [130–132] systems. In order to solve the problem related to the resulting *staggered* magnetic field, which changes sign between adjacent plaquettes, and thus failing to simulate the physics of charged particles in a constant magnetic field, it is necessary to implement a temporal modulation of the potential, which varies from site to site [133–135].

Laser-assisted tunneling - Laser-assisted tunneling between different internal atomic states is another method that has been exploited in order to engineer complex hopping amplitudes in a lattice. This is achieved by using optical potentials which act differently on atoms in different internal states, say $|g\rangle$ and $|e\rangle$, resulting in the lattice depicted in Fig. 3.4, and using an opportunely tuned laser field in order to induce a transition between them. The hopping between same states $|g\rangle \to |g\rangle$ and $|e\rangle \to |e\rangle$ occurs because of quantum tunneling, and the corresponding transition amplitudes are real. On the other hand, laser induced transitions between different atomic states imprint a phase on hopping amplitude, which becomes complex. Also in this case, the flux induced in the lattice is staggered, and need to be rectified in order to simulate a constant magnetic field. This aim is achieved for example by using counter-propagating laser field driving respectively the transitions $|g\rangle \to |e\rangle$ and $|e\rangle \to |g\rangle$. [136, 137].

3.5 Nonlinear gauge potentials

In the previous sections we have shown that orbital magnetism can be simulated with neutral atoms by exploiting geometric potentials arising from light-matter coupling. These potentials successfully reproduce the physics of charged particles in a static magnetic field, but fail in simulating truly gauge fields, as they do not rep-

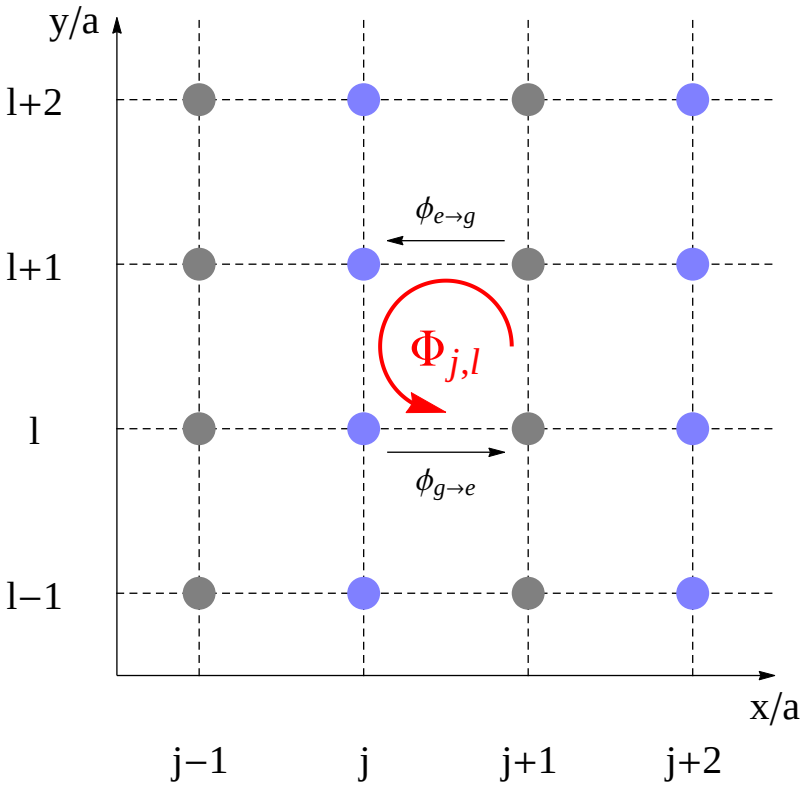

Figure 3.4: Experimental setup used in order to engineer a synthetic field acting on neutral atoms in a lattice configuration, by using laser-assisted transitions between $|g\rangle$ (blue) and $|e\rangle$ (grey) states.

resent dynamical degrees of freedom for the system. In other words, the emerging synthetic potentials do not obey the Maxwell equations or any other field theory, and lack a dynamical coupling with matter fields (that are the atoms in our case). Different proposals exist in literature, aimed to simulate dynamical gauge theories in a lattice geometry [17–22]. and in cavity QED [138–140]. By manipulating ultra-cold atoms in optical lattices, such gauge fields have been shown to emerge as effective low-energy theories from the underlying dynamics. Unfortunately, the complexity involved has so far prevented their experimental realization.

At the basis of any such proposal there is the necessity of introducing a back-reaction mechanism which locally and dynamically couples the effective gauge fields to the atoms. In this perspective, we show in the next section that synthetic potentials explicitly depending on the particle density can be engineered by including inter-particle interactions in the formalism developed so far, as first proposed in [23]. For a lattice version of this concept we refer the reader to the Refs. [141, 142]. Despite

the fact that the resulting nonlinear gauge potentials do not reproduce a truly dynamical gauge theory, they do give rise to interesting physics, with exotic nonlinear dynamics which will be addressed in this thesis.

3.5.1 Artificial gauge fields by interacting atoms

Nonlinear (density-dependent) artificial gauge potentials emerge in cold atoms systems by using collisionally induced detuning in combination with the synthetic magnetism described in the previous sections [23, 143].

For the sake of simplicity and without loss of generality, we use the atomic two-level scheme introduced in Sec. 3.3.1, bearing in mind that analogous arguments equally apply to more complex configurations such as the Λ-scheme discussed in Sec. 3.3.2. Modeling the collisional interactions by an effective zero-range pseudo-potential, the microscopic N-body Hamiltonian of the atomic gas is given by

$$\hat{H}=\sum_{n=1}^{N}\left[\left(\frac{\hat{\mathbf{p}}_n^2}{2m}+V_{\text{ext}}(\mathbf{r}_n)\right)\otimes\mathbb{I}_n+\hat{H}_{\text{int}}(\mathbf{r}_n)\right]\otimes\mathbb{I}_{\mathcal{H}\backslash n}+\sum_{n<j}^{N}G_{n,j}\,\delta\left(\mathbf{r}_n-\mathbf{r}_j\right)\otimes\mathbb{I}_{\mathcal{H}\backslash\{n,j\}},\tag{3.42}$$

where the identity matrices $\mathbb{I}_{\mathcal{H}\backslash\{n,j,...\}}$ act on the subspace excluding the particles $n, j, \ldots$. The first term in Eq. (3.42) is the sum of the single particle, non-interacting Hamiltonians, where the light-atom coupling $\hat{H}_{\text{int}}$ is modelled as in Eq.(3.21). The second term represents the pairwise interaction between the atoms, and takes the diagonal form $G_{n,j}=\text{diag}\left[g_{11},g_{12},g_{12},g_{22}\right]$ in the internal Hilbert space of the interacting particles. The coupling constants g_{ij} are related to the corresponding scattering lengths a_{ij} as $g_{ij}=4\pi\hbar^2a_{ij}/m$.

The dynamics of the system is described by the Lagrangian

$$L=\int\prod_{i=1}^{N}d^3\mathbf{r}_i\left[\mathbf{\Psi}^\dagger\left(i\hbar\partial_t-\hat{H}\right)\mathbf{\Psi}\right],\tag{3.43}$$

where $\mathbf{\Psi}=\mathbf{\Psi}\left(\mathbf{r}_1,\mathbf{r}_2,...\mathbf{r}_N\right)$ is the many-body wave function. We consider the mean field variational ansatz $\mathbf{\Psi}\left(\mathbf{r}_1,\mathbf{r}_2,...\mathbf{r}_N\right)=\prod_{i=1}^{N}\phi\left(\mathbf{r}_i\right)$, which is the symmetrized product of the single particle pseudo-spinor wave function $\boldsymbol{\phi}(\mathbf{r})$, satisfying the normalization condition $\int d^3\mathbf{r}\,\boldsymbol{\phi}^\dagger\boldsymbol{\phi}=1$. By substituting into Eq.(3.43), we obtain

the corresponding mean field Lagrangian for the order parameter of the system $\boldsymbol{\psi}(\mathbf{r}) = \sqrt{N}\boldsymbol{\phi}(\mathbf{r})$ [144]

$$L_{MF} = \int d^3\mathbf{r} \left[\boldsymbol{\psi}^\dagger \left(i\hbar\partial_t - \hat{H}_{MF} \right) \boldsymbol{\psi} \right], \tag{3.44}$$

where we defined the single particle mean field Hamiltonian H_{MF} as

$$\hat{H}_{MF} = \left(\frac{\hat{\mathbf{p}}^2}{2m} + \hat{H}_{\text{int}} + \hat{U}_{MF} + V_{\text{ext}} \right) \otimes \mathbb{I}. \tag{3.45}$$

The operator U_{MF} describes the mean field collisional effects, and is given by

$$\hat{U}_{MF} = \frac{1}{2} \begin{pmatrix} \Delta_1 & 0 \\ 0 & \Delta_2 \end{pmatrix} \tag{3.46}$$

where

$$\Delta_1 = g_{11}n_1 + g_{12}n_2, \tag{3.47}$$

$$\Delta_2 = g_{12}n_1 + g_{22}n_2, \tag{3.48}$$

and $n_i = |\psi_i|^2$ is the density of atoms in the ith internal state ($i = 1, 2$) and ψ_i the corresponding component of the order parameter. By comparing Eq. (3.45) with Eq. (3.21), we see that Δ_1 and Δ_2 can be regarded as effective detunings, induced by the collisional shift of the energy levels. In view of this result it follows that the potentials $\mathbf{A}_\pm$ and $\mathbf{W}_\pm$ in Eqs. (3.25) and (3.26) gain a density dependence.

Working in the weakly interacting limit, the strength $\hbar\Omega_r$ of the coherent coupling between the ground and the excited states is typically much larger than the mean field energy shifts. This allows us to diagonalize the Hamiltonian in Eq. (3.45) by treating the mean field interaction as a small perturbation with respect to the atom-field interaction. To order $\mathcal{O}(\Delta_d/\hbar\Omega_r)$, the eigenstates of eq. (3.45) take the form

$$|\psi_\pm\rangle = |\pm\rangle \pm \frac{\Delta_d}{\hbar\Omega_r}|\mp\rangle, \tag{3.49}$$

with the corresponding energies $E_\pm = \pm\hbar\Omega_r/2 + \Delta_\pm$. Here we defined

$$\Delta_d \equiv \langle \pm | \, U_{MF} \, | \mp \rangle = \frac{1}{2} \sin \frac{\theta}{2} \cos \frac{\theta}{2} (\Delta_1 - \Delta_2), \tag{3.50}$$

$$\Delta_+ \equiv \langle + | \, U_{MF} \, | + \rangle = \frac{1}{2} \left(\Delta_1 \cos^2 \frac{\theta}{2} + \Delta_2 \sin^2 \frac{\theta}{2} \right), \tag{3.51}$$

$$\Delta_- \equiv \langle - | \, U_{MF} \, | - \rangle = \frac{1}{2} \left(\Delta_1 \sin^2 \frac{\theta}{2} + \Delta_2 \cos^2 \frac{\theta}{2} \right), \tag{3.52}$$

where $\{|+\rangle, |-\rangle\}$ are the dressed states of the atoms in Eq. (3.24).

We retrace the arguments in Sec. 3.2 and expand the condensate wave function $|\psi(\mathbf{r}, t)\rangle$ in terms of the *interacting* dressed state basis in Eq.(3.49), as $|\psi(\mathbf{r}, t)\rangle = \sum_{i=\{+,-\}} \psi_i(\mathbf{r}, t)|\psi_i\rangle$. In order to capture the dynamics of the $\pm$ component of the condensate we use the adiabatic assumption, according to which $\psi_\mp(\mathbf{r}, t) \equiv 0$, and we consider the projection of the mean field Lagrangian in eq.(3.44) onto the subspace spanned by $|\psi_\pm\rangle$. The space dependence of the atoms-field interaction, together with the assumption of adiabatic motion, is responsible for the appearance of geometrical gauge potentials in the effective Lagrangian for the projected dynamics of the system, having the form

$$\mathbf{A}_\pm = - \langle \psi_\pm | \, \mathbf{p} \, | \psi_\pm \rangle = \mathbf{A}_{\pm,0} + \mathbf{A}_{\pm,1}, \tag{3.53}$$

$$2mW_\pm = | \, \langle \psi_+ | \, \mathbf{p} \, | \psi_- \rangle \, |^2 = 2m \left(W_{\pm,0} + W_{\pm,1} \right), \tag{3.54}$$

As expected, these are the sum of the zeroth order terms

$$\mathbf{A}_{\pm,0} = -\frac{\hbar}{2} \left(1 \mp \cos\theta \right) \boldsymbol{\nabla} \phi, \qquad 2mW_{\pm,0} = \frac{\hbar^2}{4} (\boldsymbol{\nabla}\theta)^2 + \frac{\hbar^2}{4} \sin^2\theta (\boldsymbol{\nabla}\phi)^2, \tag{3.55}$$

that are the single particle contribution in Eqs. (3.25) and (3.26), and the first order terms

$$\mathbf{A}_{\pm,1} = \pm n_\pm \mathbf{A}_1, \qquad 2mW_{\pm,1} = \frac{\hbar f_\pm}{8\Omega_r} n_\pm \cos\theta (\boldsymbol{\nabla}\phi)^2 - \hbar \boldsymbol{\nabla}\theta \cdot \boldsymbol{\nabla} \left(\frac{\Delta_d}{\Omega_r} \right), \tag{3.56}$$

which account for the meanfield collisional effects, and explicitly depends on the

particle density. Here we defined $\mathbf{A}_1 = f_\pm \left(\boldsymbol{\nabla}\phi\right)/8\Omega_r$, along with

$$\begin{aligned} f_+ &= \frac{8\Delta_d}{n_+}\sin\theta \\ &= 2\sin^2\theta\left[\cos^2\frac{\theta}{2}g_{11} + g_{12}\left(\sin^2\frac{\theta}{2} - \cos^2\frac{\theta}{2}\right) - g_{22}\sin^2\frac{\theta}{2}\right], \end{aligned} \tag{3.57}$$

$$\begin{aligned} f_- &= \frac{8\Delta_d}{n_-}\sin\theta \\ &= -f_+(1 \leftrightarrow 2). \end{aligned} \tag{3.58}$$

The mean field Lagrangian for the relevant condensate component takes thus the form (to order $\mathcal{O}(\Delta_d/\hbar\Omega_r)$)

$$L_\pm = \int d^3\mathbf{r}\left[\psi_\pm^*\left(i\hbar\partial_t - \hat{H}_\pm\right)\psi_\pm\right] \tag{3.59}$$

where

$$\hat{H}_\pm = \frac{\left(\mathbf{p} - \mathbf{A}_\pm\right)^2}{2m} + W_\pm \pm \frac{\hbar\Omega_r}{2} + \Delta_\pm + V_{\text{ext}}\left(\mathbf{r}\right) \tag{3.60}$$

is the Hamiltonian describing the dynamics of the $\pm$ component of the condensate. The Gross-Pitaevskii equation for the order parameter of the $\pm$ component is finally obtained by minimizing the Lagrangian in Eq. (3.59) with respect to variations in $\psi_\pm^*$, and takes the form

$$\begin{aligned} i\hbar\frac{\partial\psi_\pm}{\partial t} = &\left[\frac{\left(\mathbf{p} - \mathbf{A}_\pm\right)^2}{2m} + W_\pm + V(\mathbf{r}) \pm \frac{\hbar\Omega_r}{2} + 2\Delta_\pm \pm \mathbf{A}_1\cdot\mathbf{j}\right]\psi_\pm \\ &+ \left[n_\pm\left(\frac{\partial W_\pm}{\partial\psi_\pm^*} - \boldsymbol{\nabla}\cdot\frac{\partial W_\pm}{\partial\boldsymbol{\nabla}\psi_\pm^*}\right) - \frac{\partial W_\pm}{\partial\boldsymbol{\nabla}\psi_\pm^*}\cdot\boldsymbol{\nabla}n_\pm\right]. \end{aligned} \tag{3.61}$$

Eq. (3.61) is the central result of this section. It shows that new terms appear, governing the dynamics of the condensate, because of the nonlinear nature of the synthetic potentials. Of particular relevance for the work discussed in the thesis is the exotic current nonlinearity ($\pm\mathbf{A}_1\cdot\mathbf{j}$) induced by the density-dependent vector potential. Because of the presence of the vector potential, the current density is here defined as

$$\mathbf{j} = \frac{\hbar}{2mi}\left[\psi_\pm\left(\boldsymbol{\nabla} + \frac{i}{\hbar}\mathbf{A}_\pm\right)\psi_\pm^* - \psi_\pm^*\left(\boldsymbol{\nabla} - \frac{i}{\hbar}\mathbf{A}_\pm\right)\psi_\pm\right]. \tag{3.62}$$

Eq. (3.61) gives rise to novel physics in a BEC, whose investigation in specific physical situations will be the topic of the following chapters. Of particular interest is the fact that, because of the presence of the current nonlinearity, the system acquires

chiral properties. As a result, i) the effective meanfield coupling constant turns out to be stronger or weaker depending on the mutual direction of propagation between the condensate and the vector potential. ii) The dynamics of excitations such as wave packet shows a preferred direction, as well as the stability properties of solitons [23] and vortices, as is shown in the next chapter.

Part II – Rotating BECs and nonlinear synthetic magnetism

Chapter 4 Density induced vortex ground state

In this chapter we discuss how the nonlinear synthetic gauge potentials introduced in Chap. 3 affect the physics of a rotating condensate.

The discussion is based on [Butera et al. *J. Phys. B.*, **49**, 015304 (2016)] and is devoted to the study of the stability properties of a vortex state. We focus in particular on the physical conditions that make the existence of vortices energetically favorable with respect to the non-rotating state. We consider an effectively two-dimensional condensate in the Thomas-Fermi limit. We show that, as in the standard case of a constant magnetic field, the effect of the density-dependent gauge potential is to induce a rotation to the condensate. The main difference here is that the onset of vorticity depends on the number of particles that are in the condensate: the higher the particle density the more likely it is to have vortices. This condition is achieved by choosing suitable spatial profiles for the light-atom interaction parameters, such that the current nonlinearity in Eq. (3.61) leads to an exotic nonlinear term in the Gross-Pitaevskii equation, which is proportional to the angular momentum of the condensate. Its effect is to break the rotational invariance of the system, enhancing or weakening the effective interaction felt by the atoms, depending on the direction of rotation of the condensate.

4.1 Rotation-induced nonlinearity

We show in this section that by properly designing the spatial profile of the atom-light interaction parameters, a rotation-induced nonlinearity appears in the GP equation for the order parameter of the system. It is worth stressing that the specific configuration we present here is one among several by which in principle the same effect can be induced. Without loss of generality, we use the two-level formalism

introduced in Chap. 3 and choose to work with the + component of the condensate. An inspection of the definitions in Eqs. (3.53), (3.57) and (3.58) reveals that the same physics could be obtained working with the − component of the condensate, provided we change the sign of the detuning, which is proportional to $g_{11} - g_{22}$.

We work in the symmetric gauge, in which the magnitude of the zeroth order term of the vector potential in Eq. (3.53) is proportional to the radial distance from the minimum of the external potential trapping the cloud, which we assume to be harmonic and axially-symmetric along the z direction. The corresponding magnetic field is therefore constant. Its effect can be compensated by opportunely rotating the experimental apparatus. To this aim we make the assumption $|\kappa|/\Delta \equiv \epsilon \ll 1$, according to which Eqs. (3.22) and (3.57) can be expanded, to order $\mathcal{O}(\epsilon^2)$, as

$$\sin\theta = \theta = \epsilon, \tag{4.1}$$

$$\cos\theta = \left(1 - \frac{\epsilon^2}{2}\right), \tag{4.2}$$

and

$$\frac{f_+}{8\Gamma} = \epsilon^2 \frac{\gamma_{12}}{\Delta}, \tag{4.3}$$

in which we defined the combination of the mean field coupling constants $\gamma_{12} = (g_{11} - g_{12})/4$. Given the Eqs. (4.1)-(4.3), and omitting the subscript "+" in what follows, the effective vector and scalar potentials in Eqs. (3.53) and (3.54) take the form

$$\mathbf{A} = \mathbf{A}_0 [1 - 4\varepsilon], \tag{4.4}$$

$$2mW = 2mW_0^1 [1 - 4\varepsilon] + 2mW_0^2 [1 + 4\varepsilon] - \frac{\hbar^2}{2} \left(\boldsymbol{\nabla}\epsilon^2\right) \cdot (\boldsymbol{\nabla}\varepsilon), \tag{4.5}$$

where $\varepsilon = n\gamma_{12}/\hbar\Delta$ is the coherent versus collisional interaction perturbative parameter, while $\mathbf{A}_0 = -(\hbar/4)\,\epsilon^2 \boldsymbol{\nabla}\phi$, $W_0^1 = (\hbar^2/8m)\,(\boldsymbol{\nabla}\epsilon)^2$ and $W_0^2 = (\hbar^2/8m)\,\epsilon^2 (\boldsymbol{\nabla}\phi)^2$ are the single particle components of the vector and scalar potentials, respectively.

We consider a laser beam, with a phase proportional to the polar angle φ as $\phi = \ell\varphi$, where ℓ is the quantum number identifying the orbital angular momentum $\hbar\ell$ carried by the electromagnetic field. We choose the space profile $\epsilon = \epsilon_0 r$ for the perturbative parameter (with ϵ_0 constant), which can be obtained by making the intensity profile

of the coupling field linearly growing in the radial direction, and keeping the detuning Δ constant in space. This is valid in a limited region, restricted by the condition $\epsilon \ll 1$, that can be selected by properly choosing the value of ϵ_0.

Given the expressions in Eqs. (4.4) and (4.5) for the vector and scalar potentials, together with

$$\frac{\hbar\Omega_r}{2} = \frac{\hbar\Delta}{2}\left(1 + \frac{\epsilon^2}{2}\right), \tag{4.6}$$

$$2\Delta_+ = g_{11}n - 2\epsilon^2\gamma_{12}n, \tag{4.7}$$

derived from Eqs. (3.22) and (3.51) to order $\mathcal{O}(\epsilon^2)$, the Gross-Pitaevskii equation Eq. (3.61) takes, after lengthy calculations, the form:

$$i\hbar\frac{\partial\psi}{\partial t} = \left[-\frac{\hbar^2}{2m}\boldsymbol{\nabla}^2 - \Omega_\ell L_z + V_{\text{ext}}(\mathbf{r})\right]\psi + \left[g_{11}n - 2\Omega_\ell\varepsilon\left\{(\hbar\ell)\left(2 - \frac{1}{\ell^2}\right) - 4L_z\right\}\right]\psi, \tag{4.8}$$

where $\Omega_\ell = -(\epsilon_0^2/4m)(\hbar\ell)$ and $L_z = -i\hbar\partial/\partial\varphi$ is the z-component of the angular momentum operator, which is in the direction of the axis of symmetry of the external potential.

As expected, the zeroth order term of the vector potential in Eq. (4.4) results in the linear term in the first bracket of Eq. (4.8) which is proportional to the angular momentum operator. It describes the dynamics of a particle in the reference frame rotating with the effective angular velocity Ω_ℓ, when the trapping potential $V_{\text{ext}}(\mathbf{r})$ rotates with the same velocity. Equivalently, it describes the dynamics of a particle of unit charge, in the constant magnetic field $B = 2m\Omega_\ell$. The effects of this term on the physical properties of a condensate have been widely studied in the literature and are nowadays well understood [145]. More interesting is the nonlinear term in the second bracket of Eq. (4.8). It consists of the standard mean field interaction term, with the effective coupling constant $g_{\text{eff}} = g_{11} + g_\ell$, where $g_\ell \equiv -2\Omega_\ell(\varepsilon/n)(\hbar\ell)(2 - 1/\ell^2)$, plus the sought nonlinear term proportional to the orbital angular momentum L_z operator.

In order to study the role of the nonlinear term, we envisage a situation where

the effects of this term are isolated with respect to the ones which originate from the standard linear term, for instance by rotating the system with angular velocity $\Omega = -\Omega_\ell$. This might be experimentally challenging [102] but realizable in principle with existing techniques used for creating dynamical and rotating optical lattices [122, 123], and allows us to focus on the effect of the density dependent gauge potential only. In such conditions, the resulting Gross-Pitaevskii equation, takes the final form

$$i\hbar\frac{\partial\psi}{\partial t} = \left[-\frac{\hbar^2}{2m}\boldsymbol{\nabla}^2 - nC_\ell L_z + V_{\rm ext}\left(\mathbf{r}\right) + g_{\rm eff}n\right]\psi, \tag{4.9}$$

where we have labelled the experimental parameters collectively as $C_\ell = -8\Omega_\ell(\varepsilon/n)$.

4.2 Vortex ground state

In this section we investigate the rotational properties of a condensate, whose dynamics is described by the GP equation (4.9). We focus in particular on the physical conditions that make the nucleation of vortices in the condensate energetically favourable with respect to the corresponding non-rotating state. In order to extract the novel physics arising from the new nonlinearity, we consider the case of a vortex state carrying a single quantum of circulation. We carry out the analysis by looking at the nonlinear angular momentum term from two different perspectives: i) We interpret this term first as an effective, density modulated, angular velocity imprinted to the system, and look for the critical value $C_{\ell,\rm cr}$ which makes a vortex state of the condensate energetically favoured with respect to the non-rotating solution. ii) From a different point of view, we interpret the new nonlinearity as a modification of the mean field coupling constant, whose value depends on the local action of the angular momentum operator.

In the standard case of a rotating condensate, we showed in Chapter 2 that a vortex state becomes energetically favourable when its energy $E_v' = E_v - \Omega\langle L_z\rangle$, in the reference frame co-rotating with the trapping potential, is lower than the energy of the non-rotating state. For a cylindrical TF cloud, this yields the critical value for the angular velocity $\Omega_{\rm cr} = (2\hbar/mR_\perp^2)\log(0.888R_\perp/\xi_0)$ in Eq.(2.71), where $R_\perp = \sqrt{2\mu/m\omega_\perp^2}$ is the TF radius of the cloud with the harmonic potential of frequency

$\omega_\perp$, μ is the chemical potential of the system, related to the number of particles as in Eq. (4.13), and ξ_0 is the healing length in the center of the trap. In the same spirit, we can calculate the critical value $C_{\ell,\mathrm{cr}}$. Because of the nonlinear term, the energy is more appropriately calculated in terms of the energy functional from which the GP Eq.(4.9) originates. Written as an energy per unit length along the z direction, the energy has the form

$$\epsilon = \int d\mathbf{r}_\perp \psi^* \left[-\frac{\hbar^2}{2m}\boldsymbol{\nabla}^2 - \frac{C_\ell}{2} n L_z + \frac{g_{\mathrm{eff}}}{2} n \right] \psi. \tag{4.10}$$

The critical value $C_{\ell,\mathrm{cr}}$ is readily calculated by posing

$$\epsilon'_v = \epsilon_v - \frac{C_{\ell,\mathrm{cr}}}{2} \int d\mathbf{r}_\perp \, \psi^* n L_z \psi = 0. \tag{4.11}$$

Given Eq.(2.62) and using the TF density profile $n(r_\perp) = n(0)\,(1 - r_\perp^2/R_\perp^2)$, we get

$$C_{\ell,\mathrm{cr}} = 3\frac{\Omega_{\mathrm{cr}}}{n(0)}. \tag{4.12}$$

The same result can be obtained by looking at the new nonlinearity as a modification of the mean-field coupling constant. By substituting the expression $\psi(\mathbf{r}) = f(r_\perp)e^{i\varphi}$, characterizing the order parameter of a vortex state with angular momentum per particle equal to $\hbar$, in the GP equation (4.9) (or in the energy functional (4.10)), we obtain an equation for the amplitude $f(r_\perp)$, in which the effective mean field coupling constant $g'_{\mathrm{eff}} = g_{\mathrm{eff}} - \hbar C_\ell$ appears. It gets stronger or weaker depending both on the sign of the coefficient C_ℓ, and of the angular momentum of the cloud, and changes the energy scale of the system and the values of physical quantities such as the healing length. In the case in which $g'_{\mathrm{eff}} < g_{\mathrm{eff}}$, and the shift in the chemical potential is larger than the energy ϵ_v of the vortex, the rotating state becomes energetically favourable compared to the non rotating solution (see fig. 4.1).

In order to find the critical value $C_{\ell,\mathrm{cr}}$ for which this happens, we need to calculate first the shift in the chemical potential induced by a modification of the mean field coupling constant. To this aim we note that for the effectively two-dimensional TF condensate here considered, the chemical potential is related to the total number of

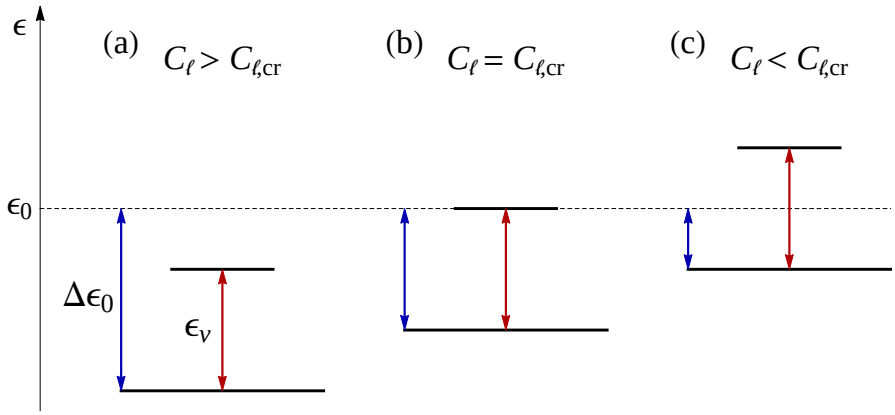

Figure 4.1: Illustration of the conditions for the onset of vorticity in the condensate, in the presence of the angular momentum nonlinearity discussed in the text. The solid long and short lines identify the energy of the non rotating and of the vortex state, respectively. The energy level ϵ_0 refers to the non-rotating state of the condensate when the laser field is not acting on the atoms. (a) When the redefined meanfield coupling constant $g' \to g - \hbar C_\ell$ induces a shift $\Delta\epsilon_0$ of the non-rotating state energy ϵ_0 which is larger than the energy ϵ_v of the vortex, then the rotating state becomes energetically favorable compared to the non rotating one. (b) When the energy ϵ_v of the vortex equates the energy shift $\Delta\epsilon_0$, the parameter C_ℓ attains its critical value. In the case (c), the energy of the vortex state is lowered by the angular momentum non linearity, but the non-rotating state of the condensate is still the lowest energy state.

particles per unit length ν by

$$\mu = \left(\frac{m\omega_0^2 g}{\pi}\right)^{1/2} \nu^{1/2}, \tag{4.13}$$

where we indicated by g the generic meanfield coupling constant. Since by definition $\mu = \partial\epsilon/\partial\nu$, the energy of the system per unit length is equal to

$$\epsilon(\nu) = \int_0^\nu d\nu' \mu(\nu') = \frac{2}{3}\mu\nu. \tag{4.14}$$

Given Eq. (4.14), the energy difference $\Delta\epsilon$ between the non-rotating states corresponding respectively to the values $g' = g + \Delta g$ and g is equal to

$$\Delta\epsilon = \frac{2}{3}\Delta\mu\nu = \frac{1}{3}\nu\mu\frac{\Delta g}{g}. \tag{4.15}$$

Equating the absolute value $|\Delta\epsilon|$ of this quantity with the energy ϵ_v of the vortex state in Eq. (2.62), given $|\Delta g| = \hbar C_\ell$ in our case, we obtain the same results as in Eq. (4.12) for the critical value $C_{\ell,\mathrm{cr}}$.

Both the interpretations discussed for the angular momentum nonlinearity, confirm the result that the critical condition for the rotating state being lower in energy than the non-rotating one, now depends on the particle number. Given Eq. (4.12) and the definition for C_ℓ reported above, a vortex ground state appears when

$$\gamma_{12} n(0) \geq \frac{3(\hbar\Delta)}{\ell \epsilon^2(R_\perp)} \log\left(0.888 \frac{R_\perp}{\xi_0}\right), \tag{4.16}$$

where the equality holds at the critical condition. In Eq. (4.16), $\epsilon(R_\perp) = \epsilon_0 R_\perp$ is the value of the perturbative parameter at the radial distance equal to the TF radius. Note that, as discussed in Chap. 3, for the adiabatic assumption of the atomic motion to be valid, the condition $\rho g_{ij} \ll \hbar\Delta$ $(i, j = 1, 2)$ has to be satisfied in the present case. In view of Eq. (4.16), this represents a limit for attaining the density induced vortex ground state. This condition is an intrinsic limit of the density-dependent gauge potentials, which arise as a first order effect of the interatomic collisions. Moreover, the presence of the perturbative parameter ϵ, in the denominator of the RHS of Eq. (4.16) make things even worse. The parameter we need to play with, in order to attain the critical conditions, is the quantum number ℓ of the orbital angular momentum per atom. In principle there is no theoretical upper limit on how many quanta a single photon can carry, its value is restricted by technological limitations. By using Spatial Light Modulators (SLM) with full HD (1920×1080) resolution, a Laguerre-Gauss mode with value of ℓ of the order of few hundreds can be achieved, before a reduction in the mode transformation efficiency occurs, due to the finite resolution of the SLM mask [146]. However, with a value $\epsilon(R) = 0.1$, which guarantees the fulfilment of the perturbative condition throughout the cloud, this unfortunately is not sufficient. Higher values for ℓ, typically of the order of ~ 1000, can be obtained by using higher resolution SLM, or spiral phase mirrors [147]. Such values of ℓ would be already enough for Eq. (4.16) to be satisfied, together with the condition that the light-atom coupling energy exceeds the atomic collisions energy. However, values of ℓ up to 10000 are in principle achievable by using more extreme optical techniques [148].

Chapter 5 Vortex dynamics with nonlinear gauge potentials

Based on [Butera et al. *New J. Phys.*, **18**, 085001 (2016)], we develop in this chapter a Lagrangian theory aimed at determining the dynamics of a vortex in a Bose-Einstein condensate, subject to a nonlinear gauge potential. By using a variational approach, we obtain the equation of motion for the vortex core, which shows the appearance of a force due to the action of the vector potential. Because of the nonlinear nature of the potential, such a force explicitly depends on the particle density in the system.

5.1 Lagrangian for the vortex core

The effective Lagrangian for the vortex core is obtained directly from the Lagrangian density of the superfluid, which is the integrand in Eq. (3.59). We choose to work with the simplest possible setup, consisting of a cloud of two-level atoms illuminated by a monochromatic laser beam with wavevector $\mathbf{k}$, whose phase varies in space as $\phi = \mathbf{k} \cdot \mathbf{r}$. We consider a symmetric atom-light interaction, characterized by the mixing angle $\theta = \pi/2$, as defined in Eq. (3.22). With these choices, the vector and scalar potentials, defined respectively in Eq.(3.53) and (3.54), take the form

$$\mathbf{A}_\pm = \mathbf{A}_0 \pm n_\pm \mathbf{A}_1, \tag{5.1}$$

$$2mW_\pm = \frac{\hbar^2 k^2}{4}, \tag{5.2}$$

where we defined $\mathbf{A}_0 = -\hbar\mathbf{k}/2$, $\mathbf{A}_1 = (g_{11} - g_{22})\mathbf{k}/(8\Omega_r)$. Using the Madelung representation for the order parameter $\psi_\pm \equiv \sqrt{n_\pm}\, e^{iS}$, the Lagrangian can be written

as

$$\begin{aligned}\mathcal{L} = &-\hbar n_\pm \frac{\partial S}{\partial t} - \frac{\hbar^2}{2m}\left(\boldsymbol{\nabla}\sqrt{n_\pm}\right)^2 - \frac{\hbar^2}{2m} n_\pm \left(\boldsymbol{\nabla} S\right)^2 + \frac{\hbar}{m} n_\pm \left(\mathbf{A}_\pm \cdot \boldsymbol{\nabla} S\right) \\ &- n_\pm \left(\frac{\mathbf{A}_\pm^2}{2m} + W_\pm \pm \frac{\hbar\Omega_r}{2} + \frac{g}{2}\right),\end{aligned} \tag{5.3}$$

where $g \equiv \Delta_\pm = \left(g_{11} + g_{22} + 2g_{12}\right)/4$ in the present configuration. In Eq (5.1), the single particle component $\mathbf{A}_0$ of the vector potential is constant and gives no contribution to the effective magnetic field felt by the atoms. Because of this reason it can be gauged away by the unitary transformation $\psi \to \exp\left(i\mathbf{A}_0 \cdot \mathbf{r}/\hbar\right)\psi$. Having performed this transformation, the Lagrangian in Eq. (5.3) keeps the same form with $\mathbf{A}_\pm = \pm n\mathbf{A}_1$. Here we dropped the subscript from the density, which is now indicated as n for brevity, and we will do the same for the other relevant physical quantities in the following. The transformation given above for the order parameter can be interpreted as just another way to split the physical velocity in the system between the contributions due to the vector potential and the phase S of the order parameter. In the presence of a vector potential $\mathbf{A}$, the physical velocity $\mathbf{u}$ has in fact the form:

$$m\mathbf{u} = \hbar\boldsymbol{\nabla} S - \mathbf{A}. \tag{5.4}$$

In our case, given the vector potential in Eq. (5.1), it can be written as

$$\begin{aligned} m\mathbf{u} &= \hbar\boldsymbol{\nabla} S - \left(\mathbf{A}_0 \pm n\mathbf{A}_1\right) \\ &= \left(\hbar\boldsymbol{\nabla} S - \mathbf{A}_0\right) \mp n\mathbf{A}_1, \end{aligned} \tag{5.5}$$

where the first line shows the splitting before, while the second line after the gauge transformation has been performed.

In order to study the dynamics of the vortex, it is convenient to consider the cloud having an effective thickness Z in the z-direction. The original condensate wave function can then be rescaled as $\psi(\mathbf{r}) \to \psi(\mathbf{r})/\sqrt{Z}$, where $\psi(\mathbf{r})$ is now two-dimensional, and normalised in such a way that $\int d\mathbf{r}\,|\psi|^2 = N$, with N the number of atoms in the condensate. Eq. (5.3) keeps the same form after this dimensional reduction, with n intended now as the effective two dimensional density, and the interaction parameters rescaled as $g \to g/Z$ and $\mathbf{A}_1 \to \mathbf{A}_1/Z$.

Since we are interested in the dynamics of a vortex state, we pose the ansatz ac-

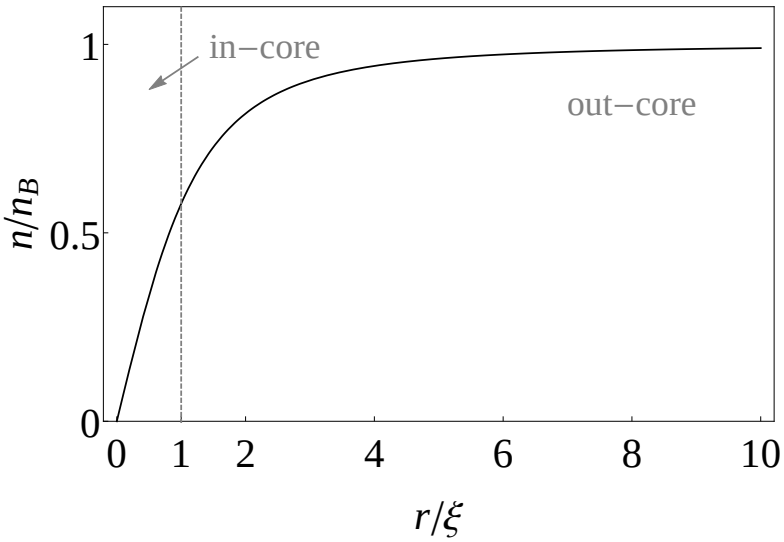

Figure 5.1: Density profile $n/n_B(x) = x/\sqrt{2+x^2}$ of a single quantized vortex state. The *in*-core and *out*-core regions are indicated.

cording to which $n = n_0(\mathbf{r} - \mathbf{r}_0(t))$, where $n_0(\mathbf{r})$ is the density profile of a vortex state, and $\mathbf{r}_0$ the position of the core. The latter depends on time in general and we define its velocity $\mathbf{v} \equiv d\mathbf{r}_0/dt$. We assume that the vortex carries a single quantum of circulation for simplicity, and write the phase of the condensate as $S = S_0 + S_v$, with $\hbar\boldsymbol{\nabla} S_0/m = \mathbf{u}_0(\mathbf{r} - \mathbf{r}_0)$ and $\mathbf{u}_0(\mathbf{r}) \equiv \boldsymbol{\kappa} \times \mathbf{r}/(2\pi r^2)$ the velocity field induced by the vortex. Here $\boldsymbol{\kappa} \equiv \kappa\,\hat{\mathbf{e}}_z$ is the circulation vector and $\kappa = |\boldsymbol{\kappa}| = h/m$ is the quantum of circulation. The term S_v represents the perturbation in the phase due to the core motion and has to be determined. Given the expression in Eq. (5.5) for the local velocity $\mathbf{u}$, and the definition of the current density $\mathbf{j} = n\mathbf{u}$, the continuity equation (2.17), yields

$$\nabla n \cdot (\hbar\nabla S_v - \mathbf{A} - m\mathbf{v}) + n\left(\hbar\boldsymbol{\nabla}^2 S_v - \nabla\cdot\mathbf{A}\right) = 0. \tag{5.6}$$

In order to derive Eq. (5.6) we used $\nabla n \cdot \nabla S_0 \equiv \nabla n_0 \cdot \nabla S_0 = 0$ and $\boldsymbol{\nabla}^2 S_0 = 0$. Assuming that the vortex motion induces a uniform field ∇S_v, Eq. (5.6) reduces to

$$\nabla n \cdot (\hbar\nabla S_v - m\mathbf{v} \pm 2n\mathbf{A}_1) = 0. \tag{5.7}$$

The Eq. (5.7) can be solved approximately, by dividing the domain of the solution in the so-called *in-core* and *out-core* region, depicted in Fig. 5.1. The extension of the former is of the order of the healing length ξ and is characterized by a density, which goes to zero for $r \to 0$, because of the centrifugal potential, and by a non-zero value

of its gradient. As a consequence we pose in this region $(\nabla n)_{\rm in} \neq 0$ and $n_{\rm in} \approx 0$. The out-core region instead is characterized by values of the physical quantities that are close to the ones corresponding to the bulk of the system, i.e. a constant and finite density, and a zero value for its gradient. We thus pose in this region $(\nabla n)_{\rm out} \approx 0$ and $n_{\rm out} \neq 0$. Given this distinction, Eq. (5.7) can be solved in the two different regions, yielding

$$\hbar \nabla S_v = m\mathbf{v} \qquad \textit{in}\text{-core}, \tag{5.8}$$

$$\hbar \nabla S_v = 0 \qquad \textit{out}\text{-core}. \tag{5.9}$$

The result in Eq. (5.8) follows straightforwardly from Eq. (5.7), while Eq. (5.9) has been chosen in order to satisfy the boundary conditions according to which the velocity field at infinity is not affected by the vortex motion.

Because of the domain distinction introduced above, it is useful to rewrite all the terms in Eq. (5.3) of the type $nf\left(\boldsymbol{\nabla} S\right)$, with $f\left(\boldsymbol{\nabla} S\right)$ any function of the phase gradient, as $\left(n - n_B\right) f\left(\boldsymbol{\nabla} S\right) + n_B f\left(\boldsymbol{\nabla} S\right)$. In this expression $n_B \equiv \lim_{r\to\infty} n(r)$ is the bulk density far from the vortex core. Following the discussion above, the term proportional to $(n - n_B)$ can be assumed different from zero within the in-core region only and, given Eq. (5.8), we can evaluate the generic function $f\left(\boldsymbol{\nabla} S\right)$ by substituting the expression $\hbar \boldsymbol{\nabla} S = m\mathbf{u}_0 + m\mathbf{v}$ for the phase gradient [149].

Considering that the phase in the condensate depends on time through the core position, we have $dS/dt = -\nabla S_0 \cdot \mathbf{v}$ and the Lagrangian density can be written in the form

$$\begin{aligned}\mathcal{L} = {} & \frac{m}{2}\left(n_0 - n_B\right) v^2 + \left[m n_B \mathbf{u}_0 + \left(n_0 - n_B\right)\mathbf{A}\right] \cdot \mathbf{v} + n_0\, \mathbf{A} \cdot \mathbf{u}_0 \\ & - \left[\frac{\hbar^2}{2m}\left(\boldsymbol{\nabla}\sqrt{n}\right)^2 + \frac{m}{2}\left(n_0 - n_B\right)\mathbf{u}_0^2 + \frac{m}{2} n_B \mathbf{u}_0^2 + n_0\left(\frac{\mathbf{A}^2}{2m} + W \pm \frac{\hbar\Omega_r}{2} + \frac{g}{2} n_0\right)\right].\end{aligned} \tag{5.10}$$

Integrating Eq. (5.10) in space we get the effective Lagrangian describing the motion of the vortex core, which is given by

$$L_v = \int d^2\mathbf{r}\, \mathcal{L} = \frac{M_v}{2} v^2 + \mathbf{A}_v \cdot \mathbf{v} - (U_0 + U_v). \tag{5.11}$$

Here we defined the effective vortex mass M_v, together with the effective vector potential $\mathbf{A}_v$ and scalar potentials U_0 and U_v:

$$M_v = m \int d\mathbf{r}\,(n_0 - n_B), \tag{5.12a}$$

$$\mathbf{A}_v = \int d\mathbf{r}\,[m n_B \mathbf{u}_0 + (n_0 - n_B)\,\mathbf{A}], \tag{5.12b}$$

$$U_v = -\int d\mathbf{r} n_0 \mathbf{A}\cdot\mathbf{u}_0, \tag{5.12c}$$

$$\begin{aligned} U_0 = \int d\mathbf{r} \Bigg[&\frac{\hbar^2}{2m}\left(\boldsymbol{\nabla}\sqrt{n}\right)^2 + \frac{m}{2}(n_0 - n_B)\,\mathbf{u}_0^2 + \frac{m}{2} n_B \mathbf{u}_0^2 \\ &+ n_0\left(\frac{\mathbf{A}^2}{2} + W \pm \frac{\hbar\Omega_r}{2} + \frac{g}{2} n_0\right)\Bigg]. \end{aligned} \tag{5.12d}$$

The scalar potential U_0 collects all the terms that do not give any contribution to the vortex dynamics, since their values do not depend on the position $\mathbf{r}_0$ of the core. As a consequence, they do not give rise to any effective forces acting on the vortex core. The vortex mass M_v takes a negative value, and accounts for the missing mass in the condensate due to the presence of the vortex. It diverges logarithmically with the size of the system, and takes the form $M_v = m_{\rm core}\zeta(L/\xi)$ [150], where $m_{\rm core} = -m n_B(\pi\xi^2/2)$ and the mass parameter of the vortex defined as

$$\begin{aligned} \zeta(L/\xi) &= 4 \times \int_0^{L/\xi} x\,(1 - n/n_B)\,dx \\ &= 4\left[2\,\mathrm{arcsinh}\left(\frac{L}{\sqrt{2}\,\xi}\right) - \frac{L}{\xi}\left(\sqrt{2 + \left(\frac{L}{\xi}\right)^2} - \frac{L}{\xi}\right)\right]. \end{aligned} \tag{5.13}$$

Here $x = r/\xi$ is the dimensionless radial length, and we used the approximate solution $n(x)/n_B = x/\sqrt{2 + x^2}$ [86]. For typical atomic clouds $L/\xi \sim 100 - 1000$, $\zeta(L/\xi)$ can take values significantly larger than one, as seen in Fig. 5.2. This means that for large clouds the mass of the vortex can attain values significantly larger than the core mass.

5.2 Effective forces

The Lagrangian in Eq. (5.11) describes the core as a point particle of (negative) mass M_v and positive unit charge ($q = 1$), which feels the action of effective vector and scalar potentials, A_v, and U_v respectively (we omitted U_0 as it has no effects

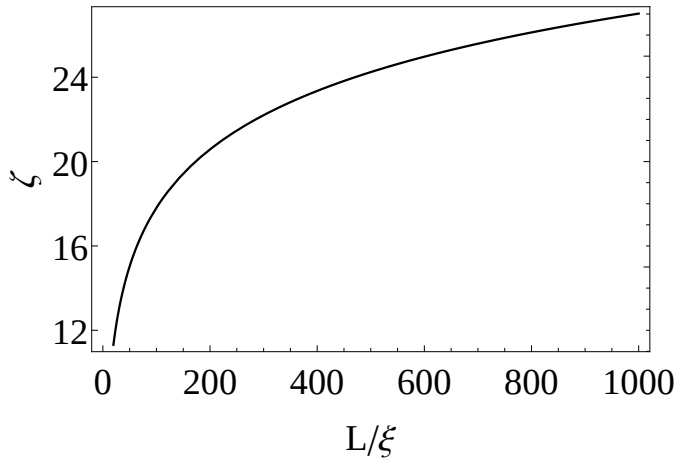

Figure 5.2: Value of the vortex mass parameter defined in the text, as a function of the extension of the cloud.

on the dynamics of the core). We therefore expect that the vortex core is subjected to two type of forces: a Lorentz-like force $f_B = q\mathbf{v} \times \mathbf{B}_v$, with $\mathbf{B}_v = \nabla_0 \times \mathbf{A}_v$ the effective magnetic field felt by the core (having defined $\nabla_0 \equiv d/d\mathbf{r}_0$) and an electric-type force due to the scalar potential, and given by $f_E = -\nabla_0 U_v$. In order to determine their explicit expressions, we start by calculating the effective magnetic field

$$\begin{aligned} \mathbf{B}_v &= \boldsymbol{\nabla}_0 \times \int d\mathbf{r}\, [m n_B \mathbf{u}_0 + (n_0 - n_B)\, \mathbf{A}] \\ &= \int d\mathbf{r}\, [m n_B \boldsymbol{\nabla}_0 \times \mathbf{u}_0 + \boldsymbol{\nabla}_0 n_0 \times \mathbf{A} + (n_0 - n_B)\, \boldsymbol{\nabla}_0 \times \mathbf{A}]. \end{aligned} \tag{5.14}$$

In order to obtain the second line in Eq (5.14) we used the vector identity $\boldsymbol{\nabla} \times (f\mathbf{V}) = (\boldsymbol{\nabla} f) \times \mathbf{V} + f\,(\boldsymbol{\nabla} \times \mathbf{V})$, where $\mathbf{V}$ is a generic vector field, and f a differentiable function. Among the three different terms in Eq.(5.14), only the first one gives a contribution different from zero, which is

$$\begin{aligned} \mathbf{B}_v^{(1)} &= \int d\mathbf{r}\, m n_B\, (\boldsymbol{\nabla}_0 \times \mathbf{u}_0) \\ &= -m n_B \int d\mathbf{r}\, \boldsymbol{\nabla} \times \mathbf{u}_0\, (\mathbf{r} - \mathbf{r}_0) \\ &= -\hbar n_B \int d\mathbf{r}\, \boldsymbol{\nabla} \times \frac{\hat{\mathbf{e}}_z \times (\mathbf{r} - \mathbf{r}_0)}{|\mathbf{r} - \mathbf{r}_0|^2} \\ &= -\hbar n_B \hat{\mathbf{e}}_z \oint d\boldsymbol{\ell} \cdot \frac{\hat{\mathbf{e}}_z \times (\mathbf{r} - \mathbf{r}_0)}{|\mathbf{r} - \mathbf{r}_0|^2} \\ &= -\hbar n_B \hat{\mathbf{e}}_z \int_0^{2\pi} d\theta \\ &= -h n_B \hat{\mathbf{e}}_z, \end{aligned} \tag{5.15}$$

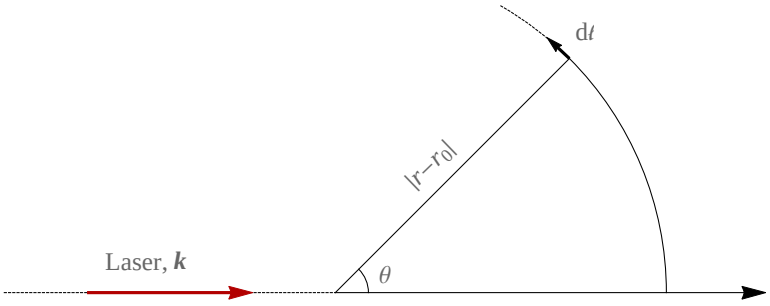

Figure 5.3: Polar coordinates used in the text.

where $h = 2\pi\hbar$ is the Planck constant, and we defined the line element as $d\boldsymbol{\ell} = (\mathbf{r} - \mathbf{r}_0)\, d\theta$. The other two contributions are zero, as

$$\begin{aligned}
\mathbf{B}_v^{(2)} &= \int d\mathbf{r}\, [\boldsymbol{\nabla}_0 n_0 (\mathbf{r} - \mathbf{r}_0)] \times \mathbf{A} \\
&= -\int d\mathbf{r}\, [\boldsymbol{\nabla} n_0 (\mathbf{r} - \mathbf{r}_0)] \times \mathbf{A} \\
&= \mp \frac{1}{2} \int_0^{2\pi} d\theta \int_0^{+\infty} dr\, r \left(\boldsymbol{\nabla} n_0^2\right) \times \mathbf{A}_1 \\
&= \mp \frac{|\mathbf{A}_1|}{2} \left(\int_0^{2\pi} d\theta\, \sin\theta\right) \left(\int_0^{\infty} dr\, r \boldsymbol{\nabla} n_0^2\right) \\
&= 0,
\end{aligned} \tag{5.16}$$

and

$$\begin{aligned}
\mathbf{B}_v^{(3)} &= \int d\mathbf{r}\, (n_0 - n_B) (\boldsymbol{\nabla}_0 \times \mathbf{A}) \\
&= \pm \int d\mathbf{r}\, (n_0 - n_B) (\mathbf{A}_1 \times \boldsymbol{\nabla} n_0) \\
&= \mp \frac{1}{2} \int d\mathbf{r}\, \boldsymbol{\nabla} \left[(n_0 - n_B)^2\right] \times \mathbf{A}_1 \\
&= \mp \frac{|\mathbf{A}_1|}{2} \left(\int_0^{2\pi} d\theta\, \sin\theta\right) \left(\int_0^{\infty} dr\, r \boldsymbol{\nabla} \left[(n_0 - n_B)^2\right]\right) \\
&= 0.
\end{aligned} \tag{5.17}$$

In Eqs. (5.16) and (5.17), θ is the angle between the radial and the laser propagation direction, the latter identified by the wave vector $\mathbf{k}$ (see Fig. 5.3). Combining the results (5.15), (5.16) and (5.17), the effective magnetic field felt by the vortex core is equal to

$$\mathbf{B}_v = \mathbf{B}_v^{(1)} = -h n_B \hat{\mathbf{e}}_z, \tag{5.18}$$

and the resulting Lorentz-like force has the form

$$\begin{aligned} f_B &= q\mathbf{v}\times\mathbf{B}_v \\ &= hn_B\hat{\mathbf{e}}_z\times\mathbf{v}. \end{aligned} \tag{5.19}$$

This force physically represents a Magnus effect, as is orthogonal to the velocity of the core, and originates from the relative motion between the vortex, which carries a net vorticity, and the condensate bulk.

The electric-like force takes instead the form

$$\begin{aligned} f_E = q\mathbf{E}_v &= -\boldsymbol{\nabla}_0 U_v \\ &= \boldsymbol{\nabla}_0\left(\int d\mathbf{r} n_0\mathbf{u}_0\cdot\mathbf{A}\right) \\ &= \pm\boldsymbol{\nabla}_0\left(\mathbf{A}_1\cdot\int d\mathbf{r} n_0^2\left(\mathbf{r}-\mathbf{r}_0\right)\mathbf{u}_0\left(\mathbf{r}-\mathbf{r}_0\right)\right), \end{aligned} \tag{5.20}$$

and can be calculated explicitly by using the vector identity $\boldsymbol{\nabla}\left(\mathbf{V}_1\cdot\mathbf{V}_2\right)=\mathbf{V}_1\cdot\left(\boldsymbol{\nabla}\mathbf{V}_2\right)+\mathbf{V}_2\cdot\left(\boldsymbol{\nabla}\mathbf{V}_1\right)+\mathbf{V}_1\times\left(\boldsymbol{\nabla}\times\mathbf{V}_2\right)+\mathbf{V}_2\times\left(\boldsymbol{\nabla}\times\mathbf{V}_1\right)$, where $\mathbf{V}_1$ and $\mathbf{V}_2$ are generic vector fields. In our case $\mathbf{V}_1\equiv\mathbf{A}_1$ and $\mathbf{V}_2=\int d\mathbf{r} n_0^2\left(\mathbf{r}-\mathbf{r}_0\right)\mathbf{u}_0\left(\mathbf{r}-\mathbf{r}_0\right)$. As a consequence, the only contribution different from zero is

$$\begin{aligned} f_E &= \pm\mathbf{A}_1\times\left(\boldsymbol{\nabla}_0\times\int d\mathbf{r} n_0^2\left(\mathbf{r}-\mathbf{r}_0\right)\mathbf{u}_0\left(\mathbf{r}-\mathbf{r}_0\right)\right) \\ &= \mp\mathbf{A}_1\times\left(\int d\mathbf{r}\,\boldsymbol{\nabla}\times\left[n_0^2\left(\mathbf{r}-\mathbf{r}_0\right)\mathbf{u}_0\left(\mathbf{r}-\mathbf{r}_0\right)\right]\right) \\ &= \mp\mathbf{A}_1\times\hat{\mathbf{e}}_z\oint_{C_\infty} n_0^2\left(\mathbf{r}-\mathbf{r}_0\right)\mathbf{u}_0\left(\mathbf{r}-\mathbf{r}_0\right)\cdot d\boldsymbol{\ell} \\ &= \mp n_B^2\frac{\hbar}{m}\left(\mathbf{A}_1\times\hat{\mathbf{e}}_z\right)\int_0^{2\pi} d\theta \\ &= \pm hn_B\hat{\mathbf{e}}_z\times\left(\frac{n_B\mathbf{A}_1}{m}\right) \\ &= \pm hn_B\hat{\mathbf{e}}_z\times\mathbf{v}_a, \end{aligned} \tag{5.21}$$

where we defined the effective velocity $\mathbf{v}_a\equiv n_B\mathbf{A}_1/m$ induced by the vector potential. In Eq. (5.21) we used the Stoke's theorem to convert the surface integral which appears in the second line, into a line integral. Such an integral is evaluated along the path C_∞ given by the boundaries of the system. Comparison of Eq. (5.21) with Eq. (5.19) shows that an extra force acts on the vortex core, due to the effective velocity $\mathbf{v}_a$ induced in the system by the vector potential. The intrinsic nonlinearity

of the vector potential makes the magnitude of this force depending on the particle density in the system.

5.3 Equation of motion

Once we know the effective forces at play, we are in the position to determine the motion of the vortex core, given suitable initial conditions. We consider here the case of an initially stationary vortex, for which $\mathbf{r}_0 = 0$ and $\mathbf{v} = 0$ at the initial time $t = 0$. The equation of motion for the vortex core

$$M_v \frac{d^2\mathbf{r}_0}{dt^2} = q\mathbf{v} \times \mathbf{B}_v + q\mathbf{E}_v, \tag{5.22}$$

can be conveniently rewritten as

$$\frac{d^2\mathbf{r}_0}{dt^2} = \omega\, \hat{\mathbf{e}}_v \times (\mathbf{v} \pm \mathbf{v}_a)\,, \tag{5.23}$$

where we defined the angular frequency $\omega = hn_B/M_v$. In order to integrate Eq. (5.23), it is convenient to project it in the directions parallel and perpendicular to the direction of propagation of the laser beam, which we indicate as $\mathbf{r}_0^{\parallel}$ and $\mathbf{r}_0^{\perp}$ respectively. In terms of the vortex velocity, the projected equations take the form

$$\frac{dv_{\parallel}}{dt} = -\omega\, v_{\perp}, \tag{5.24a}$$

$$\frac{dv_{\perp}}{dt} = \omega\, \left(v_{\parallel} \pm v_a\right), \tag{5.24b}$$

where $v_a \equiv |\mathbf{v}_a|$. Differentiating one of them and substituting into the other, they can be solved yielding the components for the velocity

$$v_{\parallel}(t) = \pm v_a \left[\cos(\omega t) - 1\right], \tag{5.25a}$$

$$v_{\perp}(t) = \pm v_a \sin(\omega t)\,. \tag{5.25b}$$

These can be readily integrated, finally giving the trajectory of the vortex core

$$r_{\parallel}(t) = \pm h_v \left[\sin(\omega t) - \omega t\right], \tag{5.26a}$$

$$r_{\perp}(t) = \pm h_v \left[1 - \cos(\omega t)\right], \tag{5.26b}$$

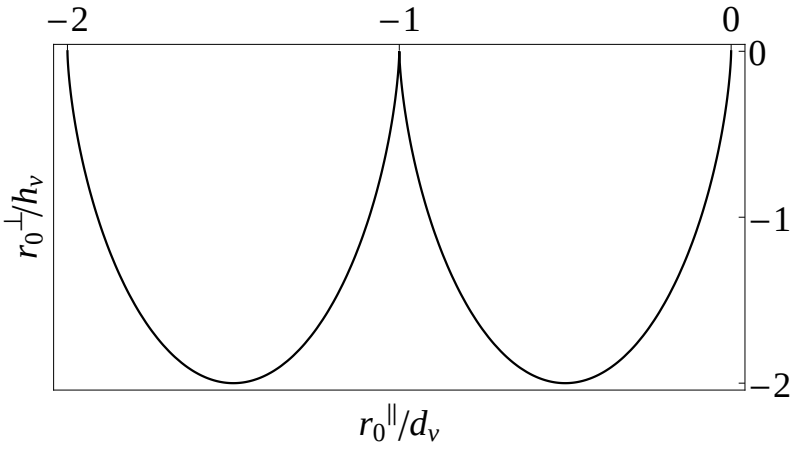

Figure 5.4: Motion of the vortex core described by Eqs. (5.26a) and (5.26b) in the text.

with $h_v = v_a/\omega = |\mathbf{A}_1|\, n_B/m\omega$. In Eqs. (5.26a) and (5.26b), the plus (minus) sign refers to the case of a condensate of atoms in the + (−) dressed state. The motion described by these equations is fully characterized by two quantities that are the frequency ω and the characteristic length h_v. The former depends only on the mass of the atomic species and on the structure of the vortex. The latter depends instead on the structure of the vortex and on the strength of the nonlinear potential, which in turn depends on the atom-light interaction parameters and on the number of particles. The motion is periodic with period $T = 2\pi/\omega$, made of a series of curved trajectories of maximum height h_v, separated by the distance $d_v = 2\pi h_v$ (see Fig. 5.4). In terms of the healing length, the characteristic length of the motion, takes the value

$$\left|\frac{h_v}{\xi}\right| = \frac{\pi}{2}\varepsilon\frac{\xi}{\lambda}\zeta\left(\frac{L}{\xi}\right), \tag{5.27}$$

where here $\varepsilon = n_B(g_{11} - g_{22})/\hbar\Omega_r$ is the coherent versus collisional interaction perturbative parameter, and $\lambda = 2\pi/|\mathbf{k}|$ is the wave length of the laser field. In typical ultra-cold atoms experiments, $\xi \sim 1\mu$m. Taking $\varepsilon \sim 0.1$, the wavelength of the laser beam to be $\lambda = 600\,$nm and a size of the atomic cloud for which $L/\xi \sim 100$, the ratio between the characteristic length h_v of the core motion and the healing length can be of the order of a few units. Despite this value being small, the motion of the vortex should be distinguishable and therefore experimentally detectable.

In order to test the analytic results, we solve numerically the Gross-Pitaevskii equation (3.61) for the + component of the condensate, with $\mathbf{A}_+$ and W_+ given in

Eqs. (5.1) and (5.2), with $\mathbf{A}_0 = 0$. We consider a cloud in a square geometry, with periodic boundary conditions in x-direction and confined by a hard-wall potential along the y, providing a homogeneous density which approximates the infinite homogeneous cloud assumed in the analytical description developed above. We determine the initial state of the system by solving Eq. (3.61) in the imaginary time without the current non-linearity, which leads to the situation represented in Fig. 5.5, where two vortices with opposite flow circulation appear in order to match the periodic boundary conditions. By running the simulations for the same system with double and half of its original size, we checked that the mutual interaction between the two vortices, as well as between the vortices and the boundaries does not affect the motion of the vortices. We solve the GP equation for the system characterized by the values of the physical parameters that, in dimensionless units, are $|\mathbf{A}_1|/(\hbar L_s Z) = 0.03, 0.06, 0.09$ and $2gm/(\hbar^2 Z) = 1.0$, where L_s is a reference length scale in the plane of the condensate, and Z is its thickness. Energy is in units of $\hbar^2/2mL_s^2$ and time in units of $2mL_s^2/\hbar$. These parameters can be related to physical values by for instance choosing the atomic mass of Ytterbium $\sim 10^{-25}\,\mathrm{Kg}$, the length $L_s = 10\,\mu\mathrm{m}$, the combinations of the scattering lengths $a_{11} - a_{22} = 100\,\mathrm{nm}$ and $(a_{11} + a_{22} + 2a_{12})/4 = 4\,\mathrm{nm}$, the Rabi frequency $\Omega_r = 10\,\mathrm{kHz}$, the wave length for the incident laser beam to be $\lambda = 628\,\mathrm{nm}$, and the density of the cloud $6.25 \times 10^{14}\,\mathrm{cm}^{-3}$, having assumed the effective thickness of the cloud to be $0.1\,\mu\mathrm{m}$.

It is important to stress here that we do not expect a perfect match between the analytical and the numerical solutions as, in the analytic model, we made the assumption that the density and phase profiles around the vortex core do not change in time, and that the motion of the vortex is adiabatic in the sense that no phonons or any other excitations are induced in the condensate. In reality the vortex is distorted by the presence of the current nonlinearity due to an effective local scattering length being different on either side of the vortex core (see Fig. 5.5(c)). The stronger the nonlinearity the more distorted the vortex becomes. This will change the value of the effective vortex mass, which consequently affects both the time scale and the length scale in the dynamics. A better match between the analytical predictions and the results of the numerical simulation can in principle be attained in the limit of very weak current nonlinearity. However, in such a limit, the time scale for the dynamics in question becomes longer, and the amplitude of the cyclic motion of the

vortex core decreases as seen from equations (5.26a), (5.26b) and (5.27).

The ansatz used to derive the analytic results presented above is the simplest one, which however is still able to capture the main features of the vortex motion. In order to reduce the spurious effects due to the actual non-adiabaticity of the motion, we look to the short time scale dynamics $\omega t \lesssim 2\pi$ (see Fig. 5.6). We recognize in the numerical curves the basic features suggested by the theoretical model: i) The direction of the forces acting on the vortices reproduce the theoretical predictions, with the transversal motion (that is in the direction $\mathbf{r}_\perp$) being in opposite directions for vortices with opposite circulation. ii) The amplitude of the motion scales linearly with the intensity of the nonlinear potential, to a good approximation. It should be noted however, that the simple model here developed is not able to closely reproduce the motion of the core, especially at long time scales.

In conclusion, we have developed a minimal model that accounts for the motion of a vortex in a condensate, when nonlinear synthetic potentials act on the system. As for the case of standard (that is linear) gauge potentials, the vortex core feels an effective force which is orthogonal to the direction of the vector potential, which explicitly depends on the particle density in our case. Comparison with numerical simulations of the GP equation shows a qualitative agreement for the motion of the vortex core, in particular at the early time, when the key features of the motion predicted by the model can be recognized. The model fails however in closely matching the results of the numerical simulation, for reasons that can be ascribed to the hypothesis of adiabatic motion, on which the model here developed relies. A better description for the vortex dynamics could be achieved by developing more complex models which take into account non adiabatic effects. Still in the framework of a variational approach to the problem, a generalization of the model here presented would be possible by introducing extra variational parameters other than the core's position, accounting for eventual asymmetries in the density and/or phase profiles of the order parameter.

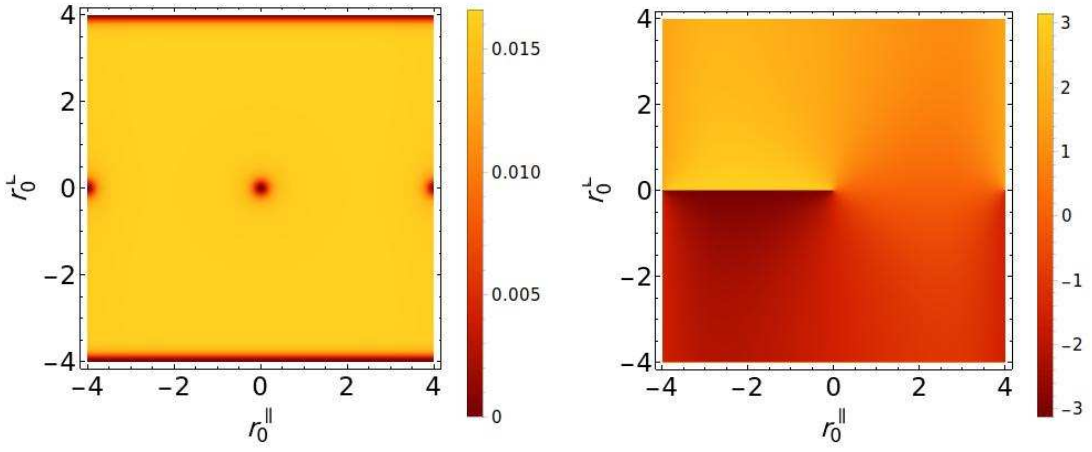

(a) (b)

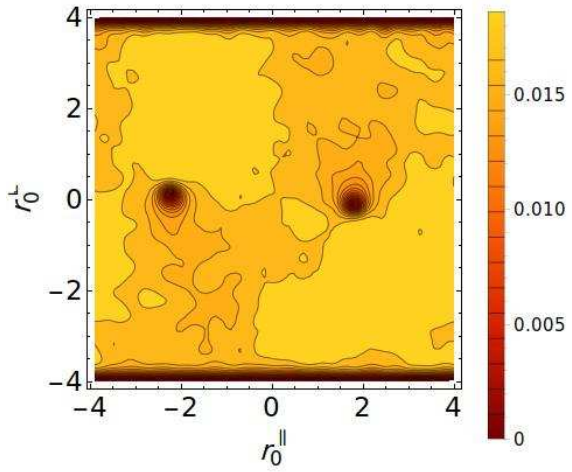

(c)

Figure 5.5: Density (a) and phase (b) profiles of the condensate wave function at $t = 0$, used as initial condition for the numerical simulation. (c) Density distribution of the cloud after $t = 2.5$ in units of $2mL_s^2\hbar$. Deformations in the density are visible, in contrast to the ideally symmetric ansatz used in the analytical model. Dimensionless units are used in the figures. We used the values of the parameters $|\mathbf{A}_1|/(\hbar L_s Z) = 0.03$ and $2gm/(\hbar^2 Z) = 1.0$

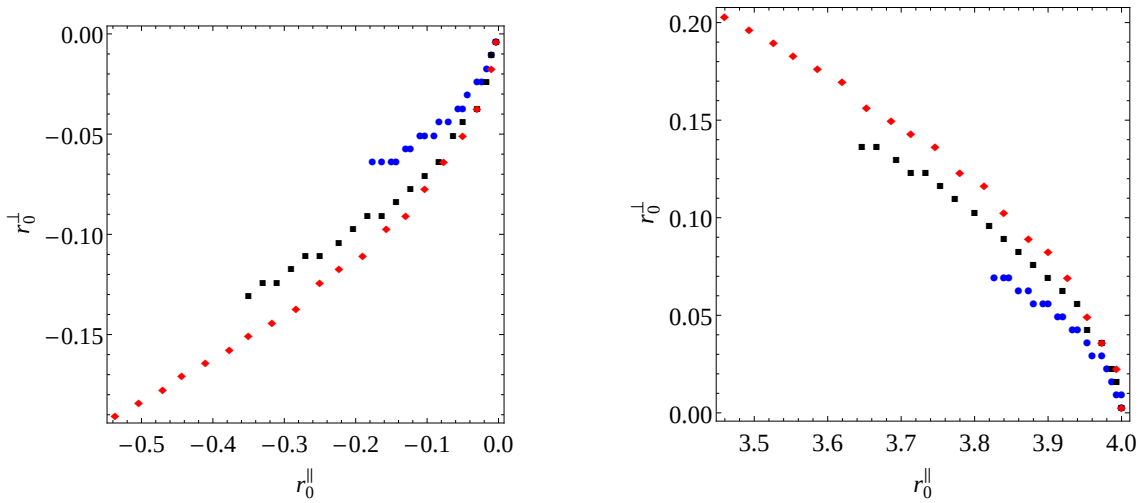

Figure 5.6: Numerical simulation of the early time motion $\hbar t/2mL_s^2 = 0.05$ ($\omega t \approx 1.5$) of the vortex and anti-vortex cores, given by the initial conditions in Figs. 5.5(a,b). We used the values of the parameters $2gm/(\hbar^2 Z) = 1.0$ and $|\mathbf{A}_1|/(\hbar L_s Z) = 0.03$ (blue), 0.06 (black) and 0.09 (red).

Part III – Analogue gravity with two-component condensates

Chapter 6 Analogue Gravity with nonlinear gauge potentials

With this chapter we start the second part of the thesis, which is devoted to the topic of analogue gravity. We will show that non-trivial effective spacetime configurations for phonons can be simulated by taking advantage of the extra degree-of-freedom introduced in the system by the nonlinear vector potential, that cannot be attained in any easy way with usual flowing condensates.

After a brief introduction to the black hole laser effect in single component condensates reported in Chapter 7, we study in Chapter 8 the equivalent phenomenon in a two-component pseudo-spin systems. There we do not consider the atoms subjected to any gauge potential. The reason is that, as we will see in the following, the nonlinear potentials are not effective in creating new horizons in the system, which are induced by the flow velocity only.

6.1 Introduction

Einstein's theory of gravitation and the Standard Model of particles and interactions represent so far our best description of nature. General relativity is the classical theory of spacetime, whose dynamics and interactions with matter fields have been postulated by Einstein in his famous equation $R_{\mu\nu} - Rg_{\mu\nu}/2 = 8\pi G T_{\mu\nu}/c^4$, which relates the geometry of spacetime to the matter and energy content of the universe (see for example [151, 152]). The Standard Model describes the building blocks of the universe we live in as quantized excitations of these fields. Both these theories have found so far an excellent experimental confirmation, but they rely on mutually contradicting hypotheses.

Modern quantum field theories (QFT) are developed in absence of gravity, i.e. based on the hypothesis of a fixed flat (Minkowskian) spacetime, which constitutes the background on which physical phenomena take place. The theory of general relativity, on the other hand, contradicts this view since it describes the spacetime as a dynamical object that bends and ripples as any other field. This implies that a fixed background metric does not exist but, instead, the physics need to be *background independent*. The origin of this apparent contradiction has to be ascribed to the fact that these theories represent approximations, at different energy scales, to a yet unknown more fundamental one. Many attempts have been made and many different routes have been pursued in order to arrive at a more general theory unifying all the known fundamental interactions, including gravity (see [153] for a comprehensive review). However, a common plague of all these attempts is the lack of any experimental data, that could lead towards one direction or the other and, eventually, provide a definitive test for the sought theory.

Quantum field theories on curved spacetime (QFTCS) represent a first step towards including the effects of gravity into the dynamics of quantum matter fields, and is expected to provide at least some insight into the structure of the still unknown more fundamental theory [24, 25]. The approach is similar to the semi-classical theory of the interaction of an atom with an electromagnetic field, where light is considered as a classical field governed by the Maxwell equations, while the internal structure of the atom is quantized. In the QFTCS case, this approach treats the interaction between spacetime and matter fields by considering the former as a classical field, whose dynamics is described by Einstein's theory of general relativity, while the latter as quantized fields. The predictions of QFTCS did open the door to a plethora of new intriguing effects which were unexpected in a Minkowskian background. Prominent example are the evaporation of black holes (BH) in the form of a thermal Hawking radiation [26, 27], or the particle creation by an expanding, or more generally non stationary universes [24, 25, 28–32].

Hawking radiation consists of the emission of thermal particles from an astrophysical black holes, characterized by a temperature whose value is inversely proportional to the black hole mass. The typical value of this temperature, for ordinary black holes is of the order of less than a micro-kelvin [26, 27], which makes its detection extremely

difficult and unlikely with state-of-the-art astrophysical observational techniques. Because of this reason, the direct observation of Hawking radiation from astrophysical objects cannot provide so far a useful test for the validity of QFTCS. However, Hawking radiation is not a phenomenon relevant only to gravitational systems, but is instead a purely kinematical effect of quantum fields living on a curved spacetime and experiencing an event horizon. This consideration has been first pointed out by Unruh in [154], which is considered a milestone of the modern field of analogue gravity.

Analogue gravity is in a sense another realization of the quantum simulators paradigm, aimed to reproduce in a fully controllable system, curved spacetime quantum field theory phenomena [3, 4, 155]. Despite its name, it is important to stress from the very beginning that analogue models for gravity do not reproduce the dynamics predicted by general relativity. In other words, the dynamics of the emerging effective spacetime is not described by the Einstein equations, but by the underlying dynamics of the system instead, which is characteristic to the specific analogue model. It instead allows us to study *kinematical* aspects of gravitation, with phenomena such as Hawking radiation and cosmological particle creation which rely on the spacetime structure only.

After Unruh's seminal paper, many proposals appeared seeking for Hawking radiation, and more generally QFTCS analogues in a multitude of physical systems. These attempts include gravity (i.e. surface) waves in flowing water [156–160], light propagation in dielectric media and slow light [161–183], phonon excitations in rings of trapped ions [184, 185], nonlinear optical systems [186–193], ultra-cold fermions [194], superconducting circuit QED [195, 196], quantum fluids of light [197, 198] and BEC [199–210]. A common purpose of all these different models is the study of the effective dynamics of the elementary excitations in the system that, in the presence of an inhomogeneous background, behave as if they were propagating in a curved effective spacetime. Choosing opportunely the background state, a specific spacetime configuration needed to investigate some QFTCS effect of interest can in principle be engineered.

Because of the high level of controllability reached in state-of-the-art experiments

with cold atoms, nowadays atomic BECs represent one of the most promising frameworks for the implementation of this program. Since the mid-2000s, a surge of activity has been devoted to this, with particular emphasis on the investigation of the Hawking physics. After the first numerical evidence of analogue Hawking radiation in atomic condensates [211] and the characterization of its observable consequences [212–214], more recently the attention has been devoted to quantum entanglement signatures [215]. Other cosmological phenomena, such as analogue particle creation by expanding universes or cosmic inflation have also been investigated [216–222].

From the experimental point of view, recent years have seen impressive advances. The first experimental realisation of sonic black hole configurations in a flowing atomic BEC has been achieved in [223], and set the root towards the experimental investigation of (sonic) Hawking radiation in an atomic condensate. The field has seen a leading role played by Jeff Steinhauer, at the Technion institute in Israel. He developed the technique useful for creating sonic horizons by accelerating a BEC down from a *waterfall*-like potential, and developed the techniques needed for detecting small fluctuations in the populations of phonons [224, 225]. In [223] he created the analogue of a charged black hole, which is endowed with two (black and white) horizons. Based on this first preliminary achievement, he investigated the black-hole lasing effect (described in details in the next chapter), claiming the observation of the related self-amplifying Hawking radiation. This result has been debated by the community, in relation to the origin of the observed instability [226–228], and in particular whether it arises because of the lasing mechanism or because of competing effects such as the Bogoliubov-Čerenkov radiation [229].

Very recently, pioneering first evidence of Hawking particles from an analogue black hole has been reported, again by Steinhauer, in [230]. Here a footprint of the particles emitted from the vacuum has been observed in the density correlation function of the system, which has been proven to have a key role in order to reveal the emission of (positive energy) Hawking particles and of its negative energy companion, respectively outside and inside the horizon [215].

Further experimental work on analogue systems has been done, with the aim of

studying particle creation phenomena originating from non-adiabatic modulation of the vacuum state of a condensate [231, 232]. The aim of the research is to elucidate physical effects such as cosmological particle creation or dynamical Casimir effect [24, 25, 233].

The aim of this chapter is to extend the theory of BEC models for gravity in order to include the effects of the nonlinear synthetic potentials introduced in Chap. 3. It is worth noting here that the same arguments hold also for models based on superfluids of light [198], in which the same kind of nonlinear potentials has been proven to arise working with nonlinear optical media [234].

6.2 The effective spacetime

An effective spacetime emerges for phonons in a condensate, whose dynamics mimic the physics of a scalar field on curved spacetime. We report here the derivation of the effective (acoustic) metric, for the case of a BEC whose atoms are subjected to the action of nonlinear gauge potentials. We show, and this is the first result of this second part of the thesis, that the presence of the nonlinear potentials endows the effective spacetime with new interesting features, enriching the physics that can be investigated.

We consider the simplest yet non-trivial case, in which two internal states of the atoms are coupled by a monochromatic laser beam with wave vector $\mathbf{k}$. It is worth stressing here that the structure of the effective spacetime depends on the details of the atom-light interaction. Different spacetime configuration can thus be engineered by properly tuning the spatial profile of the interaction parameters, which are the Rabi frequency, the detuning from the atomic resonance and the phase of the coupling field. We choose the light-matter interaction parameters in such a way that the dressed states of the atoms are symmetric superpositions of the bare internal states, in which case the mixing angle in Eq. (3.22) takes the value $\theta = \pi/2$. As already noted in Chap. 5, the linear term of the vector potential $\mathbf{A}_0 = -\hbar\mathbf{k}/2$ is constant in this case and can be disregarded, leaving the vector potential in the form $\mathbf{A} = \pm n\,\mathbf{A}_1$, with $\mathbf{A}_1 = (g_{11} - g_{22})\mathbf{k}/(8\Omega_r)$. The same happens for the scalar

potential $W = \hbar^2|\mathbf{k}|^2/8m$, which can be gauged away by a simple redefinition of the condensate wave function.

By using the Madelung representation for the order parameter $\psi = \sqrt{n}\, e^{iS}$, the nonlinear Schrödinger equation (3.61), can be written in terms of the continuity and (quantum) Euler equations

$$\frac{\partial n}{\partial t} + \boldsymbol{\nabla}\cdot\left[n\left(\frac{\hbar}{m}\boldsymbol{\nabla}S - \frac{\mathbf{A}}{m}\right)\right] = 0, \tag{6.1}$$

$$\hbar\frac{\partial S}{\partial t} = \frac{\hbar^2}{2m}\frac{\boldsymbol{\nabla}^2\sqrt{n}}{\sqrt{n}} - \frac{\hbar^2}{2m}(\boldsymbol{\nabla}S)^2 \pm 2n\mathbf{A}_1\cdot\left(\frac{\hbar}{m}\boldsymbol{\nabla}S - \frac{\mathbf{A}}{m}\right) + n\left(\frac{n|\mathbf{A}_1|^2}{2m} - g\right). \tag{6.2}$$

The dynamics of the small amplitude fluctuations of the system is obtained from Eqs. (6.1) and (6.2) by writing the density and phase field as $n = n_0 + n_1$ and $S = S_0 + S_1$ respectively, where n_1 and S_1 represent excitations on top of the background values n_0 and S_0. Retaining first order terms in n_1 and S_1 only, we obtain the linearized hydrodynamics equations

$$\frac{\partial n_1}{\partial t} + \boldsymbol{\nabla}\cdot\left[n_1\left(\mathbf{v}_0 \mp n_0\frac{\mathbf{A}_1}{m}\right) + n_0\frac{\hbar}{m}\boldsymbol{\nabla}S_1\right] = 0, \tag{6.3}$$

$$\hbar\frac{\partial S_1}{\partial t} = -\hbar\left(\mathbf{v}_0 \mp n_0\frac{\mathbf{A}_1}{m}\right)\cdot\boldsymbol{\nabla}S_1 - n_1\left(g \mp 2\mathbf{A}_1\cdot\mathbf{v}_0 + \frac{n_0|\mathbf{A}_1|^2}{m}\right), \tag{6.4}$$

with the zeroth order component $\mathbf{v}_0$ of the velocity field in the condensate defined as $m\mathbf{v}_0 = \hbar\boldsymbol{\nabla}S_0 \mp n_0\mathbf{A}_1$. Note that in Eq. (6.4) we neglected the quantum pressure term. This assumption is equivalent to working in the hydrodynamic regime $k\xi \to 0$ in which the dispersion relation of the Bogoliubov elementary excitations is linear (see Chapter 2). By substituting the density n_1, obtained from (6.4), into Eq.(6.3) we finally get the following equation for S_1

$$\frac{\partial}{\partial t}\left[-\frac{1}{g'}\left(\hbar\frac{\partial S_1}{\partial t} + \hbar\left(\mathbf{v}_0 \mp n_0\frac{\mathbf{A}_1}{m}\right)\cdot\boldsymbol{\nabla}S_1\right)\right] + \boldsymbol{\nabla}\cdot\left[n_0\frac{\hbar}{m}\boldsymbol{\nabla}S_1 - \frac{1}{g'}\left(\mathbf{v}_0 \mp n_0\frac{\mathbf{A}_1}{m}\right)\left(\hbar\frac{\partial S_1}{\partial t} + \hbar\left(\mathbf{v}_0 \mp n_0\frac{\mathbf{A}_1}{m}\right)\cdot\boldsymbol{\nabla}S_1\right)\right] = 0. \tag{6.5}$$

Here, we defined the coupling constant $g' = \left(g \mp 2\mathbf{A}_1\cdot\mathbf{v}_0 + \frac{n_0|\mathbf{A}_1|^2}{m}\right)$ which is renormalized taking into account the effect of the nonlinear potential. The analogy with

the dynamics of fields propagating on a curved spacetime relies on Eq. (6.5) which, introducing the $(3+1)$-dimensional spacetime coordinates $x^\mu \equiv (t; x^i)$, can be written in the compact form

$$\Delta S_1 \equiv \frac{1}{\sqrt{-g}} \frac{\partial}{\partial x^\mu} \left(\sqrt{-g} g^{\mu\nu} \frac{\partial S_1}{\partial x^\mu} \right) = 0. \tag{6.6}$$

It shows that the dynamics of the phase fluctuations in the condensate has the form of a wave equation for a scalar field in a spacetime characterized by the (contravariant) metric tensor

$$g^{\mu\nu} = \frac{1}{n_0 c_s} \begin{pmatrix} -1 & -\left(v_0 \mp v_a\right)^j \\ -\left(v_0 \mp v_a\right)^i & \left[c_s^2 \delta^{ij} - \left(v_0 \mp v_a\right)^i \left(v_0 \mp v_a\right)^j \right] \end{pmatrix}. \tag{6.7}$$

In Eq. (6.7), v_a^j is the component of the velocity $\mathbf{v}_a = n_0 \mathbf{A}_1 / m$ induced by the nonlinear vector potential, already introduced in Chapter 5, $c_s^2 = g' n_0 / m = c^2 \mp 2\mathbf{v}_a \cdot \mathbf{v}_0 + v_a^2$ is the local speed of sound in the condensate (with $v_a = |\mathbf{v}_a|$), while $c^2 = g n_0 / m$ is the value it would take in absence of the potential (see Chap. 2). The (covariant) metric tensor is obtained by inverting the matrix in Eq. (6.7), and reads

$$g_{\mu\nu} = \frac{n_0}{c_s} \begin{pmatrix} -\left(c^2 - v_0^2\right) & -\left(v_0 \mp v_a\right)^j \\ -\left(v_0 \mp v_a\right)^i & \delta^{ij} \end{pmatrix}. \tag{6.8}$$

It shows that the net effect of the nonlinear vector potentials is to induce an extra term in the components of the metric mixing the space and time coordinates in the laboratory reference frame. By posing $v_a = 0$, we recover the usual results of hydrodynamic models for gravity. It is an effective metric which is conformal to the Schwarzschild metric, written in the so-called Painlevè-Gullstrand coordinates [3, 235, 236]. Note that the g_{00} components (as well as the pure spatial components g_{ij}, with $i, j = 1, 2, 3$) are not affected by the nonlinear potential. This means that the sonic regime, and thus the appearance of acoustic horizons in the system is induced by the physical velocity only. As a consequence, the Hawking temperature of the acoustic black hole is not modified by the effective nonlinear potential, and keeps the form [3]

$$k_B T_H = \frac{\hbar g_H}{2\pi c_H}, \tag{6.9}$$

where c_H is the value of the bare sound velocity and g_H is the surface gravity, both

evaluated at the horizon [3]

$$g_H = \frac{1}{2} \left. \frac{\partial \left(c^2 - v_0^2\right)}{\partial n} \right|_H . \tag{6.10}$$

Despite the effective velocity $\mathbf{v}_a$ induced by the nonlinear potentials not being effective in creating sonic horizons in a condensate, it represents an extra degree of freedom that can be used in order to design effective spacetimes for photons. First and foremost, Eq. (6.8) reveals that a nontrivial curved spacetime can be induced even for a static condensate, for which the physical velocity $\mathbf{v}_0$ of particles is zero. The off-diagonal terms, mixing space and time component of the metric are characteristic of rotating spacetimes (such as the spacetime of a rotating black hole) and can be exploited for example in order to design analogues of ergoregions. Moreover, effects such as cosmological particle creations, or dynamical Casimir effect, that is the particle creation process triggered by the parametric amplification of the vacuum fluctuations in the presence of time-dependent boundary conditions, can now be relatively easily implemented by simply modulating in time light-matter interaction parameters, such as the Rabi frequency or the detuning.

Chapter 7 The Black hole laser

In this Chapter we retrace the arguments following the original paper [237], where the black hole laser has first been predicted, in the framework of a wave packet description of the fields. It is worth noting that an equivalent description of the same phenomenon exists based on the study of the spectrum of the field eigenmodes [238–241].

7.1 Introduction

Hawking's prediction that black holes emit radiation is probably the most fascinating and at the same time ambiguous consequences of quantum field theories in curved spacetime. At the origin of the ambiguity is Hawking's original derivation, which suffers from a conceptual inconsistency due to the assumption that the semi-classical theory of the interaction between gravity and quantum fields is valid at arbitrary scales. This problem is known in literature as the *trans-Planckian problem*. At high-energies, and at length scales of the order of the *Planck length*, quantum gravity effects are supposed to come into play, with signatures of the microscopic spacetime structure in the macroscopic effective dynamics of quantum fields. Such a signature is presumably encoded in a deviation from the fully relativistic invariance at energy scales of the order of the Planck scale.

In this respect, the knowledge of the microscopic physics underlying analogue models would allow us to get an insight, although very indirect, into any possible effects of trans-Planckian degrees of freedom of quantum fields on the Hawking physics. As a quantum field theory in curved spacetime is supposed to be the low-energy limit of a more fundamental theory, we have shown in the previous chapter that analogue gravity models represent an effective theory for the low-energy excitations of the

underlying system. Such an effective theory breaks down at some characteristic length scale, which is the equivalent of the Planck length. In BEC models, this length is provided by the healing length, for which the (long wave) hydrodynamic description breaks down. At such short length scales (high energies) the theory acquires superluminal (for the case of a BEC for example) or subluminal character, and Lorentz-invariance is lost.

Working with specific subluminal and superluminal models, many authors have shown that the spectrum of the particles emitted from analogue black holes is still thermal provided field modes with energy of the order of the black hole temperature are considered and the energy scale characteristic of this short scale physics is much higher than the other energy scales in the sytem [242–245]. However, things dramatically change when configurations characterized by an inner (white) and a outer (black) horizon are considered. As we will see in the next section for the case of *superluminal bosonic fields*, the Hawking emission between the two horizons is unstable and gets self-amplified, leading to a phenomenon known as black hole lasing [237]. The radiated flux of excitations grows exponentially in time, as a result of the emergence of a lasing cavity, in which the negative energy companions of the Hawking particles bounce back and forth between the two horizons stimulating further emissions.

Experimental observation of the classical counterpart of this mechanism, which is the instability of a classical field propagating in such kind of a spacetime, has been claimed in [246] in the framework of BEC analogue models. Whether the instability observed is due to the lasing phenomenon or to competing effects such as the Bogoliubov-Čerenkov radiation [229] is still debated [226, 227].

7.2 A superluminal field theory

Following the original derivation of the black hole lasing mechanism by Corley and Jacobson [237], we shall consider a non-interacting complex scalar field theory whose action is suitably modified and leads to a superluminal dispersion at high frequencies. We will use units in which $c = \hbar = 1$ throughout the chapter.

7.2.1 The action

For simplicity we consider the field propagating in a $1+1$ Lorentzian spacetime, whose ordinary relativistic (Lorentz invariant) action has the form

$$S = \frac{1}{2}\int dtdx\sqrt{-g}\, g^{\mu\nu}\,(\partial_\mu\phi^*)\,(\partial_\nu\phi). \tag{7.1}$$

We consider a spacetime of the type defined in Eq. (6.8), setting $v_a = 0$ and omitting the conformal factor, for which the line element is given by (we omit the subscript in v_0 for brevity)

$$ds^2 = dt^2 - [dx - v(x)\,dt]^2\,. \tag{7.2}$$

By inserting in Eq. (7.1) the (contravariant) metric tensor $g^{\mu\nu}$ relative to the spacetime in Eq. (7.2) (see Eq. 6.7 with $v_a = 0$ and the conformal factor omitted), the action in Eq. (7.1) can be written in the extended form

$$S = \frac{1}{2}\int dtdx\,\left[|(\partial_t + v\partial_x)\,\phi|^2 - |\partial_x\phi|^2\right]. \tag{7.3}$$

From a general relativistic point of view, the action in Eq. (7.3) can be more straightforwardly obtained from the definition of the (contravariant) metric tensor $g^{\mu\nu} \equiv u^\mu u^\nu - s^\mu s^\nu$ in terms of the unit vector fields u^μ and s^ν, which are respectively tangent and orthogonal to the free-fall world lines of the spacetime. They can be obtained by noting that the tangent vector to a generic curve $x^\mu(t)$ is defined in the standard coordinate basis (∂_t, ∂_x) as $T^\mu = \partial_t + (dx/dt)\,\partial_x$, given the free-fall world lines, with time-like curves for which $dx - v\,dt = 0$. Therefore $\mathbf{u} \equiv u^\mu\partial_\mu = \partial_t + v(x)\,\partial_x$ and $\mathbf{s} \equiv s^\mu\partial_\mu = \partial_x$. Looking at the problem from a hydrodynamic point of view, we recognize in the first term of the Lagrangian density in Eq. (7.3) the total time derivative of the field written in the Eulerian formalism. In other words, such a term represents the time derivative in the reference frame (t', x) co-moving with the flowing fluid (which is the reference frame of free-falling observers in general relativity terminology), written in the lab coordinates (t, x). Because of these considerations, we see that the action in Eq. (7.3) describes nothing else than the dynamics of a standard (that is Lorentz invariant), non-interacting, complex scalar field in the free-falling reference frame:

$$\begin{aligned} S &= \frac{1}{2}\int dt'dx\left[|\partial_{t'}\phi|^2 - |\partial_x\phi|^2\right] \\ &= \frac{1}{2}\int dt'dx\left[\left(\partial_{\mu'}\phi^*\right)\left(\partial^{\mu'}\phi\right)\right]. \end{aligned} \tag{7.4}$$

We modify this action by adding an extra term, suitably selected to provide a superluminal propagation for the high frequency modes of the field. We take this term of the form $-\left|\partial_x^2\phi\right|^2/k_0^2$, so that the action of the theory now reads

$$S = \frac{1}{2}\int dtdx\left[\left|\left(\partial_t + v\partial_x\right)\phi\right|^2 - \left|\partial_x\phi\right|^2 - \frac{\left|\partial_x^2\phi\right|^2}{k_0^2}\right]. \tag{7.5}$$

The wave vector k_0 provides the characteristic scale at which the effects of the new term becomes relevant, and thus a significant deviation from linearity appears in the dispersion relation. Physically, such a length scale is meant to be the characteristic length of the micro-structure of spacetime on which the field propagates. At such short length scales the field is able to probe this fine structure and new phenomena appear, which results in the extra term added to the effective action. In the context of BEC gravity analogues for example, this characteristic length scale is given by the healing length of the condensate at which the hydrodynamic description breaks down, and the spectrum of the (density) elementary excitations is not linear any more but get the characteristic Bogoliubov form in Eq. (2.40).

7.2.2 The spectrum

Minimising the action in Eq. (7.5), by varying ϕ^*, results in the equation of motion for the field [237, 245, 247]

$$\left(\partial_t + \partial_x v\right)\left(\partial_t + v\partial_x\right)\phi = \partial_x^2\phi - \frac{\partial_x^4\phi}{k_0^2}. \tag{7.6}$$

The invariance of the action under global phase transformations of the field $\phi \to e^{i\theta}\phi$ (with $\theta = \text{const}$) implies the existence of a conserved current, because of the Noether theorem [248, 249]. The spatial integral of the time component of this current is conserved in time and serves as a conserved inner-product of the Hilbert space, when

evaluated with solutions of the field equation. It takes the form

$$(f,g) = i\int dx\,[f^*\,(\partial_t + v\partial_x)\,g - g\,(\partial_t + v\partial_x)\,f^*], \tag{7.7}$$

with $f(x,t)$ and $g(x,t)$ both solutions of the equation of motion Eq. (7.6).

Since the metric in Eq.(7.2) is stationary (and also invariant under time reversal, that is static), a solution to the field equation Eq.(7.6) can be written in the form $\phi = e^{-i\omega t}\,f(x)$, where ω is called the *Killing frequency* and is conserved in time. In the case of BEC analogues, it corresponds to the frequency of the Bogoliubov excitations in the laboratory reference frame, respect to which the system is stationary. The name "Killing" comes from general relativity literature, and is the frequency associated with the derivative of the field in the direction given by a vector field that is a generator of an isometry for the spacetime. In our case, the metric does not depend on time and the Killing vector field is oriented in each point towards the ∂_t direction. Given this ansatz, the equation of motion (7.6) reduces to the ordinary differential equation (ODE) for the space component of the field

$$-\frac{1}{k_0^2}\phi^{(iv)} + \left(1-v^2\right)\phi'' + 2v\,(i\omega - v')\,\phi' - i\omega\,(i\omega - v')\,\phi = 0, \tag{7.8}$$

where we used the prime ($'$) to denote a derivative with respect to x. In the simplest case of constant v, the system is invariant under space translations, and plane waves of the form $f(x) = e^{ikx}$ are solutions of Eq. (7.8). By assuming that $v(x)$ is not constant but varies slowly in space compared to $\lambda = 2\pi/k$, it is reasonable to suppose that $f(x)$ keeps the same form as above, except that k (or λ) varies slowly with x. In mathematical terms this hypothesis is stated by the conditions $\partial_x v/k \ll 1$ and $\partial_x k/k^2 \ll 1$. With these assumptions Eq. (7.8) can be solved by using the WKB approximation [108] according to which, to leading order, the field solution can be written as

$$f(x) = \exp\left[i\int dx\,k(x)\right]. \tag{7.9}$$

By inserting Eq. (7.9) into (7.8), and taking into account the above assumptions, we get the dispersion relation in the lab frame [237, 245, 247]

$$[\omega - v(x)k]^2 = F^2(k) \equiv k^2 + \frac{k^4}{k_0^2}. \tag{7.10}$$

The function $F(k)$ is the positive solution to the equation above, and represents the dispersion relation in the local free-falling reference frame, as the free-fall frequency ω' is related to the Killing frequency ω by the Galilean transformation

$$\omega' = \omega - v(x)k. \tag{7.11}$$

By comparing Eq. (7.10) with Eq. (2.40), we see that the function $F(k)$ models the Bogoliubov spectrum for the sonic excitations in a BEC, with $1/k_0$ being the equivalent of the healing length. By fixing the values of ω and v, the allowable values of k are found by solving Eq. (7.10). It is a fourth order polynomial equation in the wave vector k, so four roots are expected. The nature of these solutions can be qualitatively revealed solving the equation by using a graphical method, in which we look for the intersection points between the straight line $\omega - vk$ and the $\pm F(k)$ curves. In what follows we consider $v < 0$. Analysis of Figs. 7.1(a,b) reveals that when $|v| < v_{\rm cr}$, with $v_{\rm cr} \approx 3\,(\omega/k_0)^{2/3}/2 \approx 1$ assuming $\omega/k_0 \ll 1$, only two solutions are real, the other being complex. These solutions correspond to ones we would get ($k = \pm\omega$) in the case of a standard relativistic field theory. Following the notation of [237, 245, 247] we label the positive solutions as k_{+s} and we disregard the negative one because it is irrelevant for the following analysis. In the supersonic regime $|v| > 1$, all the four roots are real instead. We denote the largest positive root as k_+, disregard the other positive norm solution because it is not relevant for what follows, and indicate the two negative solutions (with negative norm) as k_- and k_{-s} respectively (the subscript s indicates the solution smaller in magnitude). A key feature of the supersonic regime ($v < -1$), which we will see will be crucial for the onset of the Hawking physics, is the appearance of solutions with negative free-fall frequencies.

The group velocity v_g of a wave packet in the lab frame is defined as

$$v_g = \frac{\partial\omega}{\partial k} = -|v| \pm \frac{dF}{dk}, \tag{7.12}$$

where $\pm dF/dk$ is the corresponding quantity in the free-fall reference frame. It is thus determined by the relative weight between the free-fall group velocity and $|v|$. From Figs. 7.1(a,b) it is easy to deduce that this quantity is positive for solutions belonging to the $(+s)$ and $(\pm)$ branches of the dispersion relation, while is negative

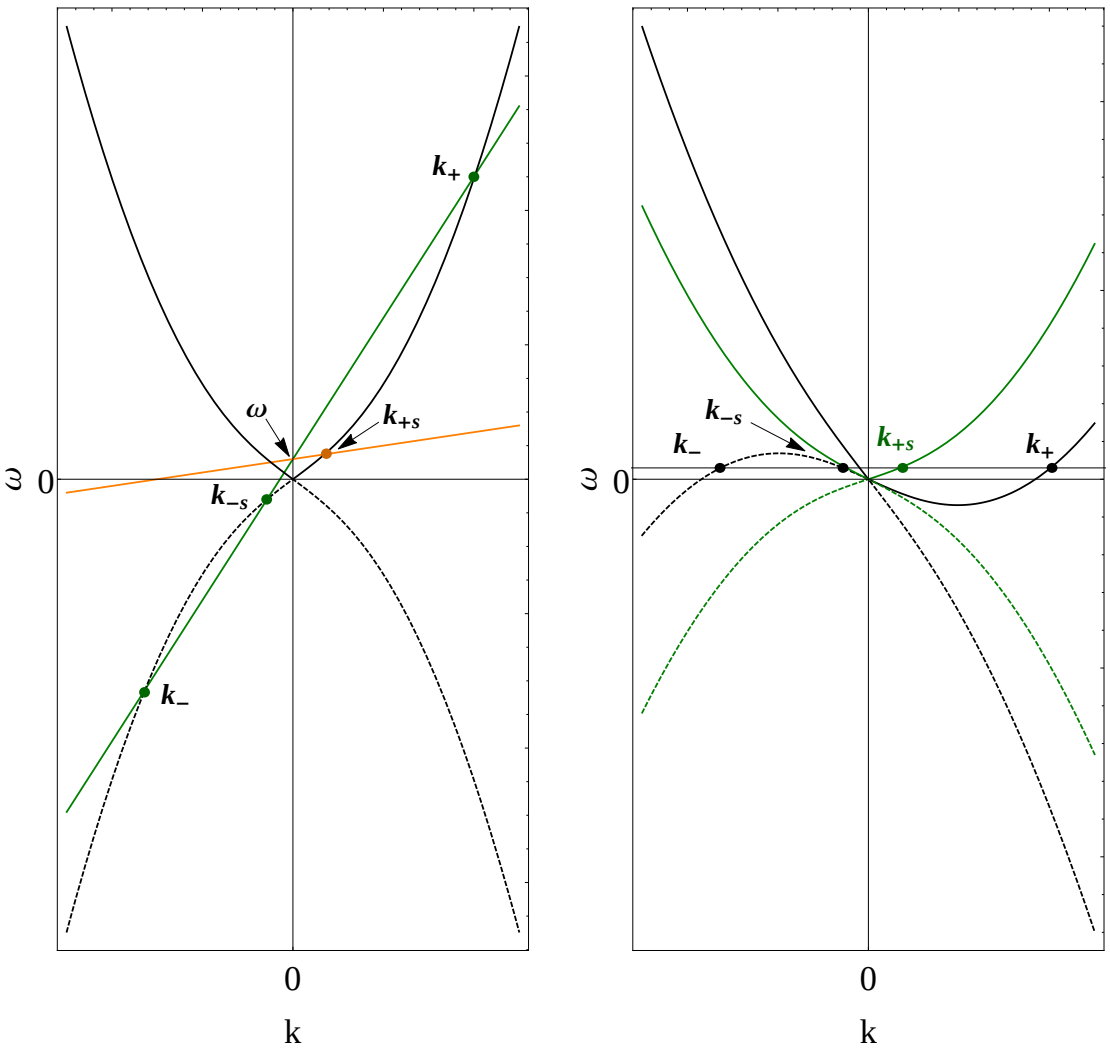

(a) (b)

Figure 7.1: Modes of the superluminal field in the laboratory reference frame. (a) Graphical solution of Eqs. (7.10) and (7.11) in the text. Continuous (dashed) black lines represent the dispersion relation relative to positive (negative) norm solutions, in the co-moving reference frame. The green and yellow straight lines allows for Galilean transformation into the laboratory frame for $|v| > 1$ and $|v| < 1$, respectively. (b) Dispersion relation of the field modes in the laboratory frame, for supersonic (black) and subsonic (green) velocities.

for $(-s)$.

7.2.3 Quantization

In order to identify the amount of particles created by the black hole, we briefly illustrate the quantization procedure of the field. Other than the positive Killing

frequency modes, the positive free-fall frequency modes will also be relevant for the quantization. They are formally defined as solutions of Eq. (7.6) satisfying the relation

$$(\partial_t + v\partial_x)\, f(t,x) = -i\omega' f(t,x), \tag{7.13}$$

with $\omega' > 0$. Positive free-fall or Killing frequency *wave packets* are given by sums of the corresponding solutions.

To quantize the field we assume that $\hat{\phi}(t,x)$ is a self-adjoint operator, solution of Eq. (7.6), satisfying the canonical commutation relations $\left[\hat{\phi}(t,x), \hat{\pi}(t,x')\right] = i\delta(x - x')$, where $\hat{\pi}(t,x) \equiv \delta\mathcal{L}/\delta\,(\partial_t\phi) = (\partial_t + v\partial_x)\,\hat{\phi}$ is the conjugate momentum (density) field. We define the operator $a(f)$ associated to a normalized solution $f(t,x)$ of the wave equation as

$$a(f) \equiv (f, \hat{\phi}). \tag{7.14}$$

Given Eq. (7.14) and the above commutation relation for the field and its conjugated momentum, the commutation relation between annihilation and creation operators of particles respectively in the f and g solution of the field equation, takes the form

$$[a(f), a^\dagger(g)] = (f, g). \tag{7.15}$$

Eq. (7.15) shows that the nature of the $a(f)$ operator depends on the norm of f. For positive norm solutions $a(f)$ behaves as an annihilation operator while, for negative norm solutions instead, it acts as a creation operator, and in particular it is equal to

$$a(f) = -a^\dagger(f^*), \tag{7.16}$$

where $a(f^*)$ is an annihilation operator since f^* has positive norm. The remaining commutation relations read [237, 245, 247]

$$[a(f), a(g)] = -(f, g^*) \qquad [a^\dagger(f), a^\dagger(g)] = -(f^*, g). \tag{7.17}$$

7.3 Lasing mechanism

Retracing the work [237], we present here a qualitative analysis of the propagation of a wave packet in a spacetime of the type described by Eq. (7.2), with $v(x)$ changing

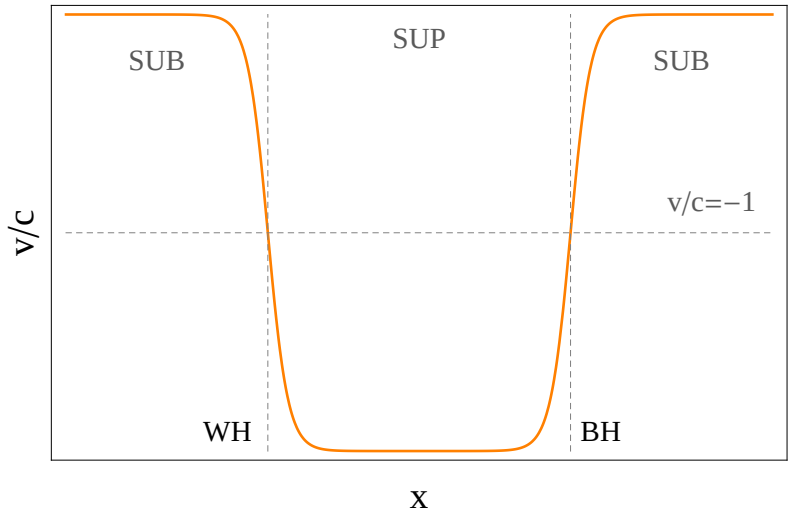

Figure 7.2: Velocity profile $v(x)$ giving rise to a lasing cavity. A supersonic region is enclosed between two subsonic regions and delimited by a white hole and a black hole.

in space in such a way that an outer (black) and an inner (white) horizon are present in the system (see Fig. 7.2). We assume that $v(x)$ changes slowly enough that the wave packet propagation can be described through the WKB approximation. Such a description is valid except in the vicinity of the two horizons, where the WKB approximation breaks-down [237, 245, 247] and mode conversion between positive and negative wave vector branches of the dispersion relation takes place. We aim to demonstrate that, whenever the spacetime is endowed with two horizons, the system is unstable and gives rise to the so-called black hole lasing.

To this aim, we follow the procedure commonly used in the literature on Hawking physics, and trace the evolution of a given final state of the field backward in time. Such backward evolution is depicted in Fig.7.3. Outside the black horizon, the velocity field $v(x)$ is subsonic and, as it can be inferred from Fig. 7.1(a), two field solutions exist with fixed $\omega > 0$. In terms of these solution, the wave packet can be decomposed in general as

$$\phi(x) = a_{+s}\psi_{+s}(x) + a\psi(x). \tag{7.18}$$

Here we indicated by $\psi(x)$ the positive norm mode with negative wave vector. We indicate by ϕ_{out} the final state of the field, which represents the boundary condition of the problem, and we consider given by an outgoing (right-moving) wave packet

prepared in the $(+s)$ branch of the dispersion relation, which leaves the black horizon on the outer side. Such a wave packet is detected at the late times by an observer placed outside far from the outer horizon, and can be regarded as a Hawking particle leaving the black horizon. Far away from the black horizon, in the subsonic upstream region, the field is thus given as

$$\phi_{\rm out}(x) = \psi_{+s}(x). \tag{7.19}$$

Following its evolution backward in time, the packet moves leftward, and approaches the black horizon from the outer side. Getting closer to the horizon, it blue-shifts (its wave vector grows) as the magnitude of v increases and so does the slope of the straight line in Fig. 7.1(a), while the intercept is fixed since the spacetime is stationary and thus ω is conserved during the evolution. Once it reaches the horizon, the packet propagates superluminaly and crosses it, ending up into the + branch of the dispersion relation.

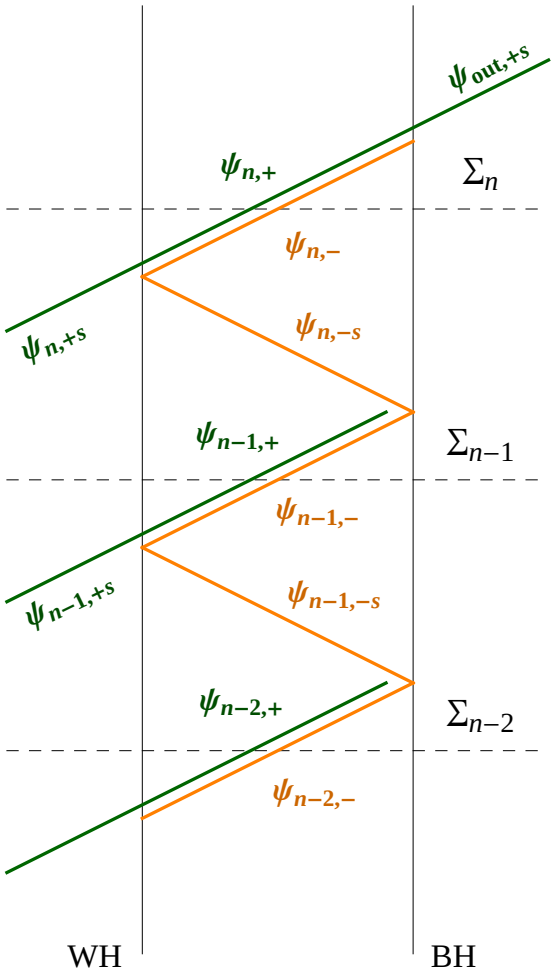

Figure 7.3: Illustration of the lasing mechanism discussed in the text. Green (yellow) lines refer to positive (negative) norm field wave packets.

As it can be seen from Fig.7.4(a), the transition from the outer to the inner side of the black horizon is smooth within the WKB approximation, with the packet remaining in the same (positive wave vector, positive free-fall frequency) branch of the dispersion relation. In the same figure, such smooth evolution is indicated by arrows in the dispersion curve. However, as anticipated above, close to the horizon the WKB approximation breaks-down and mode

conversion from a positive wave vector, positive free-fall frequency, into negative wave vector, negative free-falling frequency modes takes place. Between the two horizons, the velocity field is supersonic, and four field solutions exist. In terms of these solutions, the field can in general be decomposed in this region as

$$\phi(x) = a_+\psi_+(x) + a\psi(x) + a^*_{-s}\psi^*_{-s}(x) + a^*_-\psi^*_-(x). \tag{7.20}$$

Since the final state of the field is a purely outgoing wave packet, only conversion into modes with positive group velocity is allowed. As a consequence, only packets with wave vectors in the branches + and − are created in the region between the horizons. In Figs.7.3 and 7.4, such non-WKB evolution is indicated by a line originating from a point, in contrast to the continuous lines which represent the smooth WKB evolution. We indicate these packets by $\psi_{n,+}$ and $\psi_{n,-}$, where the subscript n is a discrete index having the meaning of time. The field is thus composed by the combination $\phi(x) = a_{n,+}\psi_{n,+}(x) + a^*_{n,-}\psi^*_{n,-}(x)$. Going further backwards in time, they keep propagating leftwards away from the black horizon, until they reach the inner (white) horizon. The group velocity of the $\psi_{n,+}$ packet remains positive across it, and therefore it reaches the region on the left of the horizon in the form of a $\psi_{n,+s}$ packet. Also in this case, partial mode conversion into the $(-s)$ branch of the dispersion takes place, so that a left-moving (in the case of forward in time evolution) packet is generated, which propagates backward in time toward the black horizon. On the other hand, the $\psi_{n,-}$ packet cannot cross the inner horizon where its group velocity drops to zero. It thus remains in the negative wave vector branch and propagates back toward the black horizon as a $(-s)$ packet. Again, partial mode conversion from the negative to the positive wave vector modes occurs, with part of the $\psi_{n,-}$ packet crossing the horizon as a $(+s)$ packet. Combining the contributions from $\psi_{n,+}$ and $\psi_{n,-}$, the state of the field is composed by the $\psi_{n,+s}$ packet emitted in the inner side of the white horizon, which propagates away from it backward in time, and the $\psi_{n,-s}$ packet which propagates instead back towards the black horizon (see Fig. 7.4(b)). When the $\psi_{n,-s}$ packet reaches the black horizon, its group velocity drops to zero and again partial mode conversion to the positive wave vector modes occurs. A pair of $\psi_{n-1,+}$ and $\psi_{n-1,-}$ packets are thus created, which run again towards to the inner horizon (see Fig. 7.4(c)) and the evolution described above repeats.

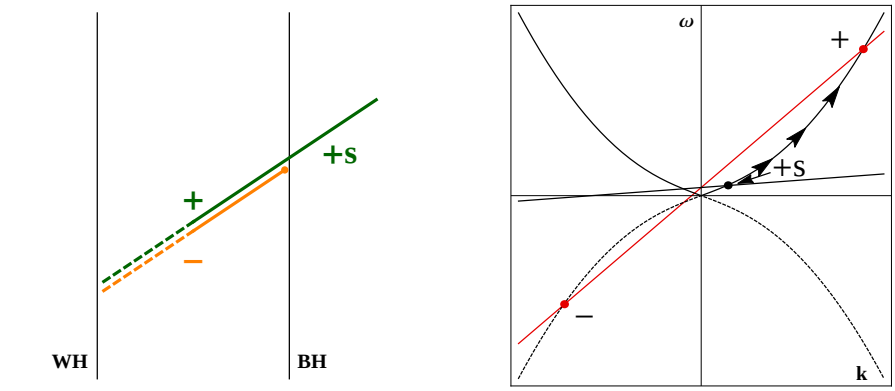

(a)

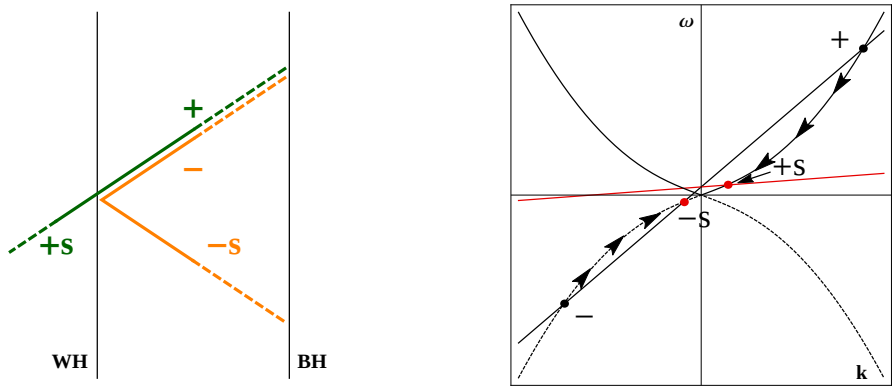

(b)

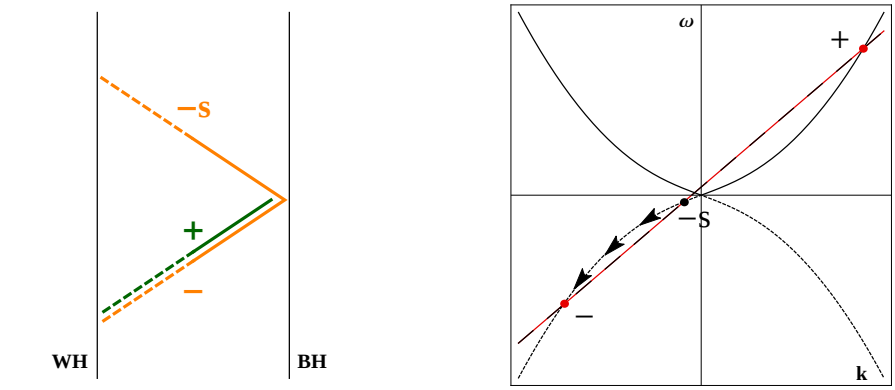

(c)

Figure 7.4: Illustration of the WKB and mode conversion processes involved in the lasing mechanism.

The result of the above analysis is that, because of the superluminal character of the dispersion relation of the field, the wave packet propagates indefinitely backward in time, in a cyclic bouncing of the negative free-fall frequency component of the field back and forth between the two horizons. In order to deduce the (past) fate of the system, we note that the fundamental process of the described cyclic evolution is the transformation of a wave packet $(-s)$ at the generic time step n, into orthogonal $(+s)$ and $(-s)$ packets at the time step $n-1$ (see Fig.7.3):

$$\psi_{n,-s} \to \psi_{n-1,+s} + \psi_{n-1,-s}. \tag{7.21}$$

Since the norm is conserved we have, after one cycle

$$||\psi_{n,-s}||^2 = ||\psi_{n-1,+s}||^2 + ||\psi_{n-1,-s}||^2, \tag{7.22}$$

where we indicated the norm in terms of the inner product as $||f||^2 = (f, f)$. Since a packet belonging to the $(+s)[(-s)]$ branch has positive [negative] free-fall frequency and therefore positive [negative] norm under Eq.(7.7), it follows from Eq. (7.22) that $||\psi_{n-1,-s}||^2$ is larger in magnitude than $||\psi_{n,-s}||^2$. As this process repeats during the (past) evolution, the magnitude of the negative free-fall frequency component of the field between the horizons, as well as of the emitted $(+s)$ component, gets amplified by a fixed amount each cycle, resulting in a exponential amplification in time.

We have thus shown that a so-called *lasing cavity* is created in the system, which is delimited by the two horizons. Here the negative free-fall frequency component of the field experiences an endless exponential amplification, together with the emitted positive free-fall frequency component.

7.4 Particle production

Let us consider now the case of a quantum field. We show in what follows that the quantum counterpart of the black hole lasing instability can be read in terms of spontaneous creation of particles by the double horizons geometry. To this aim, we need to define the state of the field in some space-like hypersurface Σ of the space-time. This would represent the initial condition, to which the particle production is

referred. Since we are interested in spontaneous particle creation (as the Hawking radiation is), we assume that the field is in the free-fall vacuum $|0_\Sigma\rangle$ defined by the condition $a(f)|0_\Sigma\rangle$ for all positive free-fall frequency modes f on the initial time hypersurface. The amount and the nature of the particles created from vacuum, crucially depends on the hypersurface Σ on which the initial condition is posed. We consider first the hypersurface $\Sigma \equiv \Sigma_n$ shown in Fig.7.3. We showed in the previous section that, propagating the final state of the field backward in time, in correspondence of Σ_n, the field is composed by the combination of + and − components: $\psi_{\Sigma_n} = \psi_{n,-} + \psi_{n,+}$ (note that here ψ_{Σ_n} is normalized but $\psi_{n,+}$ and $\psi_{n,-}$ are not). Since the inner product in Eq.(7.7) is conserved in time, we have

$$(\psi_{\text{out}}, \hat{\phi}) = (\psi_{n,-}, \hat{\phi}) + (\psi_{n,+}, \hat{\phi}) \tag{7.23}$$

or, in terms of the annihilation and creation operators defined in Eqs.(7.14) and (7.16)

$$a(\psi_{\text{out}}) = -||\psi_{n,-}||\, a^\dagger(\psi^*_{n,-}) + ||\psi_{n,+}||\, a(\psi_{n,+}). \tag{7.24}$$

Given the Eqs.(7.24) and (7.15), it results that the number of particles created in the final wave packet from the vacuum at the hypersurface Σ_n, is equal to

$$N(\psi_{\text{out}}) = \left\langle 0_\Sigma \right| a^\dagger(\psi_{\text{out}}) a(\psi_{\text{out}}) \left| 0_\Sigma \right\rangle = -||\psi_{n,-}||^2. \tag{7.25}$$

Analogously, if we pose the initial condition on Σ_m instead, with $m < n$, the amount of particles created results in

$$N(\psi_{\text{out}}) = \left\langle 0_{\Sigma_m} \right| a^\dagger(\psi_{\text{out}}) a(\psi_{\text{out}}) \left| 0_{\Sigma_m} \right\rangle = -||\psi_{m,-}||^2. \tag{7.26}$$

Both Eqs. (7.25) and (7.26) show that the amount of particles created is given by the (negative of the) norm of the negative free-fall frequency component of the wave packet. Thus, following the results of the previous section, the number of particles created from vacuum grows exponentially in time. Moreover, because of the multiple bounces that the final state of the system undergoes between the two horizons in its backward evolution, the spectrum of the emitted particles deviates in general from the thermal Hawking prediction [237, 245, 247]. A thermal distribution is found just for the particles that are emitted from a single horizon, that is if we consider the initial conditions to the field on the hypersurface Σ_n. In this case, the norm

of the negative free-frequency packet follows a thermal distribution at the Hawking temperature $T_H = \kappa/2\pi$ where κ is the surface gravity at the horizon. This result is valid for wave packets with Killing frequency $\kappa \leq \omega \ll k_0$ and shows that the standard Hawking effect occurs even in the presence of a superluminal field theory, provided we consider a temperature of the horizon and energies of the field much less than the energy scale at which the new physics appears [237, 245, 247].

Chapter 8 Spin Black hole laser

In this chapter we present a numerical study of the (classical) black hole laser phenomenon in the context of pseudo-spin two-component atomic BECs. See Butera et al. *arXiv:1702.07533* (to appear in Phys. Rev. A). Our goal is to prove the occurrence of the lasing effect in the *spin* modes rather than in the usual *density* modes of the system. The latter are equivalent to the elementary excitations we introduced in Chapter 2 for single component condensates, and represent local oscillations in the density of the total number of particles, while the former are fluctuations in the excess of atoms in one component with respect to the other. As we will show in what follows, this setup brings with itself a number of experimental advantages that are promising, in contrast to standard single-component systems. Despite very recent pioneering first evidence of Hawking particles originating from an analogue black hole in a single component atomic BEC [230] has been claimed, the Hawking radiation is in fact an extremely tiny effect, and its observation is exceptionally challenging also in the framework of ultra-cold gases.

We address the problem using a mean-field approach based on the Gross-Pitaevskii theory, introduced in Chapter 2 for single component condensates. Its generalization to two-component systems is straightforward and will be introduced in this chapter. As we will show, this approach is successful in proving the possibility of achieving, under suitable conditions, a black hole lasing instability in the spin branch of the elementary excitation of the system, and the existence of Hawking conversion phenomena at the horizons. However, it of course fails in describing the quantum features of Hawking emission, when it is triggered by the zero-point fluctuations of the fields. The work presented in this chapter represents a first step towards the study of (spontaneous) Hawking physics in a coherently coupled two-component BEC, which may lead to a more complete understanding of the fundamental quan-

tum aspects of the phenomenon.

We start the chapter in Sec. 8.1 by describing in detail the physical system at hand, and introduce the generalization of the Gross-Pitaevskii theory for a two-component condensate. We will see that a symmetric and a polarized ground state exist for the system, depending on the value of the coherent and collisional interaction parameters. We then discuss the Bogoliubov theory for the elementary excitations showing that, because of the dual component nature of the system, two different branches appear, which are the aforementioned spin and density modes. We will address in Sec. 8.2 a number of experimental considerations, aimed to show the advantages brought by the proposed setup to the investigation of the Hawking physics (and its related phenomena), compared to standard single component condensates. In the following sections we present the main results of the work. Working with an effective one-dimensional uniform condensate, we study first in Sec. 8.3 the propagation of a wave packet, initially prepared in the spin branch of the excitations, when a lasing region is prepared in the system. We will show that all the relevant physics emerges straightforwardly in this case, such as the mode conversion at the two horizons, the self-amplification of the radiation inside the cavity, and the exponentially growing amplitude of the Hawking emission from the cavity.

We will consider in Sec. 8.4 again the uniform system, but with a random noise initially imprinted over its ground state. The aim here is to characterize the strength of the instability in terms of the interaction parameters of the system, which determine the supersonic regime inside the lasing region. We finally discuss in Sec. 8.5 the same physics, but in the experimentally more feasible case of a one-dimensional cloud confined by a harmonic potential. Here we highlight some observable consequences of the higher-order coupling between the spin and the density modes.

8.1 The physical system

8.1.1 Gross-Pitaevskii equations and the ground state

We consider a condensate composed by two-level atoms which are assumed to interact via a spin-dependent s-wave contact interaction, and whose internal states are coherently coupled between each other. Such coupling can be provided for example by an external laser field, as we discussed in the previous sections, which we consider perfectly resonant with the atomic transition for simplicity, and thus described by the Hamiltonian in Eq. (3.21), with $\Delta = 0$. Within the meanfield approximation, the dynamics of the system is described by a generalization of the GP equation (2.13), that takes into account the multiple internal degrees of freedom of the atoms. Two coupled equations arise in our case, for the order parameters ψ_i ($i = a, b$) of the two components, which read [250]

$$i\hbar\frac{\partial\psi_a}{\partial t} = \left[-\frac{\hbar^2}{2m}\boldsymbol{\nabla}^2 + V_{a,\text{ext}}(\mathbf{r}) + g_a|\psi_a|^2 + g_{ab}|\psi_b|^2\right]\psi_a + \kappa\psi_b, \tag{8.1}$$

$$i\hbar\frac{\partial\psi_b}{\partial t} = \left[-\frac{\hbar^2}{2m}\boldsymbol{\nabla}^2 + V_{b,\text{ext}}(\mathbf{r}) + g_b|\psi_b|^2 + g_{ab}|\psi_a|^2\right]\psi_b + \kappa^*\psi_a. \tag{8.2}$$

In Eqs. (8.1) and (8.2) κ is the Rabi frequency defined in Eq. (3.21) (with the factor $\hbar/2$ included into the definition) whose magnitude determines the strength of the coherent coupling, while g_i (with $i = a, b, ab$) are the meanfield interaction parameters relative to the different scattering channels, and are related to the corresponding scattering lengths a_i as $g_i = 4\pi\hbar^2 a_i/m$, with m the mass of the atomic species. Any external confining potentials, selectively applied to the two components, are taken into account by the terms $V_{i,\text{ext}}$ ($i = a, b$). The Eqs. (8.1) and (8.2) can be obtained by extremezing the action $S = \int dtd\mathbf{r}\,\mathcal{L}$, with the Lagrangian density having the form

$$\mathcal{L} = \sum_{i=a,b}\left(-i\hbar\psi_i^*\frac{\partial\psi_i}{\partial t} + |\boldsymbol{\nabla}\psi_i|^2 + V_{i,\text{ext}}\,n_i + \frac{g_i}{2}n_i^2\right) + \sum_{\substack{i,j=a,b\\ i\neq j}}\left(\frac{g_{ij}}{2}n_i n_j + \kappa_i\psi_i^*\psi_j\right), \tag{8.3}$$

where $\kappa_a \equiv \kappa$ and $\kappa_b \equiv \kappa^*$.

In what follows we work in the Thomas-Fermi limit introduced in Chapter 2, according to which the the kinetic energy terms can be neglected in Eq. (8.3). By writing

the order parameters in the Madelung representation as $\psi_j = \sqrt{n_j} e^{i\phi_j}$ $(j = a, b)$, the energy density reads

$$\epsilon = \frac{g_a}{2} n_a^2 + \frac{g_b}{2} n_b^2 + g_{ab} n_a\, n_b + 2|\kappa| \cos\phi \sqrt{n_a n_b} + V_{a,\mathrm{ext}} n_a + V_{b,\mathrm{ext}} n_b - \mu(n_a + n_b), \quad (8.4)$$

where μ is the chemical potential. Here we introduced the phase $\phi \equiv \phi_{ab} + \phi_\kappa$, with $\phi_{ab} \equiv \phi_b - \phi_a$ and ϕ_κ the phase characterizing the coherent coupling $\kappa = |\kappa|\, e^{i\phi_\kappa}$. The energy density in Eq.(8.4) is minimum when $\cos\phi = -1$, that is for $\phi_{ab} + \phi_\kappa = (2n+1)\pi$ with $n \in \mathbb{N}$. In the following we will choose $\kappa < 0$, so that the phase of the two components is the same ($\phi_{ab} = 0$). Given these assumptions, the ground state of the system is obtained by minimizing Eq.(8.4) with respect to variations in the densities n_a and n_b. We consider the fully symmetric case, in which the strength of the mean field interaction parameters between atoms in the same states a and b is the same, as well as the external trapping potential. In these conditions $g_a = g_b = g$ and $V_{a,\mathrm{ext}} = V_{b,\mathrm{ext}} = V_{\mathrm{ext}}$, and we obtain the following equations which define the ground state of the system

$$\left(g - g_{ab} + \frac{|\kappa|}{\sqrt{n_a n_b}} \right) (n_a - n_b) = 0, \quad (8.5)$$

$$\left(g + g_{ab} - \frac{|\kappa|}{\sqrt{n_a n_b}} \right) (n_a + n_b) = 2\,(\mu - V_{\mathrm{ext}})\,. \quad (8.6)$$

From Eq. (8.5) we see that two possible solutions exists, corresponding to the vanishing of one or the other factor in the left-hand-side. By denoting the local density of particles $n = n_a + n_b$ and the population difference $\delta n = n_a - n_b$, these are [250]

$$\text{(GS)}\ \delta n = 0 \qquad (g_{ab} \leq \tilde{g}_{ab})\,, \quad (8.7)$$

$$\text{(GA)}\ \delta n_\pm = \pm n \sqrt{1 - \left(\frac{1 - \tilde{g}_{ab}/g}{1 - g_{ab}/g} \right)^2} \qquad (g_{ab} > \tilde{g}_{ab})\,. \quad (8.8)$$

The *GS* state is symmetric (that is neutral) since there is an equal number of particles in both the internal states, while *GA* is anti-symmetric (or polarized) in the sense that there is an excess of atoms in one of the internal atomic levels with respect to the other. The equilibrium of one or the other state depends on the strength of the inter-species interaction parameter g_{ab} with respect to the critical value $\tilde{g}_{ab} = g + 2|\kappa|/n$. For values $g_{ab} < \tilde{g}_{ab}$ the symmetric state is the true ground state for the system, until a bifurcation occurs at $g_{ab} = \tilde{g}_{ab}$ and the minimum

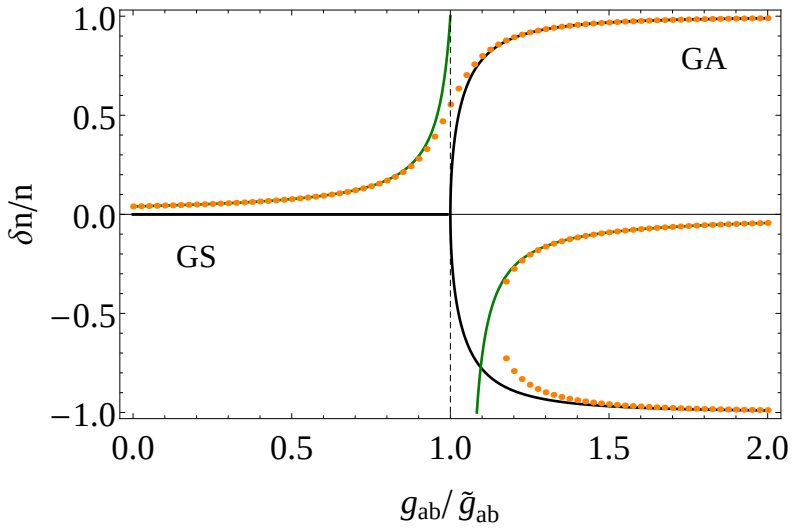

Figure 8.1: Ground state polarization as a function of the inter-species mean field interaction parameter g_{ab}, with a fixed value the value of the Rabi frequency $|\kappa|/gn = 0.1$. The black curves identify the fully symmetric system, for which $\delta g = \delta V_{\rm ext} = 0$. A sharp bifurcation occurs in this case for $g_{ab} = \tilde{g}_{ab}$. The yellow dotted curves show the numerical solution of Eq. (8.10) for the non-symmetric case $\delta g/g = 0.1$, $\delta V_{\rm ext} = 0$. The green curves reproduce the approximate solution in Eq. (8.10).

energy state become polarized (see Fig. 8.1, were the polarization of the system is shown as a function of g_{ab}). This sharp bifurcation characterizes the perfectly symmetric condensate only, and is removed by introducing any kind of asymmetry in the system. This happens for example by choosing different trapping potentials for the two species, that is $V_{a,\rm ext} \neq V_{b,\rm ext}$, and/or a different interaction strength between atoms in the same level a and b, that is $g_a \neq g_b$. Under such conditions, a certain polarization is always present in the system. Taking for example $g_a = g$, $g_b = g + \delta g$ and $V_{a,\rm ext} = V_{\rm ext}$, $V_{b,\rm ext} = V_{\rm ext} + \delta V_{\rm ext}$, the excess of particles δn is found by solving the equation

$$\left(\tilde{g}_{ab} - g_{ab} + \frac{\delta g}{2}\right)\delta n - \frac{\delta g}{2} n + \frac{2|\kappa|}{n}\delta n \left(\frac{1}{\sqrt{1-(\delta n/n)^2}} - 1\right) - \delta V_{\rm ext} = 0, \qquad (8.9)$$

whose numerical solution is shown in Fig. 8.1 for $\delta V_{\rm ext} = 0$, with particular values of the interaction parameters. In the limit $\delta n/n \ll 1$ a simple solution can be found in the form

$$\delta n = \frac{\delta g\, n/2 + \delta V_{\rm ext}}{\tilde{g}_{ab} - g_{ab} + \delta g/2}. \qquad (8.10)$$

Eq. (8.6) provides instead information about the particle density, and yields the TF

profile

$$n(\mathbf{r}) = 2\left(\frac{\mu + |\kappa| - V_{\rm ext}(\mathbf{r})}{g + g_{ab}}\right). \tag{8.11}$$

Here we note that the particle density explicitly depends on the atom-light interaction energy that is, in other words, on the magnitude of the Rabi frequency κ. We will see in Sec. 8.2, and this represents the main advantage of working with two- instead than single-component systems, that such dependence can be removed by working with more complex atomic structures such as the Λ-scheme introduced in Chapter 3. In such a configuration, with suitable choices of the values of the parameters, the density is insensitive to variations in the strength of the coherent coupling and we will show that a lasing cavity for the spin modes can be relatively easily created drastically limiting the onset of spurious excitations in the system.

Working with non-homogeneous systems, it is important to note that the critical value $\tilde{g}_{ab}$ defined above becomes space dependent. It could thus happen that $g_{ab} < \tilde{g}_{ab}$ in some regions of the condensate and $g_{ab} > \tilde{g}_{ab}$ in others. In this case we are in a situation in which both the neutral and polarized phases coexist in the system [250]. Considering a trapping potential with the minimum at $\mathbf{r} = 0$, we work in what follows in the conditions for which $g_{ab} < \tilde{g}_{ab}(\mathbf{r} = 0)$, which guarantees that the entire system is in the symmetric ground state. The reason of this choice is due to the fact that the spin and density branches of the Bogoliubov excitations decouple on a symmetric background, while they hybridize in the case of an asymmetric ground state. This is a condition that we need in order to demonstrate the occurrence of the lasing effect in the spin branch only.

8.1.2 Bogoliubov excitations

We treat the elementary excitations of the system within the Bogoliubov formalism introduced in Chapter 2, and write the order parameters in the form

$$\psi_i = e^{-i\mu t/\hbar}(\psi_{i0} + e^{i\phi_{i0}}\psi_{i1}) \qquad (i = a, b), \tag{8.12}$$

where we indicated by ψ_{i0} and ψ_{i1} the condensed and the excited components respectively. By substituting Eq. (8.12) into Eqs. (8.1) and (8.2), with

$$\begin{pmatrix} \psi_{i1}(\mathbf{r}) \\ \psi_{i1}^*(\mathbf{r}) \end{pmatrix} = \begin{pmatrix} u_i(\mathbf{r}) \\ v_i(\mathbf{r}) \end{pmatrix} e^{-i\omega' t} + \begin{pmatrix} v_i^*(\mathbf{r}) \\ u_i^*(\mathbf{r}) \end{pmatrix} e^{i\omega' t} \quad (i = a, b), \tag{8.13}$$

and retaining terms up to first order in ψ_{i1}, we obtain the eigenvalue problem for the Bogoliubov u_i and v_i functions, and the corresponding spectrum. We consider the simplest case of a homogeneous system ($V_{a,\mathrm{ext}} = V_{b,\mathrm{ext}} = 0$ for example), for which the eigenmodes take the form of plane waves $u_i(\mathbf{r}) = u_i e^{i\mathbf{k}\cdot\mathbf{r}}$, $v_i(\mathbf{r}) = v_i e^{i\mathbf{k}\cdot\mathbf{r}}$, with u_i and v_i constant coefficients. The following results can be extended to non-homogeneous TF condensates, for which the local density approximation can be safely applied. We restrict ourself to the case of a symmetric mean field interaction $g_a = g_b = g$ and consider excitations living on top of a neutral background state, which is characterized by $n_a = n_b = n/2$, $\delta n = 0$. With these assumptions, the Bogoliubov-De Gennes equations take the form

$$\mathcal{L}\mathbf{v} = \hbar\omega'\mathbf{v}, \tag{8.14}$$

where $\mathbf{v} = (u_a, v_a, u_b, v_b)^T$ is the vector collecting the u and v Bogoliubov coefficients, and the Bogoliubov operator $\mathcal{L}$ is defined as

$$\mathcal{L} = \begin{pmatrix} h & \frac{gn}{2} & \frac{g_{ab}n}{2} & \frac{g_{ab}n}{2} \\ -\frac{gn}{2} & -h & -\frac{g_{ab}n}{2} & -\frac{g_{ab}n}{2} \\ \frac{g_{ab}n}{2} & \frac{g_{ab}n}{2} & h & \frac{gn}{2} \\ -\frac{g_{ab}n}{2} & -\frac{g_{ab}n}{2} & -\frac{gn}{2} & -h \end{pmatrix}, \tag{8.15}$$

with $h \equiv \frac{\hbar^2 k^2}{2m} + \frac{gn}{2} + |\kappa|$. Due to the symmetry of the underlying condensate, the excitations decouple into two channels that are the density and the spin branches introduced above. The problem is thus more conveniently written in the density

$\psi_{d1} = (\psi_{a1} + \psi_{b1})/2$ and spin $\psi_{s1} = (\psi_{a1} - \psi_{b1})/2$ basis. An expansion analogous to Eq. (8.13) can be defined for ψ_{d1} and ψ_{s1}, with the density and spin Bogoliubov coefficients u_d, v_d and u_s, v_s related to u_a, v_a and u_b, v_b by

$$u_d = \frac{(u_a + u_b)}{2}, \qquad v_d = \frac{(v_a + v_b)}{2}, \tag{8.16}$$

$$u_s = \frac{(u_a - u_b)}{2}, \qquad v_s = \frac{(v_a - v_b)}{2}. \tag{8.17}$$

In this basis, the full eigenvalue problem in Eq. (8.14) diagonalizes into the two independent sets of equations:

$$\mathcal{L}_d \mathbf{v}_d = \hbar\omega'_d \mathbf{v}_d, \tag{8.18}$$

$$\mathcal{L}_s \mathbf{v}_s = \hbar\omega'_s \mathbf{v}_s, \tag{8.19}$$

where $\mathbf{v}_d = (u_d, v_d)^T$, $\mathbf{v}_s = (u_s, v_s)^T$, and the density and spin Bogoliubov operators are defined respectively as

$$\mathcal{L}_d = \begin{pmatrix} \frac{\hbar^2k^2}{2m} + \frac{n}{2}(g + g_{ab}) & \frac{n}{2}(g + g_{ab}) \\ -\frac{n}{2}(g + g_{ab}) & -(\frac{\hbar^2k^2}{2m} + \frac{n}{2}(g + g_{ab})) \end{pmatrix}, \tag{8.20}$$

and

$$\mathcal{L}_s = \begin{pmatrix} \frac{\hbar^2k^2}{2m} + \frac{n}{2}(g - g_{ab}) + 2|\kappa| & \frac{n}{2}(g - g_{ab}) \\ -\frac{n}{2}(g - g_{ab}) & -(\frac{\hbar^2k^2}{2m} + \frac{n}{2}(g - g_{ab}) + 2|\kappa|) \end{pmatrix}. \tag{8.21}$$

Diagonalization of Eqs. (8.20) and (8.21) yields the spectra for the two branches, which have the form [250]

$$(\hbar\omega'_d)^2 = \frac{\hbar^2k^2}{2m}\left[\frac{\hbar^2k^2}{2m} + (g + g_{ab})n\right], \tag{8.22}$$

$$(\hbar\omega'_s)^2 = \frac{\hbar^2k^2}{2m}\left[\frac{\hbar^2k^2}{2m} + (g - g_{ab})n + 4|\kappa|\right] + 2|\kappa|\left[(g - g_{ab})n + 2|\kappa|\right]. \tag{8.23}$$

The spectrum in Eq. (8.22) is analogous to the result in Eq. (2.40), obtained for the case of a single component condensate, and corresponds to density fluctuations in the system. Here both the g and g_{ab} mean field coupling constants appear, since collisions for particles both in the same and different internal state takes place. Eq. (8.23) gives instead the spectrum of the spin excitations, that are oscillations in the relative population of atoms in different internal state. As usual, in the Bogoliubov formalism, the positive (negative) energy solutions correspond to modes with

the positive (negative) norm defined in Chapter 2, that is $||\psi_{i1}||^2 = \int d\mathbf{r}\,(|u_i|^2 - |v_i|^2)$ $(i = d, s)$.

As can be seen from Fig. 8.2(a), a peculiar feature of the spin spectrum is the

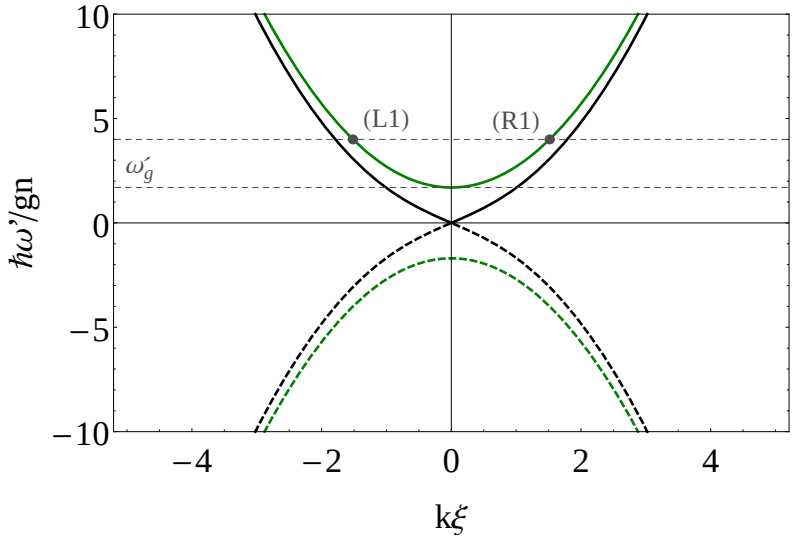

(a)

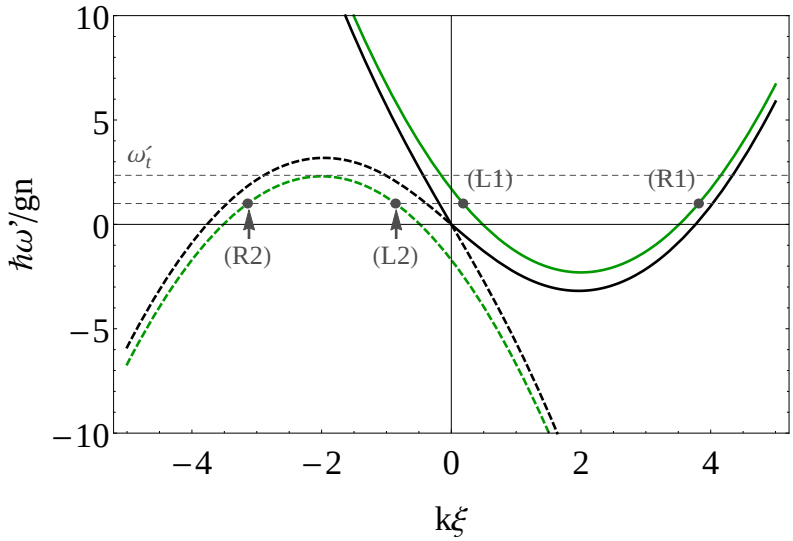

(b)

Figure 8.2: Dispersion relation for the density (black) and spin (green) modes, in the laboratory reference frame. Continuous and dashed curves represent positive and negative norm solutions, respectively. Values of the parameters used: $|\kappa|/gn = 0.8$, $g_{ab}/g = 0.8$. (a) Subsonic (subcritical) case, $v = 0$. (b) Supersonic (supercritical), $2m\xi v/\hbar = -4$.

gap appearing in the low energy limit. This prevents us from introducing a hydrodynamic description for these excitations, since the dispersion relation is not linear

in the long wave length limit and a characteristic propagation speed cannot be defined. As a consequence, the definition of an effective metric for these (massive) quasi-particles, as done in Chapter 2 for phonons, is not obvious [201]. Moreover, the low-energy gap is in principle a drawback for the investigation of the lasing effect in the spin modes, since it makes it more difficult to attain the supersonic regime. However, we shall see in the following that the supersonic regimes for spin modes can still be achieved.

8.1.3 Moving condensates

The spectra in Eqs. (8.22) and (8.23) have been calculated in the reference frame in which the condensate is at rest, that is the frame *co-moving* with the superfluid. In the laboratory reference frame, i.e. the one in which the condensate is seen by static observers as moving with velocity v, the corresponding expressions are obtained by the Galilean transformation

$$\hbar\omega_i = \hbar\omega_i' + \hbar k v \qquad (i = d, s)\,, \tag{8.24}$$

where ω_i is the frequency in the laboratory frame, and ω_i' is the corresponding value in the co-moving frame, given by Eqs. (8.22) and (8.23). In this reference frame, we say that the superfluid is moving supersonically (subsonically) with respect to the density modes, when the magnitude $|v|$ of its background velocity exceeds (is smaller than) the local speed of sound, which is defined as $c_d = \lim_{k\to 0}\omega_d(k)/k = \sqrt{(g+g_{ab})\,n/2m}$. The corresponding regimes for the spin modes can be defined by adopting a more general definition according to which, in the supersonic regime, there exist modes with positive (negative) norm having a negative (positive) energy in the laboratory frame. Conversely, in the subsonic regime, modes with positive (negative) norm can only have positive (negative) energy in the laboratory frame. This definition coincides with the one reported above for the density modes, and gives the *critical* velocity

$$v_{\rm cr} = \left\{ \frac{\hbar^2}{2m}\left[(g-g_{ab})\,n + 4|\kappa|\left(1+\sqrt{1+\frac{(g-g_{ab})n}{2|\kappa|}}\right)\right]\right\}^{1/2}, \tag{8.25}$$

for the spin excitations. The relation between the particular hydrodynamic regime and the properties of the excitations modes stated above, can be inferred by comparing Fig. 8.2(a) and Fig. 8.2(b), where the density and spin spectra are shown for a condensate moving in the laboratory frame with supersonic (or supercritical in the case of spin modes) speed. From the same figures we see that the number and the type of solutions to Eq. (8.24) strictly depends on the hydrodynamic regime. In particular, for the spin branch, whenever the flow is subcritical, two positive (negative) norm solutions exist with wave vectors $k = k_{R1}$ and $k = k_{L1}$ for each $\omega > \omega_g$ ($\omega < -\omega_g$), where ω_g is a threshold value equal to the size of the gap of the dispersion relation when $v = 0$. The labels R and L we used in the above definitions, indicate solutions with positive (right-moving solutions) or negative (left-moving solutions) group velocity $v_g = d\omega/dk$ in the laboratory frame. Since the dispersion relation is of fourth order in k, two other complex solutions exist, conjugated to each other, which represent exponentially growing or decreasing evanescent waves and are thus unable to sustain a propagating particle. If the flow is supercritical instead, the scenario is much richer since for $|\omega| < |\omega_t|$, with ω_t a threshold value which depends on the strength of the supersonic regime, two additional positive (negative) norm propagating solutions appear with negative (positive) frequency $\omega < 0$ ($\omega > 0$), indicated in Fig. 8.2(b) as $R2$ and $L2$. The appearance of these extra solutions is exactly what makes the onset of the Hawking physics possible, as pairs of particles with opposite energy can be created in such conditions, while conserving the total energy of the system. The same considerations apply to the density branch, with the difference that, in such a case, $\omega'_g = 0$ since the dispersion relation is not gapped.

8.2 Experimental considerations

8.2.1 Λ-level atomic scheme

The discussion in the previous section gives a hint on the techniques that could be used in order to create effective horizons in a condensate. What we need is to make the velocity of the superfluid exceeding a certain critical velocity, which is the speed of sound for the density modes or the velocity in Eq. (8.25) for the spin modes. To this aim, we can either change in space the former, by opportunely designing the

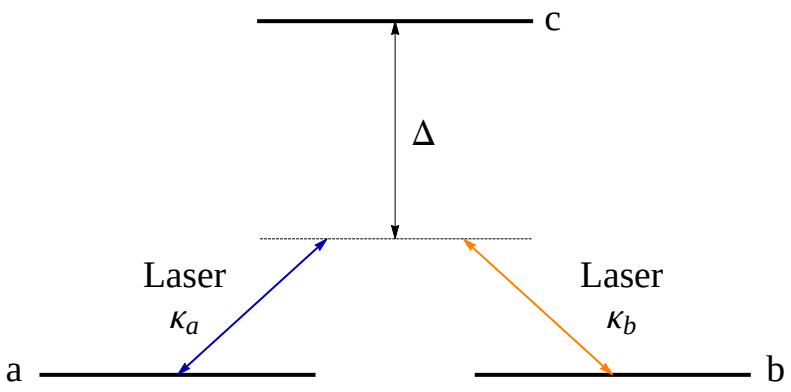

Figure 8.3: Resonant Raman coupled Λ-level atom.

trapping potentials in order to accelerate part of the superfluid up to supersonic speed [223, 230, 246], or modulate in space the latter. Working with the density modes, this can be accomplished by locally modifying the speed of sound by tuning the mean field interaction constants g and g_{ab}. This can be done by exploiting for example Feshbach resonances in order to modify the scattering lengths of the atomic interactions. In the case of spin modes instead, the supercritical regime can be attained by locally modifying the gap in the dispersion relation. This can be done by tuning the magnitude of the Rabi frequency κ, which is the amplitude of the field which couples the internal states of the atoms. It is in this respect that the investigation of the Hawking physics in a two-component system brings the main advantages. As can be seen from Eq. (8.11), the a posteriori local modification of the interaction parameters induces an inhomogeneity in the chemical potential and, consequently, the onset of spurious excitations in the condensate, which could overwhelm the Hawking signal and, for the case here addressed, the self-amplification mechanism of black hole lasing. This effect could be in principle compensated by suitably tailoring external potentials $V_{\rm ext}(\mathbf{r})$, a task that is exceptionally challenging as it requires an extreme fine tuning of the experimental parameters.

This difficulty can be overcome by working with the spin modes of a condensate, once we replace the simple two-level atomic configuration discussed so far, with the Raman-coupled Λ-scheme for the atomic levels introduced in Chapter 3 and reported here in Fig. 8.3. We show in the following that the effective Hamiltonian describing the ground subspace projection of the internal dynamics of the atoms, naturally allows us to compensate any inhomogeneity in the chemical potentials

due to a spatial dependence of the coherent coupling strength. For simplicity, and without affecting the generality of the following arguments, we consider the case of a two-fold degenerate ground manifold spanned by the $\{|a\rangle, |b\rangle\}$ states, each of them we assume coupled to the excited state $|c\rangle$ by a far off-resonant electromagnetic field of Rabi frequency κ_a and κ_b respectively, and detuned by Δ from the atomic resonance. With this choice of the parameters, the Raman transition between the ground states $|a\rangle$ and $|b\rangle$ is resonant, that is $\delta = 0$ (see Chapter 3).

The operator describing the internal coupling between the atomic levels has been introduced in Chapter 3 and reads

$$U_\Lambda = \kappa_a |c\rangle\langle a| + \kappa_b |c\rangle\langle b| + \kappa_a^* |a\rangle\langle c| + \kappa_b^* |b\rangle\langle c|. \tag{8.26}$$

To derive the effective ground state dynamics, we start from the Schrödinger equation describing the full internal dynamics of the atoms, which reads

$$\left[H_0 + U_\Lambda\right] |\psi\rangle = E|\psi\rangle. \tag{8.27}$$

Here we indicated by $H_0 = \Delta\, |c\rangle\langle c|$ the free atomic Hamiltonian (see Eq. (3.30) with $\delta = 0$ in the present case), and by $|\psi\rangle = \sum_{i=a,b,c} c_i |i\rangle$ the generic internal state of the atom, with energy E. By projecting Eq. (8.27) onto the excited state (via the projector $Q \equiv |c\rangle\langle c|$) and onto the ground state manifold (via the projector $P \equiv |a\rangle\langle a| + |b\rangle\langle b|$), we get the coupled equations

$$H_0 \left(Q|\psi\rangle\right) + Q U_\Lambda P \left(P|\psi\rangle\right) = E \left(Q|\psi\rangle\right), \tag{8.28}$$

$$H_0 \left(P|\psi\rangle\right) + P U_\Lambda Q \left(Q|\psi\rangle\right) = E \left(P|\psi\rangle\right), \tag{8.29}$$

having used the properties of the projectors

$$P = P^\dagger, \qquad P^2 = P, \tag{8.30}$$

$$Q = Q^\dagger, \qquad Q^2 = Q. \tag{8.31}$$

By solving for $(P|\psi\rangle)$ from Eq.(8.29), and substituting into Eq.(8.28), we get the energies of the interacting system. Because of the far off-resonance nature of the coherent coupling to the $|c\rangle$ state, the interaction U_Λ can be treated as a small perturbation with respect to the free Hamiltonian H_0. In other words this means

considering $|\kappa_a|, |\kappa_b| \ll \Delta$ so that, to the first order, the perturbed energies reads

$$E_+ = \Delta + \Delta E, \tag{8.32}$$

$$E_- = -\Delta E, \tag{8.33}$$

where $\Delta E = \left(|\kappa_a|^2 + |\kappa_b|^2\right)/\Delta$ is the first order correction due to the coherent coupling. Conversely, we can solve for $(Q|\psi\rangle)$ from Eq. (8.28) and substitute the result into Eq. (8.29), obtaining the projection of the Schödinger equation onto the ground subspace, which reads

$$\left[H_0 + U_{\text{eff}}\right](P|\psi\rangle) = E\,(P|\psi\rangle)\,, \tag{8.34}$$

with

$$U_{\text{eff}}(E) = (PU_\Lambda Q)\,\frac{1}{E - H_0}\,(QU_\Lambda P), \tag{8.35}$$

the energy dependent effective coupling Hamiltonian. Eq. (8.35) is still exact at this stage. By evaluating it for the unperturbed ground energy $E = 0$, we finally get the effective coupling Hamiltonian up to second order in U_Λ

$$U_{\text{eff}}(E_0) = \left[\frac{|\kappa_a|^2}{-\Delta}|a\rangle\langle a| + \frac{|\kappa_b|^2}{-\Delta}|b\rangle\langle b| + \frac{\kappa_a^*\kappa_b}{-\Delta}|a\rangle\langle b| + \frac{\kappa_a\kappa_b^*}{-\Delta}|b\rangle\langle a|\right]. \tag{8.36}$$

The Eq. (8.36) describes the effective interaction between the internal levels $|a\rangle$ and $|b\rangle$, mediated by their coupling with the excited state $|c\rangle$. It shows the same type of non-diagonal terms as in Eq. (3.30), with κ replaced by the combination $-\kappa_a\kappa_b^*/\Delta$. Moreover, diagonal terms appear that were not present in the simple two-level model, and that represent the main advantage in considering the atomic Λ-configuration instead of the simpler two-level scheme. These terms have the role of extra potentials, and can be used to balance an eventually inhomogeneous spatial profile of the Rabi frequencies, in order to maintain the value of the chemical potential constant through the system. This prescription can be accomplished for example by considering the real and equal amplitudes for the Rabi frequencies $\kappa_a = \kappa_b = \tilde{\kappa}$. In this case, the effective coherent coupling takes the form $\kappa = -\tilde{\kappa}^2/\Delta$, which is the same as the extra potential term for both the $|a\rangle$ and $|b\rangle$ atomic states. Inserting these quantities into Eq.(8.11), we see that the two contributions cancel out and the chemical potential no longer depends on the coherent coupling. As a consequence, any inhomogeneity in the Rabi frequency, introduced in order to create a supercrit-

ical region for the spin modes of the condensate, does not modify the local value of the chemical potential, which remains constant through the system.

8.2.2 Efficiency of the mode conversion

A further issue concerning the experimental investigation of the Hawking physics in the spin modes of a two-component condensate is related to the efficiency of the mode conversion at the horizons between the positive and negative norm modes. The efficiency of such a process is related to the strength of the off-diagonal coupling in the Bogoliubov operator for the spin excitations in Eq.(8.21), which is proportional to the difference $g-g_{ab}$ between the interaction parameters for atoms in the same and different internal states. For typical atoms used in modern cold-atoms experiments, such values are close to each other. In Rb^{87} for example, the relevant scattering lengths are such that $g_{ab} \approx 0.97\, g$ [251]. Because of this reason, the mode conversion at the horizons is strongly attenuated, practically inhibiting any possible observation of the lasing phenomenon, or any other effect related to the Hawking physics.

Higher values of $|g - g_{ab}|$ can be attained for example by exploiting Feshbach resonances, in order to modulate the relative value of the cross-state versus same-state scattering lengths. Another method that could be pursued consists in using three different one-dimensional atomic clouds condensed in three parallel potentials of the type depicted in Fig.8.4. In this configuration the coherent coupling is provided by the hopping of particles from the clouds a and b into c, a process that could even be artificially assisted, for example by using a laser field, if necessary. The contact interaction between particles in a and b is due to the superposition of the two condensate wave functions, and is thus much weaker than the contact interaction between particles in the same cloud, that is $g_a, g_b \gg g_{ab}$. However, the lasing mechanism will not be affected since, as noticed, the relevant quantity in this case is the difference $g - g_{ab}$. A lasing region can be prepared with this set-up by tuning in space the hopping strength. This can be done by suitably tailoring the spatial profile of the coupling fields and/or the geometry of the potentials, varying the distance between the atomic guides a and b or changing the height of the potential which confines the cloud c.

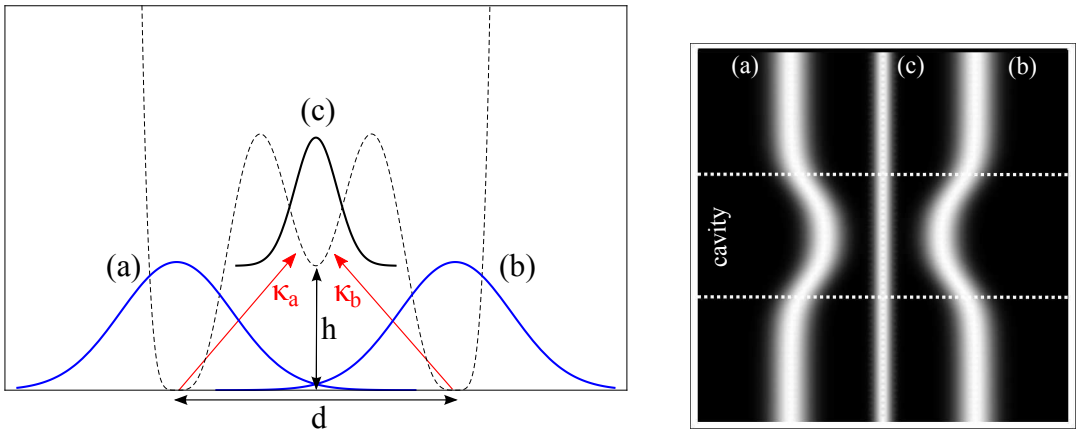

(a) (b)

Figure 8.4: Coherently coupled Λ-scheme implemented with three atomic clouds in elongated potentials. The coupling is provided by the hopping of atoms from the clouds a and b into c, whose strength can be controlled by modulating the horizontal d and/or vertical h distance between the clouds. a) Cross-section, b) top-view of the experimental setup.

8.3 Wave packet propagation

In this section we show how the black hole lasing comes about in the spin modes of a two-component condensate. We perform numerical simulations for a one-dimensional system, which represents the simplest configuration useful to investigate the lasing phenomena. As already mentioned in the previous chapters, effective one-dimensional configurations can be experimentally realized by tightly confining an atomic cloud in the transverse direction, in order to freeze-out the corresponding atomic degree of freedoms. In these quasi-one-dimensional systems, the interaction between particles preserves a three-dimensional character, even though the effective kinematic is one-dimensional.

We start by discussing the propagation of a (spin) wave packet through an infinite untrapped condensate. In the numerical simulations we model such a system as a ring with periodic boundary conditions, in which an absorbing region has been implemented, where all the excitations on top of the condensate are suppressed. This prescription allows us to avoid interference effects between packets traversing the ring, effectively simulating a spatially unbounded system.

We prepare a lasing cavity for the spin excitations only, by modulating the strength of the coherent coupling in space, i.e. the spatial profile of the Rabi frequency κ, keeping the values of g and g_{ab} fixed. Here we use the simplest configuration, involving a piece-wise constant profile, and choose the values of κ in such a way that the spin modes attain the supercritical regime in a finite region (the lasing cavity), while they are subcritical elsewhere. Following the consideration in Sec. 8.2, we included in the simulation the potential terms needed to compensate the resulting inhomogeneity in the chemical potential.

In the following, we investigate the dynamics of the system both in the absence and in presence of the lasing conditions, in order to emphasize the different behaviour in the two situations. In the former case we observe standard scattering phenomena because of the discontinuities in the Rabi frequency profile, which is the emission of transmitted and reflected components. The physics in the latter case is instead much richer, because of the appearance inside the cavity of negative norm solutions with positive energy, and the onset of the lasing instability. As we will see, the early time dynamics shows the conversion between positive and negative norm packets (and vice versa) at the BH and WH horizons. At late times instead, the appearance of unstable modes in the cavity dominates the scene, resulting in the exponential amplification of the field, and of the emitted Hawking radiation.

For the sake of generality, we express the results of the simulations in the dimensionless units $\bar{L} = L/\xi$, $\bar{t} = \hbar t/(2m\xi^2)$, $\bar{\omega} = \hbar\omega/gn$ and $\bar{n} = n\xi$ for lengths, time, energy and density respectively. Here we took as reference value for lengths the healing length $\xi = \sqrt{\hbar^2/2mgn}$, where by g is hereafter meant the effective one-dimensional mean field coupling constant. It is defined in terms of the corresponding three-dimensional value g_{3d} and the effective transverse area S_t of the cloud as $g = g_{3d}/S_t$. The following simulations have been run considering a condensate of $N = 10^3$ atoms, leftward flowing through a ring of length $\bar{L} = 1000$. The initial state of the condensate is characterized by a linear phase profile $\theta(\bar{x})$, which is equal for both the components, and characterized by the winding number $w = \left[\theta(\bar{L}) - \theta(0)\right]/2\pi = 90$. For standard condensates of atoms with masses of the order $m \sim 10^{-25}$ Kg and $\xi \sim 1\mu$m, this value corresponds to a physical flow velocity v of the order $v \sim 1\,$mm/s. The value for the (dimensionless) meanfield coupling strength we used is $g_{ab}/g = 0.8$.

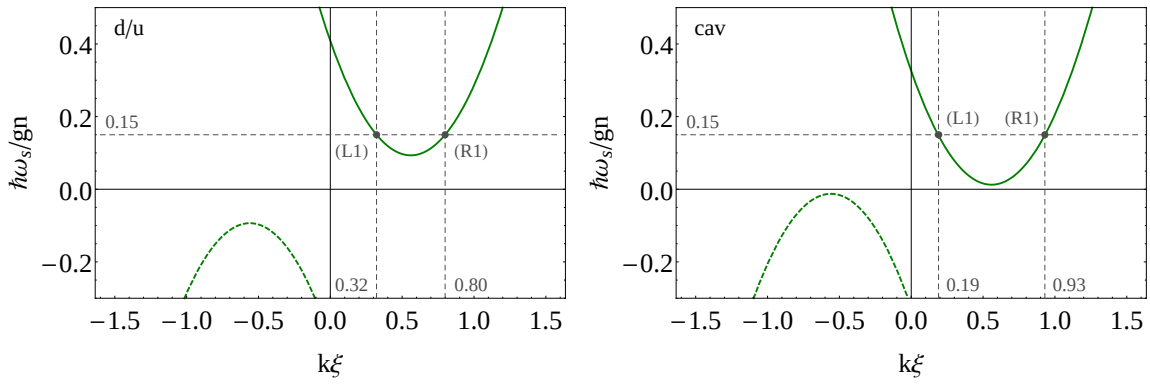

(a) (b)

Figure 8.5: Spin-modes dispersion relations: non-lasing configuration. (a) Downstream and upstream regions: $\kappa/gn = -0.16$, $g_{ab}/g = 0.8$. (b) Cavity region: $\kappa/gn = -0.12$, $g_{ab}/g = 0.8$.

8.3.1 Non-lasing regime

We start by discussing the simpler non-lasing case. The Figs. 8.5(a,b) show the dispersion relations of the spin modes, relative to the values $\bar{\kappa} = -0.16$ and $\bar{\kappa} = -0.12$, that we choose respectively inside and outside the cavity region. The latter is $\bar{L}_c = 79$ long and located around $\bar{x} = 500$, while the absorbing region has been designed around the edges of the ring at $\bar{x} = 0$ and $\bar{x} = 1000$. We solved the time evolution of the system by implementing a step-by-step integration of the GP equations (8.1) and (8.2), using the time-splitting method, and solving the kinetic terms by the iterated Crank-Nicholson algorithm. We discretize the space domain with a grid of 1024 points and chose the time step $\Delta\bar{t} = 0.001$ which guarantees the numerical stability of the integration scheme.

We take as initial condition of the simulation, at $\bar{t} = 0$, a spin wave packet living on top of the homogeneously flowing condensate described above (see Fig. 8.6(a)), and located in the downstream region on the left of the cavity. Such a packet is composed by wave vector components Gaussian distributed around the value $\bar{k} \equiv k\xi = 0.80$, with width $\Delta\bar{k} = 0.04$, in the *d-R1* branch of the dispersion relation (hereafter we will add the prefixes *d, u, cav* to the mode labels, in order to identify the downstream, upstream and cavity regions of the system to which they refer). The group velocity of the packet is positive in the laboratory frame, and propagate rightwards towards the cavity. Its energy is $\bar{\omega} = 0.15$ in the laboratory frame.

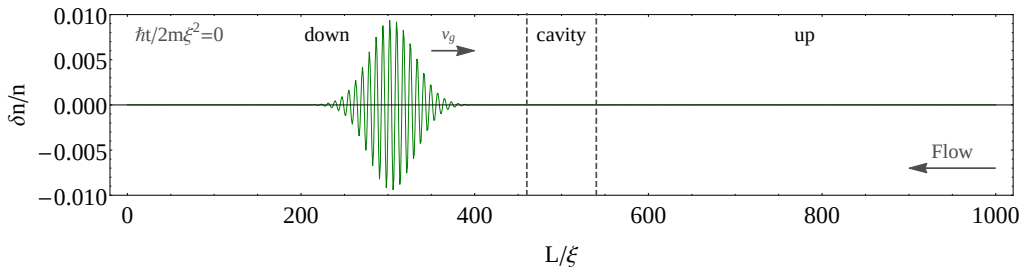

(a)

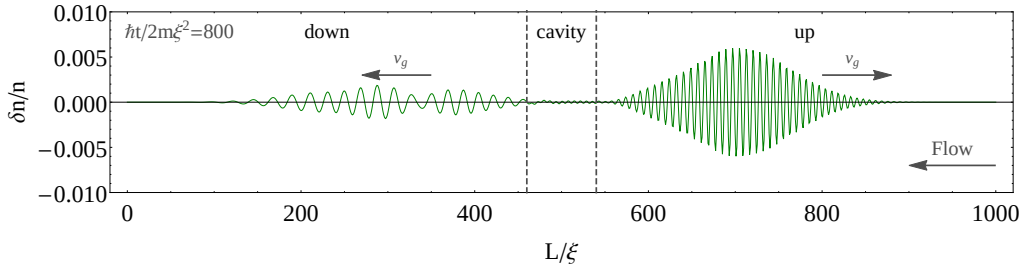

(b)

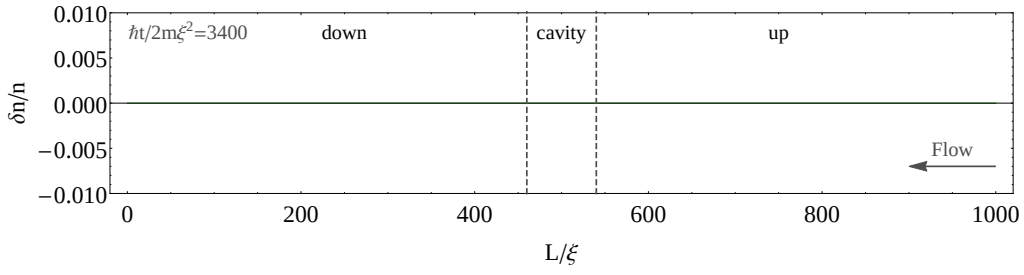

(c)

Figure 8.6: Wave packet propagation in the real space, for the non-lasing configuration of the system defined by the set of parameters given in the text. The dashed lines enclose the cavity region. (a) Initial condition of the simulation. (b,c) State of the spin density respectively at $\hbar t/2m\xi^2 = 800$ and 3400.

We report the result of the simulation both in the physical and in the wave vector domains. From the state of the system in the real space, reported in Figs. 8.6(b,c) respectively at the time instants $\bar{t} = 800$ and $\bar{t} = 3400$, which in real units correspond to $t = 16\,\mathrm{ms}$ $t = 68\,\mathrm{ms}$ for the condensate parameters mentioned before, we clearly see the absence of the lasing instability. Fig. 8.6(b) show the propagation of the components transmitted and reflected by the cavity, respectively in the upstream and downstream regions, with a residual component still present inside the cavity. At the late time instead (Fig. 8.6(c)) no excitations are left in the system, since all the wave packets have been annihilated by the absorbing region. More information about the processes involved can be gained from the evolution of the system in the

wave vector domain, reported in Figs. 8.7(a-c). Here we show the time evolution of the spatial Fourier transform of the spin density δn respectively in the downstream, cavity and upstream regions. Since the density is a real quantity, the negative and positive wave vector regions of the Fourier transform carry the same information, being one the complex conjugate of the other: $\delta n(-k) = \delta n^*(k)$. For this reason, we just report the positive ($k > 0$) Fourier components.

By inspection of the dispersion relations in Figs. 8.5(a,b), we deduce the expected central wave vectors components for the transmitted and reflected packets in the regions inside and outside the cavity. Since the frequency in the laboratory frame is conserved in time, such wave vectors are given by the spin modes with $\bar{\omega} = 0.15$ which comply with the boundary conditions (that is a rightward propagating packet, located in the downstream region at $\bar{t} = 0$). These modes are identified by dashed lines in Figs. 8.7(a-c), and match the results of the simulations. Fig.8.7(a) shows the initial wave packet in the *d-R1* mode, which is visible up to time $\bar{t} \approx 300$ at which it enters into the cavity with the simultaneous emission of a leftwards propagating reflected *d-L1* packet, which in turns disappears around $\bar{t} \approx 1500$ annihilated by the absorbing region close to $\bar{x} = 0$. Fig.8.7(b) reports the wave vector content of the field inside the cavity, and shows at $\bar{t} \approx 300$ the appearance of the wave packet transmitted from the downstream region. It is localized in the *cav-R1* branch of the dispersion relation, and propagates rightwards towards the up-stream region, until it gets reflected, around $\bar{t} \approx 450$, by the right edge of the cavity, onto the *cav-L1* branch. This latter component is too weak for being visible in the figure, but it can be recognized in the cut shown in fig.8.8(d). Fig.8.7(c) finally shows the wave vector content of the spin density in the up-stream region. Here we see, at $\bar{t} \approx 450$, the wave packet transmitted by the cavity, which is annihilated by the absorbing regions at $\bar{t} \approx 1400$. Figs.8.8(a-d) finally show the plots of the spatial Fourier transform of the spin density at the time instants indicated in Figs. 8.7(a-c), in order to provide a clearer comparison between the observed and the expected radiation content.

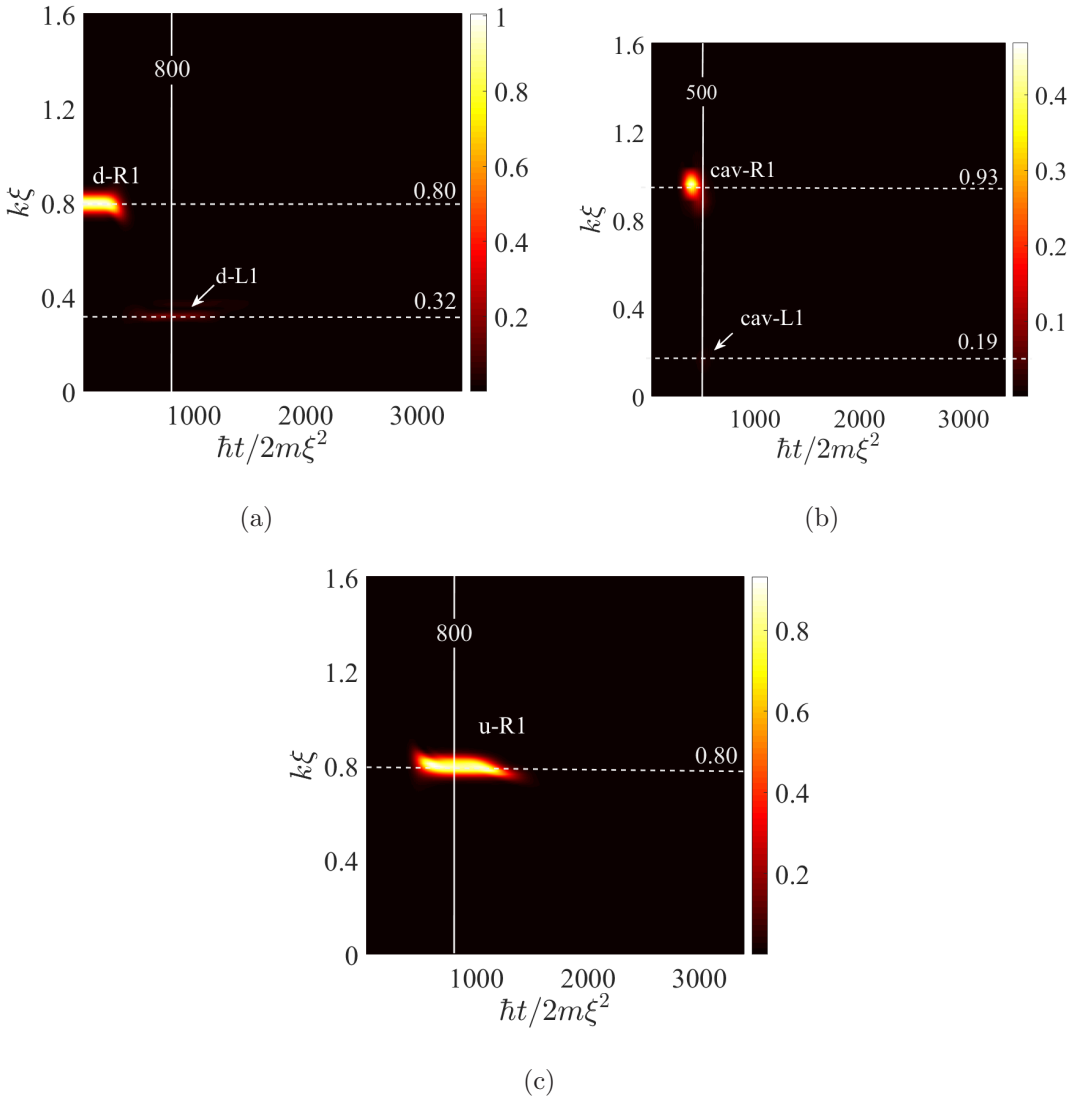

Figure 8.7: Wave packet propagation in the wave vector domain, for the non-lasing configuration of the system defined by the set of parameters given in the text. (a) *Downstream region.* The *d-R1* wave vector components of the initial wave packet are clearly visible. The *d-L1* components corresponding to the wave packet reflected by the WH are barely visible and indicated by an arrow. (b) *Cavity region.* The *cav-R1* and *cav-L1* wave packets, transmitted through the WH horizon and reflected by the BH horizon respectively. The latter is indicated by an arrow and is barely visible in the figure. (c) *Upstream region.* The *u-R1* packet transmitted through the cavity.

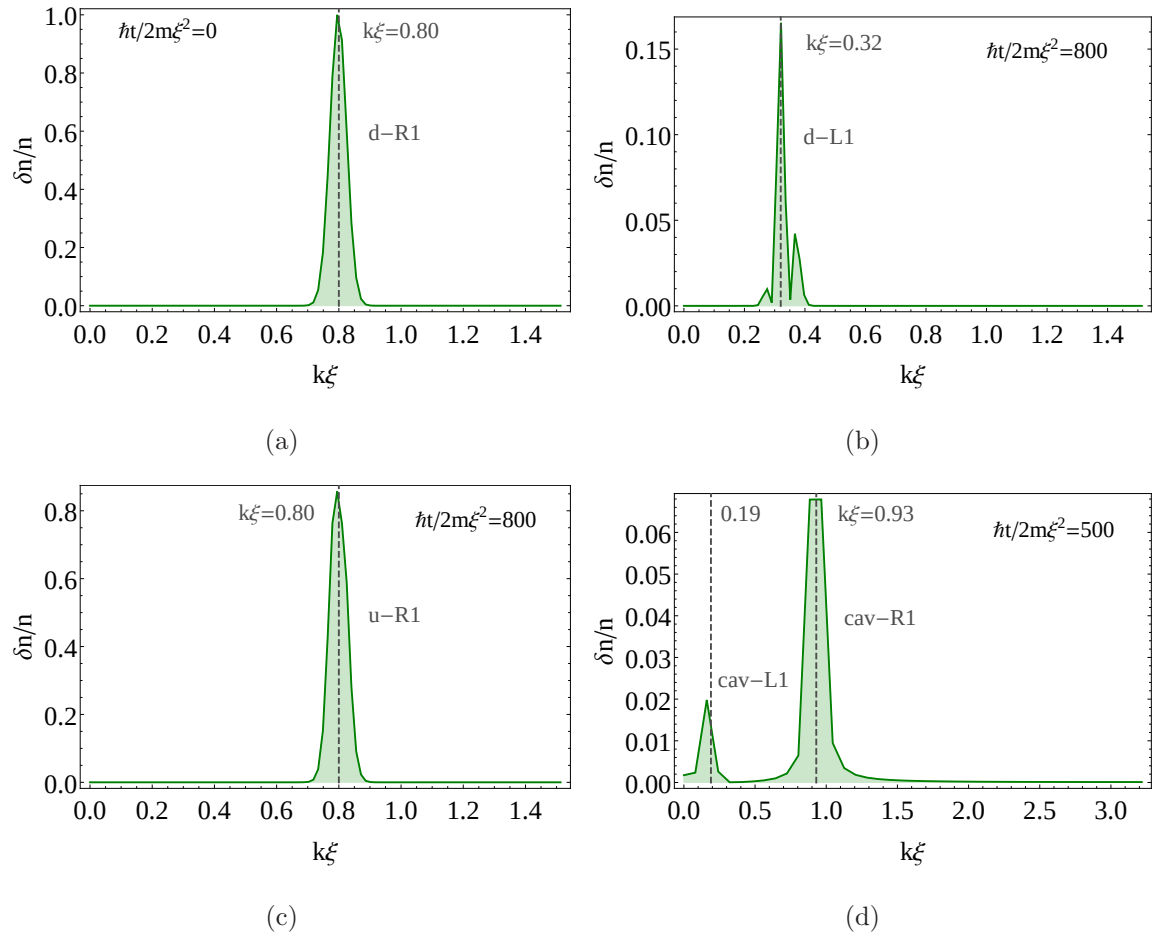

Figure 8.8: Non-lasing configuration. Wave vector content of the spin density of the system, at the time instants indicated in Figs. 8.7(a-c) by the vertical lines. In the figures, the dashed lines indicate the central wave vector expected by inspection of the dispersion relations shown in Figs. 8.5(a) and 8.5(b). (a,b) *Downstream region.* a) Initial condition of the simulation, b) $\hbar t/2m\xi^2 = 800$, wave packet reflected by the WH horizon. (c) *Upstream region.* $\hbar t/2m\xi^2 = 800$, wave packet transmitted through the cavity. (d) *Cavity region.* $\hbar t/2m\xi^2 = 500$, wave packets transmitted through the WH and reflected by the BH horizon.

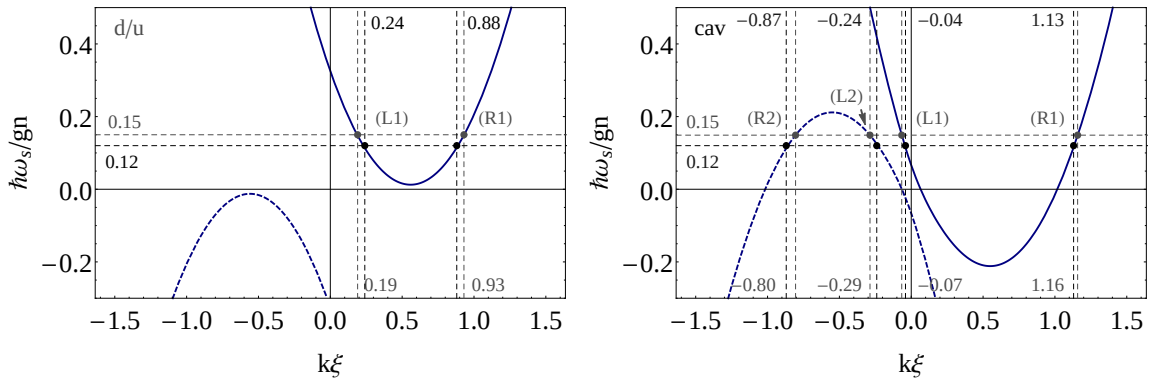

(a) (b)

Figure 8.9: Spin-modes dispersion relations: lasing configuration. (a) Downstream and upstream regions: $\kappa/gn = -0.12$, $g_{ab}/g = 0.8$. (b) Cavity region: $\kappa/gn = -0.01$, $g_{ab}/g = 0.8$.

8.3.2 Lasing regime

We consider here the same system as before, given the values $\bar{\kappa} = -0.01$ and $\bar{\kappa} = -0.12$ for the coherent coupling strength inside and outside the cavity respectively. We see from the dispersion relations in Figs. 8.9(a,b) that the cavity region is supercritical in this case and is delimited by a WH horizon on the downstream side and a BH horizon on the upstream side. The downstream and upstream regions are still subcritical, and the instability is expected to arise. We study the propagation of a wave packet, initially located again in the downstream region, and prepared in the *d-R1* branch of the subsonic dispersion relation with wave vector content centred on the value $\bar{k} = 0.93$. Its group velocity is positive in the laboratory frame, and propagates rightwards towards the WH horizon. The energy is again equal to $\bar{\omega} = 0.15$. As before we reported the results of the simulation both in the physical (Fig. 8.10) and the wave vector (Fig. 8.11) domains. With respect to the previous section, novel phenomena arise in the present case because of the presence inside the cavity of negative norm modes with the same energy $\bar{\omega} = 0.15$. Colliding with the WH horizon, the wave packet gives rise to a reflected component propagating leftwards back into the downstream region as a *d-L1* packet, and a transmitted components propagating rightwards through the cavity, towards the BH horizon, on the *cav-R1* branch. At the same time, mode conversion takes place at the WH horizon, generating a negative norm *cav-R2* transmitted component, propagating rightwards along the cavity towards the BH horizon. The same type of processes take place

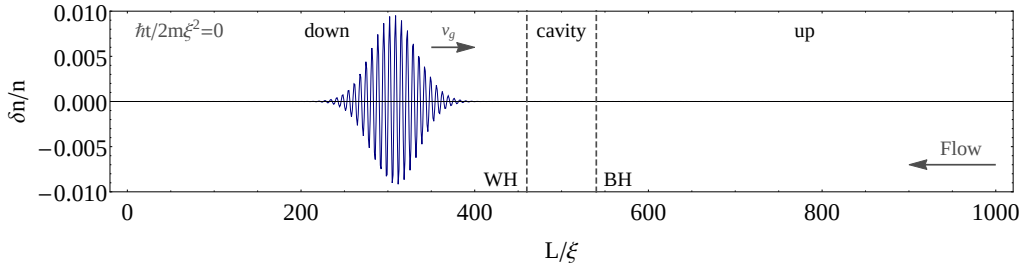

(a)

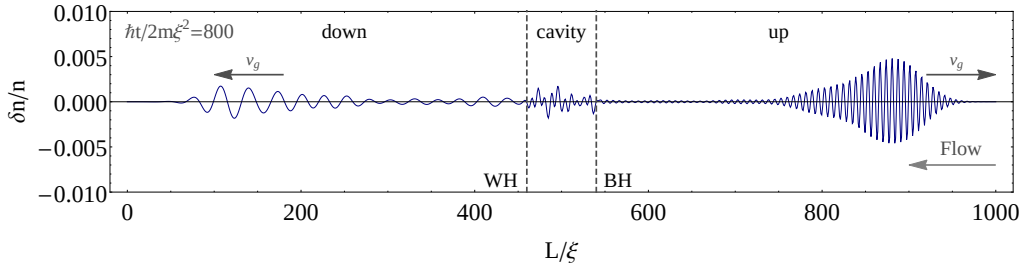

(b)

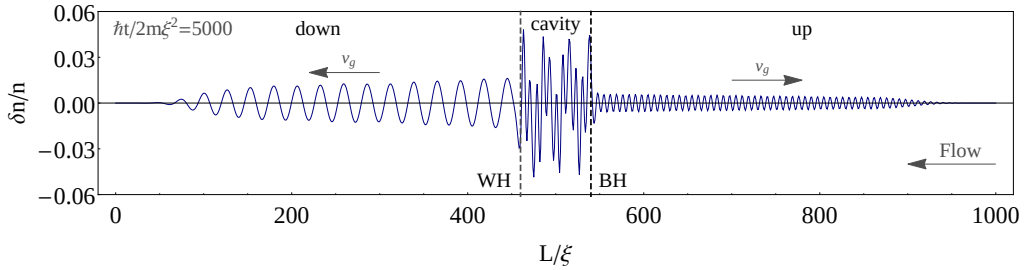

(c)

Figure 8.10: Wave packet propagation in the real space, for the lasing configuration of the system defined by the set of parameters given in the text. The dashed lines enclose the cavity region. (a) Initial condition of the simulation. (b) State of the spin density at $\hbar t/2m\xi^2 = 800$: transmitted and reflected components are visible in the upstream and downstream regions respectively. The incipient instability can be seen inside the cavity. (c) State of the spin density at $\hbar t/2m\xi^2 = 5000$: the unstable modes are clearly visible inside the cavity, together with the corresponding radiation emitted in the down- and up-stream regions.

when the *cav-R1* and *cav-R2* packets encounter the BH horizon. A transmitted *u-R1* component appears in the subcritical upstream region, and leaves the cavity, whose quantum counterpart represents a Hawking particle propagating towards a static observer far from the BH horizon. In addition, reflection and mode conversion processes takes place at the BH, generating positive norm *cav-L1* and negative norm *cav-L2* packets leftwards propagating through the cavity and heading back towards the WH horizon. This phenomenon is visible in the results of the numerical simulation reported in Figs 8.11(a-d), at early times ($\bar{t} \lessapprox 1500$), and in the cuts shown in Fig. 8.12. Fig. 8.10(b) shows the solution in the physical space at an intermediate time instant: wave packets transmitted and reflected in the upstream and downstream subcritical regions respectively are visible, together with a radiation component inside the cavity. The onset of the lasing mechanism is evident in Figs. 8.11(a-e) at the later times. Here we see that certain modes of the supercritical cavity region are unstable and get amplified in time (Fig. 8.11(b)). By comparing the characteristic wave vectors of these modes with the spectrum in Fig. 8.9(b), we notice that the most unstable modes are the one with energy $\bar{\omega} = 0.12$. However, by the procedure illustrated in the next section, we verified that the most unstable modes are actually the ones close to $\bar{\omega} = 0$, in accordance with [240]. In the present case the modes close to $\bar{\omega} = 0.12$ are dominant since they are closest to the triggering wave packets, and so are excited first. Growing modes of the same energy are visible also in the subcritical downstream and upstream regions, as a consequence of the leakage of radiation from the cavity. The exponential character of the amplification is shown in the plots in Figs. 8.13(a-i).

The unstable dynamics of the system can be inferred also from the results in the physical space, and at later times, shown in Fig. 8.10(c).

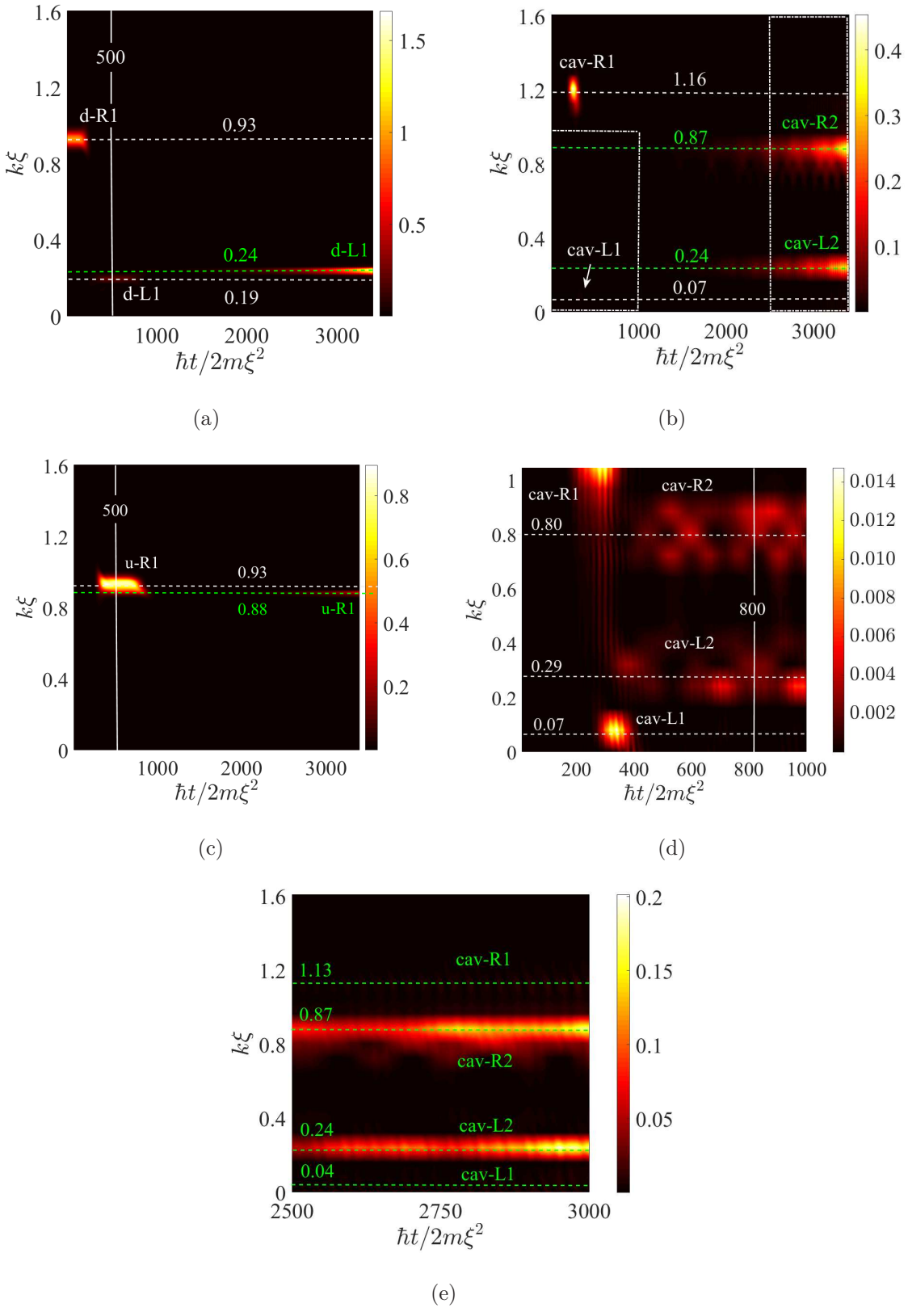

Figure 8.11: (Continued in the following page).

Figure 8.11: Wave packet propagation in the wave vector domain, for the lasing configuration of the system defined by the set of parameters given in the text. Qualitatively different *early time* ($\bar{t} \leq 1500$) and *late time regimes* ($\bar{t} \geq 1500$) can be identified. Features corresponding to these regimes are reported in white and green, respectively. (a) *Downstream region.* At early times, the *d-R1* wave vector components of the initial packet appear, together with the *d-L1* components relative to the packet reflected by the WH horizon. At the late times, the leakage of the self-amplified radiation from the cavity appears in the *d-L1* modes. (b) *Cavity region.* The *cav-R1* packet transmitted through the WH appears, together with the *cav-L1* component reflected by the BH, which is barely visible in the figure and indicated by an arrow. At the late times unstable modes appear in the simulation. (c) *Upstream region.* At the early time, the *u-R1* packet transmitted through the cavity appears while, at the late times, it is evident the leakage into the *u-R1* mode of the self-amplified radiation from the cavity. (d,e) Magnified views of the regions enclosed by the dashed white rectangles in panel (b). In (d), the *cav-L1* packet reflected by the BH horizon is now clearly visible, together with the early times excitation of the *cav-R2* and *cav-L2* modes. In (e) the focus is on the unstable mode.

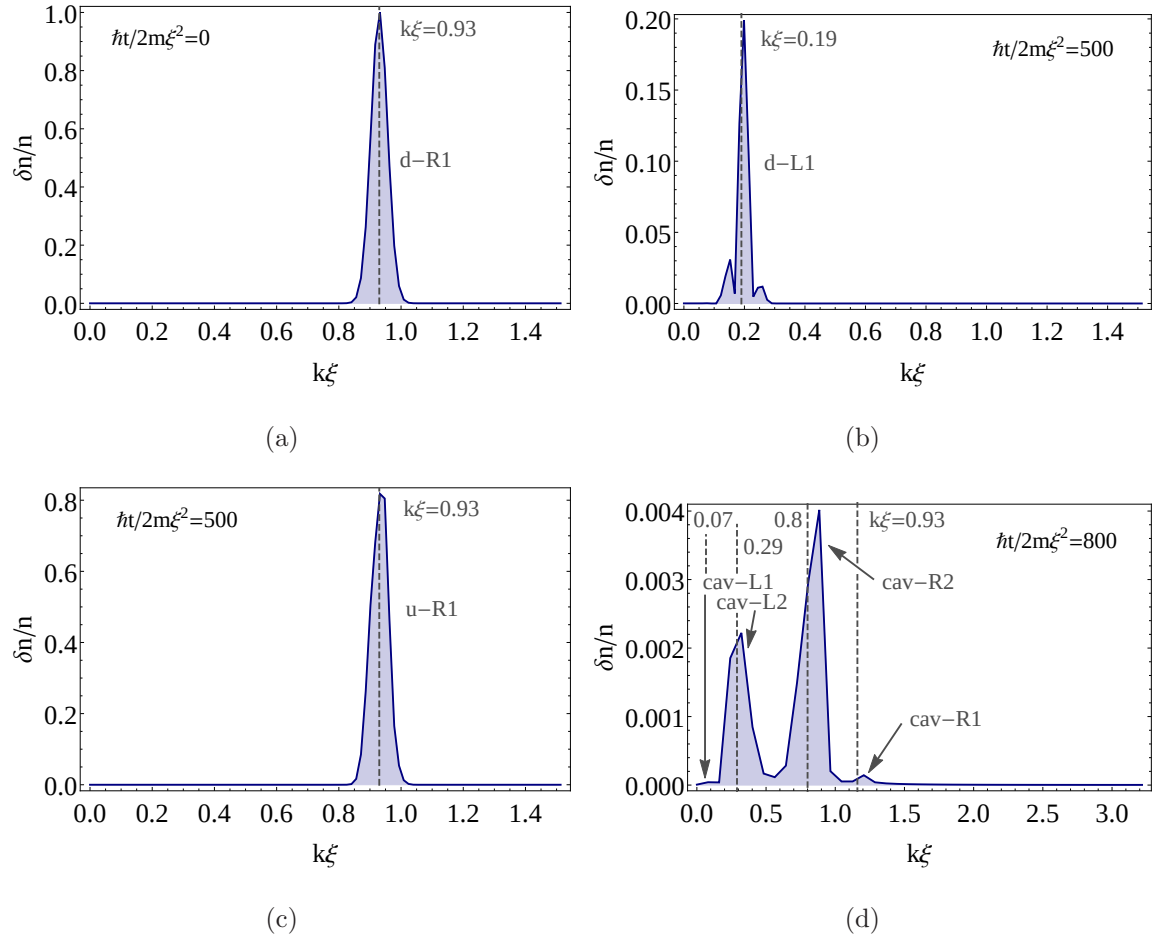

Figure 8.12: Lasing configuration at the early time. Wave vector content of the spin density of the system at the time instants indicated in Figs. 8.11(a-e), in the downstream, upstream and cavity regions. The dashed lines indicate the central wave vector expected by inspection of the dispersion relations shown in Figs. 8.9(a) and 8.9(b). (a,b) *Downstream region.* a) Initial condition, b) $\hbar t/2m\xi^2 = 500$, reflected wave packet by the WH horizon. (c) *Upstream region.* $\hbar t/2m\xi^2 = 500$, wave packet transmitted through the cavity. (d) *Cavity region.* $\hbar t/2m\xi^2 = 800$, negative norm components are now present because of the supercritical motion of the condensate for the spin modes.

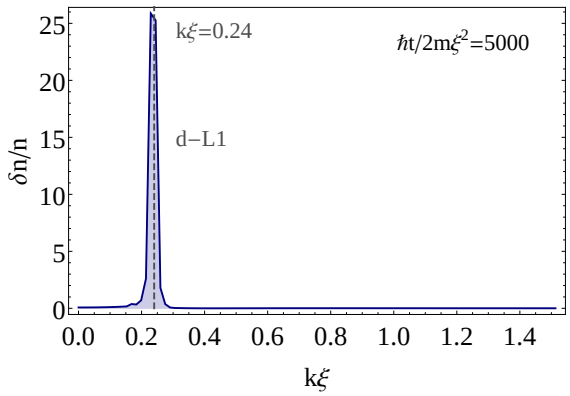
kξ=0.24
ħt/2mξ²=5000
d−L1
δn/n
kξ

(a)

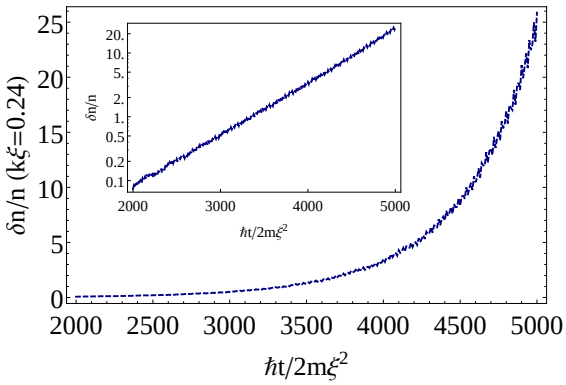
δn/n (kξ=0.24)
δn/n
ħt/2mξ²

(b)

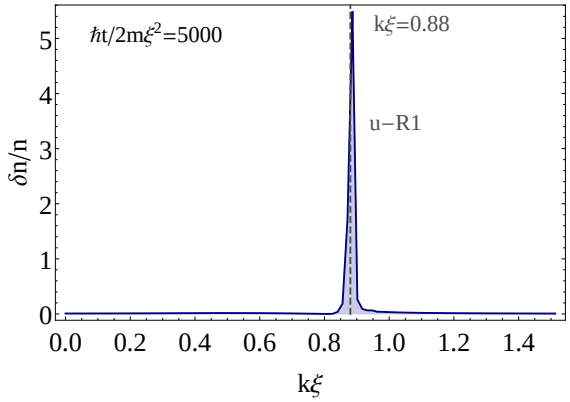
ħt/2mξ²=5000
kξ=0.88
u−R1
δn/n
kξ

(c)

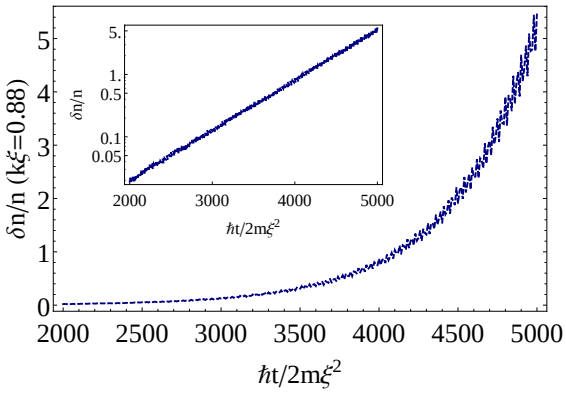
δn/n (kξ=0.88)
δn/n
ħt/2mξ²

(d)

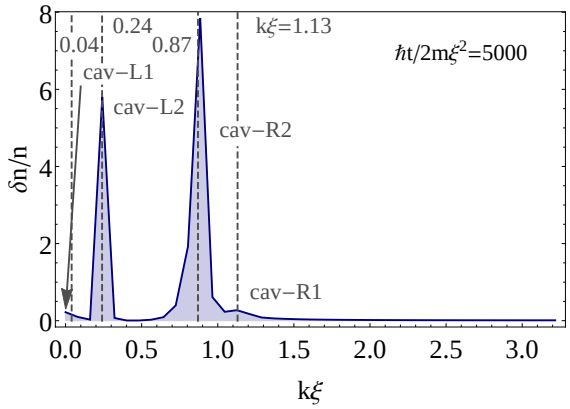
0.04
0.24
0.87
kξ=1.13
ħt/2mξ²=5000
cav−L1
cav−L2
cav−R2
cav−R1
δn/n
kξ

(e)

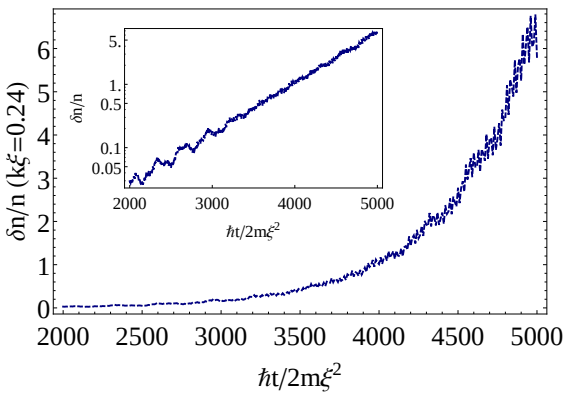
δn/n (kξ=0.24)
δn/n
ħt/2mξ²

(f)

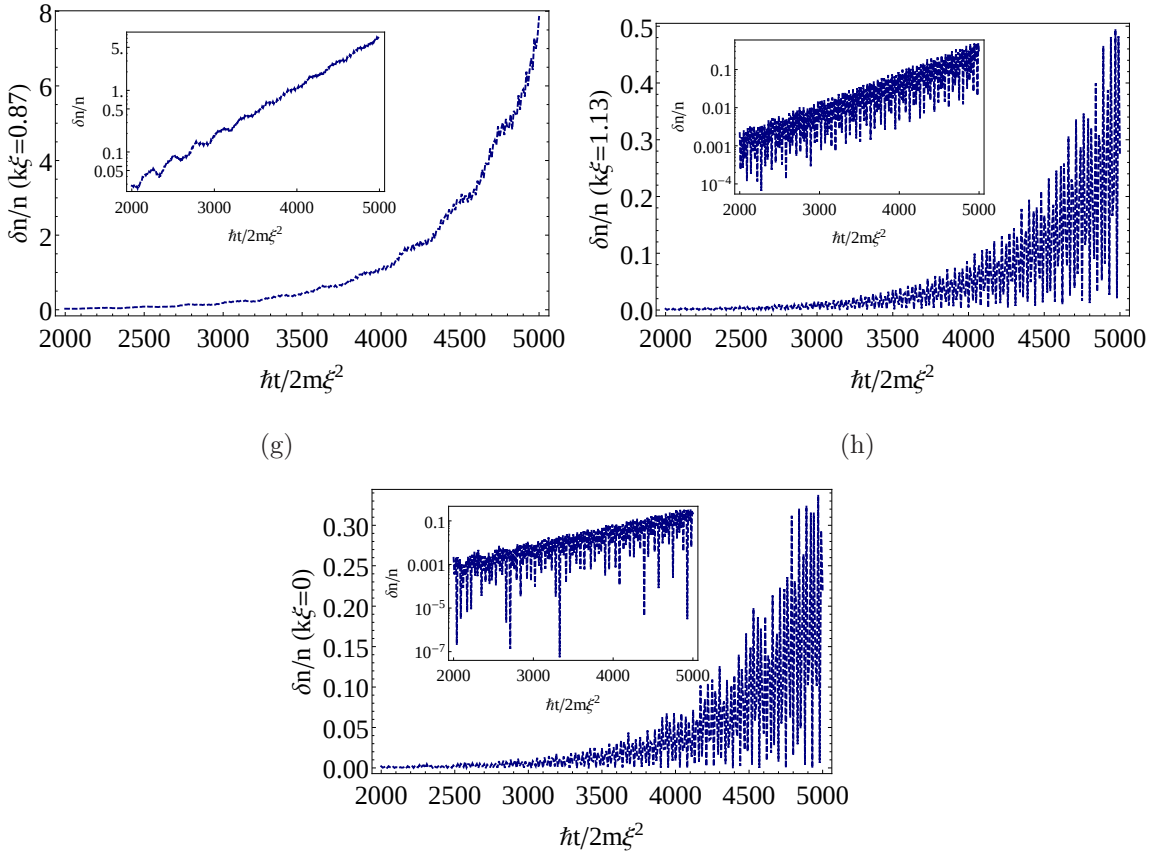

Figure 8.13: Lasing configuration at the late times: (a,c,e) wave vector content of the spin density at $\hbar t/2m\xi^2 = 5000$, in the downstream, upstream and cavity regions, respectively. The pictures show the dominant unstable modes in the cavity and their leakage in the downstream and upstream regions. (b,d,f,g,h,i) Time evolution of the unstable modes in the three different regions. The exponential character of the self-amplification is clearly visible. The panel (i) (as well as (e)) shows the $k\xi = 0$ instead of the expected unstable $k\xi = 0.04$ because the wave vector resolution in the simulation is equal to 0.08.

8.4 White noise amplification

The analysis of the wave packet propagation discussed in the previous section, allowed us to unravel the new physics which emerges because of the supercritical flow of the condensate. We showed that negative (positive) norm modes with positive (negative) energy appear, and mode conversion between modes with different norm take place at the WH and BH horizons. Moreover, the results of the previous section showed the existence of unstable modes in a cavity, which is a consequence of the black hole lasing mechanism. The purpose of this section is to characterize such an instability, and qualitatively investigating its dependence on the strength of the supercritical regime attained in the cavity.

To this aim, we analyze the dynamics of the same system considered in the previous section, with a cavity length now equal to $\bar{L} = 196$, posing different initial conditions for the simulation: we prepare the condensate in its ground state, and superimpose a random noise on it. We pose a cut-off to the noise, at a wave vector k_{cut} larger than the one at which $\omega = 0$ in the dispersion relation of the spin modes, around which the most unstable modes are expected and which thus result seeded by the initial condition. Also, we ensure that the Nyquist prescription $2k_{cut} < k_{max} = 2\pi/\Delta x$ is satisfied, preventing the possible occurrence of spurious aliasing effects. The scope of the analysis is to identify the most unstable modes, characterize their frequency, and qualitatively study the relative instability in terms of the strength of the supercritical regime attained in the cavity. The initial random noise imprinted on the system is justified from an experimental point of view, as fluctuations in the local particle and spin components are always present in an experiment for both technical and thermal reasons.

We run the simulations considering again a piece-wise constant profile for the Rabi frequency, with the value $\bar{\kappa} = -0.5$ in both the subcritical downstream and upstream regions, and values inside the cavity in the range $\bar{\kappa} = -0.011 - -0.030$. We take the value of the mean field coupling constant $g_{ab}/g = 0.8$, and use the same integration scheme as before. We discretize the space domain using a grid of 4096 points, and choose the time step $\Delta t = 0.0004$. In Fig. 8.14 are reported a few snapshots of the spin density of the system at different time instants, for the case $\bar{\kappa} = -0.015$ inside

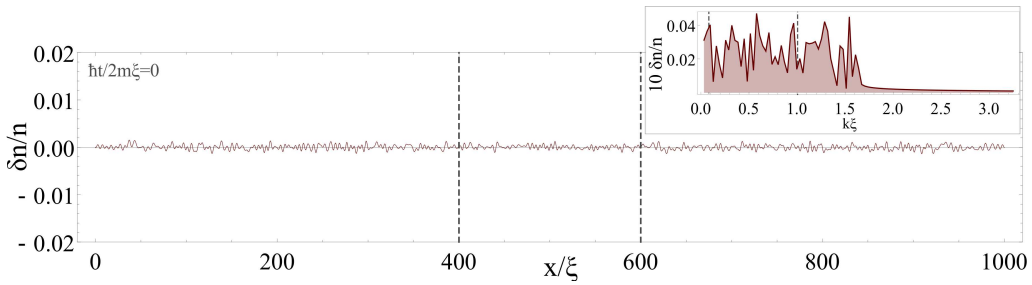

(a)

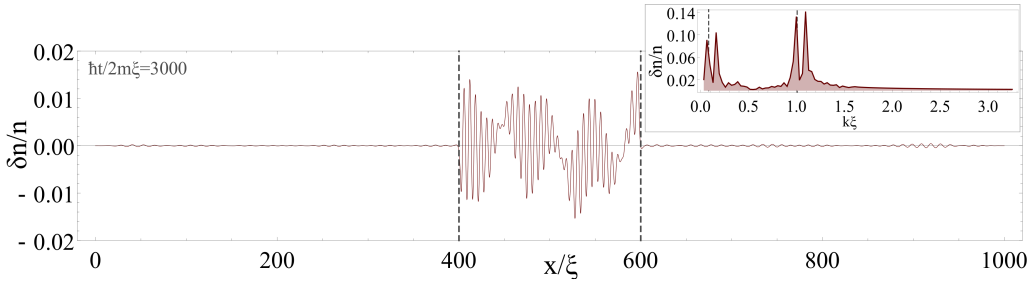

(b)

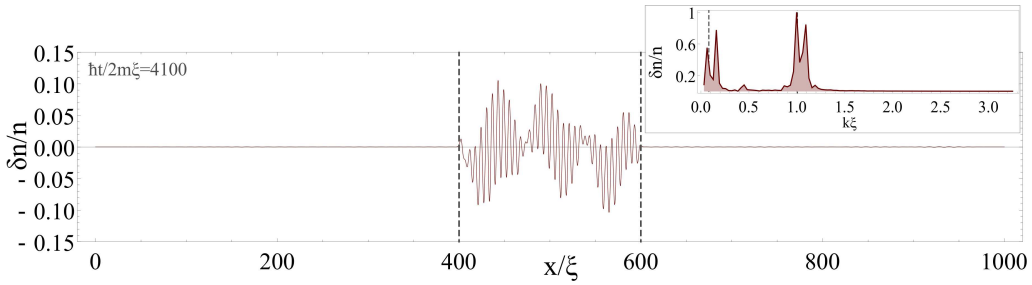

(c)

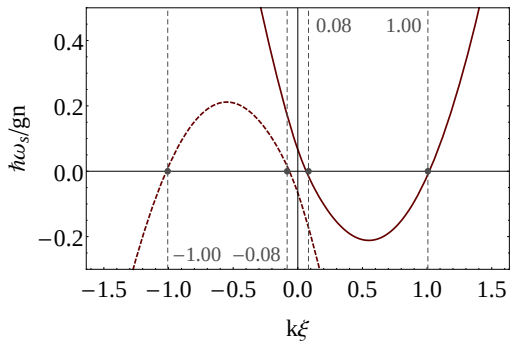

(d)

Figure 8.14: Noise amplification in the lasing configuration characterized by the values $g_{ab}/g = 0.8$ and $\bar{\kappa} = -0.015$ ($\bar{\kappa} = -0.5$) for the interaction parameters inside (outside) the cavity. Panels (a-c) show the spatial profile of the spin density at the times $\bar{t} = 0$, $\bar{t} = 3000$, and $\bar{t} = 4500$ respectively, given the random white noise initially imprinted to the system. (d) The supercritical dispersion relation for the spin modes inside the cavity, given the above values of the parameters.

the cavity. The dynamical evolution of the system shows the onset of rightwards propagating unstable modes with short wavelength, which get converted at the BH horizon into leftward propagating, long wavelength modes. These in turn collide on the WH horizon, get converted into short wavelength modes, rightwards propagating towards the BH horizon, and the cycle repeats, enhancing the content of the field inside the cavity. It is interesting to note that, since the dispersion relation outside the cavity is highly gapped, no modes are available where the zero frequency radiation enclosed in the cavity could leak, and the coupling between the cavity and the downstream and upstream subcritical regions results extremely weak. This is evident from the time evolution of the spin component of the system reported in Fig. 8.14(a-c). The negative and positive energy radiation created by the mode conversion precesses which take place at the horizons, remains thus confined within the cavity. This can be seen from the insets in the same figures, where it is shown the spectral content of the radiation inside the cavity. This result in contrast with what obtained in Sec. 8.3 for the case of the wave packet propagation. There, propagating modes were available outside the cavity, which thus resulted strongly coupled with the outside subcritical regions (see Fig. 8.10).

The exponential character of the self-amplification can be inferred from Fig. 8.15. Given different values of the Rabi frequency κ, here we show the time evolution of the magnitude Mn of the spin density inside the cavity, which we define as

$$Mn = \int_{cavity} dx\, \delta n^2(x). \tag{8.37}$$

From these and analogous results for the other values of the Rabi frequency, the amplification rates displayed in Fig. 8.16 are readily deduced by evaluating the steepness of the curves at the earlier times. At the later times, nonlinear behaviour of the system beyond the Bogoliubov theory come into play.

The wave vector characterizing the unstable modes can be inferred from the spectral content of the signal inside the cavity, shown in the insets of Figs. 8.14(a-c). In the case examined two pairs of peaks appear, close to the intersection point of the spin dispersion relation with $\bar{\omega} = 0$ (indicated in the insets by the dotted lines), which confirms that the most unstable modes are the one closest to the zero frequency, as

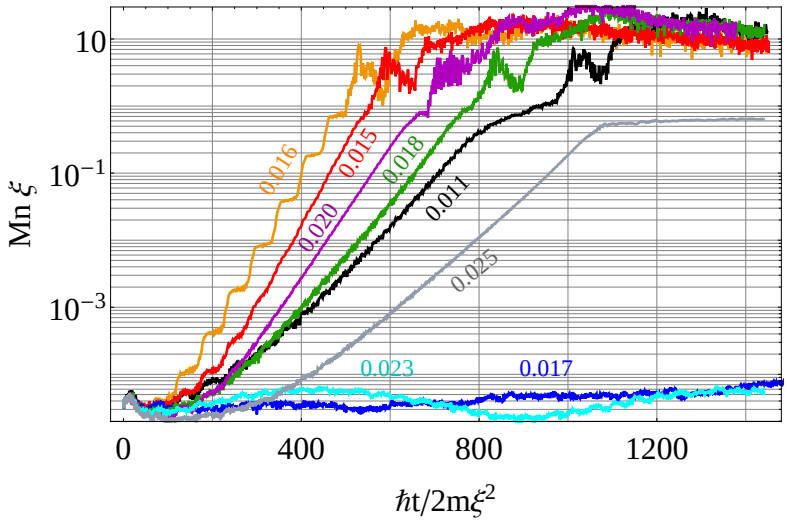

Figure 8.15: Evolution in time of the magnitude of the spin density inside the lasing cavity, for different values of the amplitude $|\kappa|$ of the Rabi frequency. The values used for $|\kappa|$ are indicated in the figure aside each curves.

predicted in [239, 240]. Similar behaviour occurs for the other values of the Rabi frequency we considered, for which the system is also unstable. These values can be deduced from Fig. 8.16, where the dimensionless value of the amplification rate $\Gamma = 1/t_c$ (with t_c the characteristic time scale of the exponential self-amplification $Mn \sim \exp(t/t_c)$) as a function of κ is reported. The figure shows an oscillatory behaviour of Γ, convoluted with an overall decreasing trend with the strength of the coherent coupling. Such oscillations can be ascribed to the discrete nature of the modes sustained by the cavity between the two horizons: by varying the value of $|\kappa|$, we are in fact effectively changing the amplitude of the gap in the dispersion relations and therefore the wave-vectors for which it attains the zero energy. As a consequence, new cavity modes enter or leave the supersonic regime, resulting in the observed oscillatory profile. Moreover we infer, again from the same figure, that the instability is switched off when the spin modes become subcritical inside the cavity, as expected. A close analysis of the dispersion relations reveals that such a transition happens close to the value $\bar{\kappa} = -0.11$ which is not far from the value $\bar{\kappa} = -0.10$ which can be inferred from Fig. 8.16. The reason for this small discrepancy is due to the limit of the resolution achievable in determining the amplification rate, which is intrinsic to the time-splitting algorithm we used to solve the time evolution of the system.

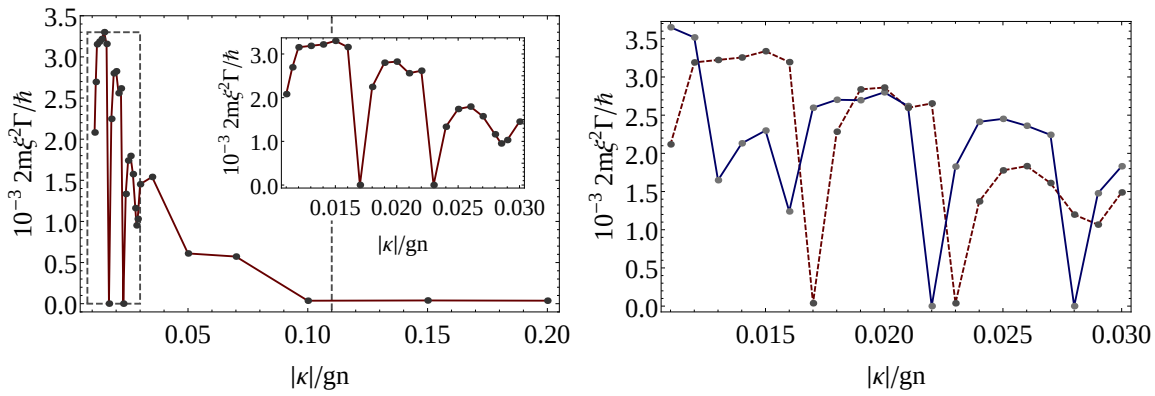

(a) (b)

Figure 8.16: (a) The rate $\bar{\Gamma}$ of the exponential amplification $\exp(\bar{\Gamma}\bar{t})$ of the spin excitations inside the cavity, plotted as a function of the strength of the coherent coupling. The value of κ/gn at which the supercritical-subcritical transition is expected to occur in the cavity is indicated by the dotted line. The inset shows a magnified view of the region inside the dashed rectangle. (b) Comparison of the amplification rate profile for two different lengths of the lasing cavity: $L/\xi \approx 196$ (solid blue), $L/\xi \approx 195$ (dashed red).

As a final remark, we analyze how the amplification rate is modified by a change in the length of the cavity. To this aim we focus the analysis on the range of values of the Rabi frequency used in the inset in Fig. 8.16. We consider the cavity 0.5% shorter than its original size, obtaining the amplification rate shown in Fig. 8.16(b), where it is contrasted with the one obtained with the original length of the cavity. The overall shape of the two profiles look very similar, where the two curves are slightly shifted only. The shift is due to the fact that variations in the cavity length are in fact effectively equivalent to varying the value of the Rabi frequency. A change in the value of the Rabi frequency modifies the gap of the spin dispersion relation, and thus the wave-vector at which the dispersion relation intersect the $\omega = 0$ axes, leaving unchanged the characteristic wavelength of the cavity modes. Conversely, by changing the cavity length we change the wavelength of the cavity modes, without affecting the gap in the dispersion relation.

8.5 The trapped condensate

The aim of the previous sections was to give a clear evidence of the occurrence of the black hole lasing in the spin branch of the excitations in a symmetric, coherently coupled, quasi-one-dimensional two-component condensate. The choice to work with a uniform configuration was not casual, but deliberately made in order to take advantage of the translational invariance of the system, and the consequent continuity of the Bogoliubov spectra. This allowed us to precisely identify in the simulations the phenomenology of the Hawking physics, which is the appearance of negative (positive) norm modes with positive (negative) energy, the mode conversion mechanism at the WH and BH horizons, and the existence of unstable modes in the cavity, which is at the basis of the black hole lasing phenomenon.

We consider in this section the experimentally more feasible case of a harmonically trapped condensate. It is not our intention to provide in the following any quantitative analysis of the phenomena since this was the object of the previous sections. Moreover, for a more complete study, the exact Bogoliubov spectrum for the spin excitations in the non-homogeneous system should be calculated. The latter could be relatively easily calculated numerically, but this is not the purpose of the present work. With an experimental investigation in mind of the spin black hole lasing, our aim in this last section is to show the occurrence of this phenomenon in the spin modes of a non-homogeneous system, when the lasing conditions are met. In order to define the latter conditions, we take as guide a local density approximation of the spectrum in Eq. (8.23).

We modulate in space the strength of the coherent coupling in order to create a finite supercritical cavity in the center of the trap, once the condensate is set in motion with a proper velocity. Rather than using a step-like profile for the Rabi frequency κ as in the previous sections, we use here the more realistic shape

$$\kappa = \frac{\Delta}{2}\left[\tanh\left(\frac{x-x_l}{s}\right) - \tanh\left(\frac{x+x_r}{s}\right)\right] + \kappa_0, \tag{8.38}$$

depicted in Fig. 8.17. This profile is characterized by the following parameters: i) the asymptotic value κ_0 of the Rabi frequency far from the cavity, ii) the difference

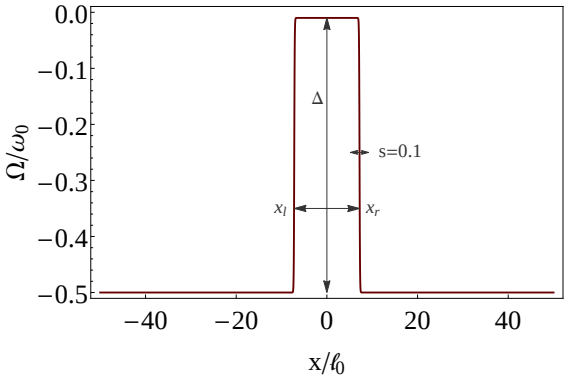

Figure 8.17: Spatial profile of coherent coupling strength $\kappa/\hbar\omega_0$ (in units of χ) used in the simulations.

Δ between the values of the Rabi frequency inside and outside the cavity, iii) the left and right delimiting positions x_l and x_r of the latter, iv) the steepness of the walls which is related to s. In contrast to what was done in the previous sections, it is more convenient here to define lengths in units of the oscillator length $\ell_0 = \sqrt{\hbar/2m\omega_0}$, where ω_0 is the characteristic frequency of the trapping potential, and time is in units of $1/\omega_0$. We indicate quantities in these units by a double bar on top of the symbols, to distinguish with the single bar used in previous sections. The values of the parameters can be translated between the two units by the coefficient $\chi \equiv gn/\hbar\omega_0$, in which n is the particle density of the homogeneous system considered in the previous sections. In particular we have the following transformation laws, respectively for length and time

$$\bar{\bar{L}}/\bar{L} = \sqrt{\frac{1}{\chi}}, \qquad \bar{\bar{t}}/\bar{t} = \frac{1}{\chi}, \tag{8.39}$$

from which immediately follows that $\bar{\bar{E}}/\bar{E} = \bar{\bar{\omega}}/\bar{\omega} = \chi$, $\bar{\bar{n}}/\bar{n} = \sqrt{\chi}$ for energy, frequency and particle density respectively.

In order to show the occurrence of the lasing phenomenon in the harmonically trapped condensate, we consider a set of parameters already used in Sec. 8.4 for the ring geometry. We use in particular the values $g_{ab}/g = 0.8$ and $\bar{\kappa} = -0.01, -0.5$ for the mean field and coherent coupling respectively, with the latter values referring to the regions inside and outside of the cavity. We reproduce the same physical conditions as for the ring geometry, by choosing the number of particles in the cloud in such a way that the density in the center of the trap is equal to the density considered for the uniform system. In the Thomas-Fermi approximation (see Eq. (8.11)),

this is equal to $n(0) = 2\left(\mu + |\kappa|\right) / \left(g + g_{ab}\right)$, with the chemical potential related to the number of particles by the normalization condition

$$N = \int dx\, n(x) = \frac{2}{3\pi} \left(\frac{\mu + |\kappa|}{\hbar \omega_0} \right)^{3/2} \frac{S_t}{\ell_0 \left(a + a_{ab}\right)}. \tag{8.40}$$

In terms of the particle density in the center of the trap we can thus write $\chi = gn(0)/\hbar\omega_0$. Its value provides a measure for the validity of the Thomas-Fermi approximation (that is $\chi \gg 1$). In the simulations we considered $\chi = 200$. We use the values $\bar{\bar{x}}_r = -\bar{\bar{x}}_l = 7.2$, so that the cavity has approximatively the same length as in the Sec. 8.4. The same velocity $\bar{v} = 2\bar{k} = 4\pi \times (90/L) = \bar{\bar{v}}/\sqrt{\chi}$ considered in the previous section is achieved in the center of the trap ($\bar{x} = 0$), by initially locating the condensate in $\bar{\bar{x}} = \bar{\bar{v}} = 16$ at $\bar{\bar{t}} = 0$ and letting it freely oscillate under the effect of the harmonic potential, while the spatial profile of $\bar{\bar{\kappa}}$ is kept constant. We finally choose the steepness parameter $\bar{\bar{s}} = 0.1$. The results shown in Fig. 8.18 confirm the occurrence of the lasing in the spin modes also for the harmonically trapped condensate. As a further check, the same simulation has been run with the value $\bar{\kappa} = -0.2$ inside the cavity, for which the flow is everywhere subsonic. As expected, no instability appears in this case.

Fig. 8.18 also show that, while at early times the total density profile remains smooth and unaffected by the instability in the spin degrees of freedom, at later times, when the amplitude of the spin excitation has grown large enough, a significant modulation shows up also in the total particle density profile. This interplay between the spin and density modes is due to the higher-order, nonlinear couplings beyond the Bogoliubov theory. From a heuristic point of view, this effect can be associated to the back-reaction of Hawking radiation on the background metric, in which the spin degrees of freedom play the role of the quantum field theory, while the density represent the underlying metric.

The higher order character of this effect can be quantitatively assessed in Fig. 8.18(h), where we display the time evolution of the standard deviation of the modulation in the density and spin components with respect to their equilibrium values. With exception made for the early times, where the system is in a transient regime, a fast exponential-like amplification appear for both quantities. In particular, it is

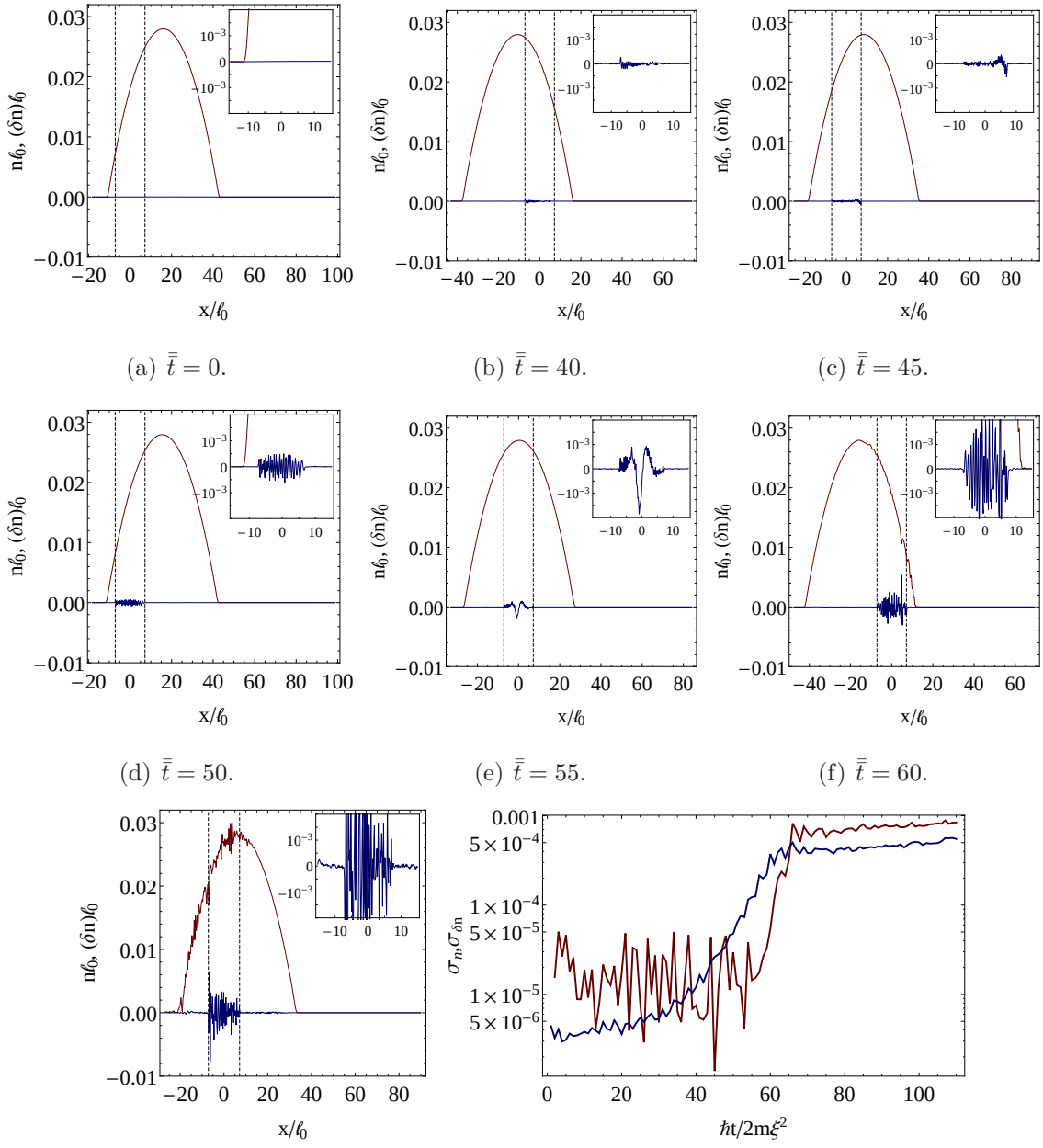

(a) $\bar{\bar{t}} = 0$. (b) $\bar{\bar{t}} = 40$. (c) $\bar{\bar{t}} = 45$.

(d) $\bar{\bar{t}} = 50$. (e) $\bar{\bar{t}} = 55$. (f) $\bar{\bar{t}} = 60$.

(g) $\bar{\bar{t}} = 64$. (h)

Figure 8.18: a-g) Lasing in a harmonically trapped condensate. The figures show snapshots of the spin (blue) and density (red) components at different time instants. The insets show magnified views focused around the lasing cavity. The values of the parameters are given in the text. h) Lin-log plot of the time evolution of the standard deviation of the fluctuations in the density (red) and spin (blue) components with respect to their equilibrium values.

evident that the modulation in the total density grows faster than the one in the spin component of the system, confirming that the former are indeed a higher-order effect beyond the Bogoliubov theory.

Chapter 9 Conclusions

The work presented in this thesis places itself in the general framework of quantum simulation with cold atomic gases, and in particular in the context of synthetic magnetism with neutral atoms and BEC based analogue models for gravity. In the former case, we worked with synthetic gauge fields in a particular configuration which makes them nonlinear, that is explicitly depending on the particle density in the system. This type of a gauge field emerges due to a collisionally induced detuning in combination with synthetic magnetism arising from light-atom coupling. The nonlinear character gives rise to interesting novel dynamics. The current-dependent nonlinearity that results in the mean field description of the condensate, induces a chirality that opens up unexpected perspectives in applications which require a directionality in the system, such as in the emerging fields of atomtronics and analogue gravity.

We investigated in the first part of the thesis, the effects the chirality has on the stability and dynamical properties of the rotating state of a condensate. In Chap. 4 we showed that by properly shaping the profile of the light-matter interaction parameters, a nonlinear term appears in the Gross-Pitaevskii equation, which is proportional to the angular momentum of the condensate itself. We highlighted that two different interpretations can be made for this nonlinearity in terms of a density modulated angular velocity added to the cloud or as a modification of the mean field coupling constant. In the latter case, the resulting effective interaction gets stronger or weaker depending on the sign of the angular momentum of both the condensate and the external laser beam. As a consequence, it may happen that the rotating state of the condensate is energetically favourable compared to the corresponding non-rotating state. We showed that this regime is attained for configurations of the laser light characterized by high values of the orbital angular momentum per

photon.

In Chap. 5 we studied the effects of the nonlinear gauge fields on the effective dynamics of a vortex in a condensate. We developed the simplest, yet nontrivial, variational formulation of the problem, obtaining the equation of motion for the vortex core, in which a density dependent additional force appears as an effect of the nonlinear potentials acting on the atoms.

Apart from their fundamental interest, the above results gives an example of how the chirality induced by the nonlinear fields provides a tool to control the physical behaviour and the properties of a condensate. These novel phenomena could find applications for example in the fields of atomtronics, where the goal is to exploit the tunability of a BEC in order to build the atomic analogues of electronic devices such as diodes or switches, and eventually new quantum devices for measuring and sensing. In this respect, the directional dependence built into the system by the nonlinear synthetic gauge fields, provides a crucial ingredient to this goal, which is not straightforward to achieve with standard BECs.

The results presented in Chapters 6 and 8 form the second part of the thesis, which is devoted to the topic of analogue gravity models with two-component systems. We analyzed first the effects of the aforementioned density-dependent gauge fields in this context, showing that they provide an extra degree of freedom that can be used in order to design novel spacetimes experienced by phonons in a condensate. By properly designing the space profiles and temporal modulation of the light-matter interaction parameters, a wide range of nontrivial effective spacetimes can be implemented, enriching the physics that can be simulated compared to standard, single-component, analogue models.

The results of Chapter 6 concluded the work dedicated to the study of density-dependent gauge fields. In the last part of the thesis, we discussed the promise of multicomponent, spinorial atomic Bose-Einstein condensates as analog models of gravity. The motivation for using these more complex set-ups is due to the fact that, while preliminary claims of the observation of correlated excitations emanating from a sonic black hole have been recently reported [230], a clear and widely accepted

experimental evidence of the occurrence of Hawking physics is not available yet and many questions are still open. The spontaneous Hawking radiation is in fact a tiny effect, and its experimental observation is extremely challenging also in the framework of analogue systems. In this respect, we showed that the two-component set-up is promising, compared to single-component configurations. Working with the spin rather than the density branch of the excitations offers clear advantages from an experimental point of view, since many spurious effects that typically plague the experimental realization of effective horizons and the detection of the Hawking signal in single component condensates can be tamed. Moreover, by simply shaping the amplitude profile of the coherent coupling between the internal states of the atoms, a wide variety of hydrodynamic regimes for the spin modes, and different number and shapes of the horizons can be achieved.

The work presented in Chap. 7, discusses first steps towards the investigation of the spontaneous Hawking radiation originating from analogue black holes, in the spin modes of a coherently coupled, two-component, atomic Bose-Einstein condensates. Using a mean-field formalism based on a (classical) Gross-Pitaevskii theory, we investigated the so-called black hole lasing mechanism in the spin branch of the excitations of the system. This approach successfully revealed the possibility of achieving a black hole lasing instability under suitable conditions, and the existence of Hawking conversion phenomena at the horizons. We showed how a black hole lasing phenomenon can emerge in the spin modes of a flowing one-dimensional, two-component atomic condensate in both spatially homogeneous and harmonically trapped geometries. For the homogeneous case, we studied the propagation of a wave packet of spin excitations through the lasing cavity, and identified the self-amplification of the unstable modes inside the cavity. The rate of such self-amplification was further characterized as a function of the coherent coupling amplitude between the two components by initially imprinting a random noise into the system. The oscillatory behaviour found in the amplification rate reflects the discreteness of the modes sustained by the lasing cavity. We finally confirmed that the effect is preserved also in the experimentally more realistic situation of a harmonically trapped condensate. Furthermore, we highlighted that the nonlinear coupling, at higher order in the Bogoliubov theory, between the spin and density degrees of freedom may be heuristically associated to the back-reaction of Hawking radiation onto the background

metric. The classical mean field approach developed of course fails in correctly describing the quantum features of the Hawking emission when this is triggered by zero-point fluctuations of the fields, but represents a solid starting point towards future investigations of the quantum features of the phenomenon, since the classical process of conversion between positive and negative norm modes at the two horizons is at the basis of the fully quantum Hawking emission.

At a much higher level of technical difficulty, and as a further and most challenging perspective, the experimental advantages provided by the two-component set-up could be useful in the investigation of the finer details of Hawking radiation, such as the back-reaction of the emitted particles on the black hole horizon, where it is crucial to isolate the quantum effects from the background hydrodynamics. We expect this to provide a deeper understanding of the microscopic mechanism underlying the process of (analogue) black hole evaporation due to Hawking emission, hopefully providing a deeper (even if very indirect) insight also on more fundamental questions related to astrophysical black holes and the so-called information paradox [252].

As a last point concerning the promise of spinorial BECs as analog models of gravity, it is worth mentioning the perspectives for investigating the phenomenon of *superradiance* originating from an analogue rotating black hole. Compared to single component systems, using spin modes appears advantageous because of the different length scales that characterize the spin and density component, respectively. The much larger value of the spin healing length, compared to the density one, ensures in fact the existence of a wide ergoregion where radiation enhancement effects can take place on top of a homogeneous density background far from the vortex core, where negative norm spin modes are well defined.

Bibliography

[1] J. Dalibard, F. Gerbier, G. Juzeliūnas, and P. Öhberg. *Rev. Mod. Phys.*, 83:1523–1543, 2011.

[2] N. Goldman, G. Juzeliūnas, P. Öhberg, and I. B. Spielman. *Rep. Prog. Phys.*, 77:126401, 2014.

[3] C. Barceló, S. Liberati, M. Visser, et al. *Living Rev. Rel.*, 8:214, 2005.

[4] D. Faccio, F. Belgiorno, S. Cacciatori, V. Gorini, S. Liberati, and U. Moschella. *Analogue Gravity Phenomenology: Analogue Spacetimes and Horizons, from Theory to Experiment*. Springer, Heidelberg, 2013.

[5] R. P. Feynman. *International Journal of Theoretical Physics*, 21:467–488, 1982.

[6] M. P. A. Fisher, P. B. Weichman, G. Grinstein, and D. S. Fisher. *Phys. Rev. B*, 40:546–570, 1989.

[7] D. Jaksch, C. Bruder, J. I. Cirac, C. W. Gardiner, and P. Zoller. *Phys. Rev. Lett.*, 81:3108–3111, 1998.

[8] M. Greiner, O. Mandel, T. Esslinger, T. W. Hänsch, and I. Bloch. *Nature*, 415:39–44, 2002.

[9] M. Greiner, C. A. Regal, and D. S. Jin. *Nature*, 426:537–540, 2003.

[10] T. Bourdel, L. Khaykovich, J. Cubizolles, J. Zhang, F. Chevy, M. Teichmann, L. Tarruell, S. J. J. M. F. Kokkelmans, and C. Salomon. *Phys. Rev. Lett.*, 93:050401, 2004.

[11] M. Bartenstein, A. Altmeyer, S. Riedl, S. Jochim, C. Chin, J. Hecker Denschlag, and R. Grimm. *Phys. Rev. Lett.*, 92:120401, 2004.

[12] M. W. Zwierlein, C. A. Stan, C. H. Schunck, S. M. F. Raupach, A. J. Kerman, and W. Ketterle. *Phys. Rev. Lett.*, 92:120403, 2004.

[13] J. Kinast, S. L. Hemmer, M. E. Gehm, A. Turlapov, and J. E. Thomas. *Phys. Rev. Lett.*, 92:150402, 2004.

[14] X.-L. Qi and S.-C. Zhang. *Rev. Mod. Phys.*, 83:1057–1110, 2011.

[15] M. Z. Hasan and C. L. Kane. *Rev. Mod. Phys.*, 82:3045–3067, 2010.

[16] C. Nayak, S. H. Simon, A. Stern, M. Freedman, and S. Das Sarma. *Rev. Mod. Phys.*, 80:1083–1159, 2008.

[17] E. Zohar and B. Reznik. *Phys. Rev. Lett.*, 107:275301, 2011.

[18] E. Zohar, J. I. Cirac, and B. Reznik. *Phys. Rev. Lett.*, 109:125302, 2012.

[19] D. Banerjee, M. Bögli, M. Dalmonte, E. Rico, P. Stebler, U.-J. Wiese, and P. Zoller. *Phys. Rev. Lett.*, 110:125303, 2013.

[20] E. Zohar, J. I. Cirac, and B. Reznik. *Phys. Rev. Lett.*, 110:125304, 2013.

[21] E. Zohar, J. I. Cirac, and B. Reznik. *Phys. Rev. Lett.*, 110:055302, 2013.

[22] L. Tagliacozzo, A. Celi, P. Orland, M. W. Mitchell, and M. Lewenstein. *Nat. Commun.*, 4:2615, 2013.

[23] M. J. Edmonds, M. Valiente, G. Juzeliūnas, L. Santos, and P. Öhberg. *Phys. Rev. Lett.*, 110:085301, 2013.

[24] S. A. Fulling. *Aspects of quantum field theory in curved spacetime*. Cambridge university press, Cambridge, 1989.

[25] N. D. Birrell and P. C. W. Davies. *Quantum fields in curved space*. Cambridge university press, Cambridge, 1982.

[26] S. W. Hawking. *Nature*, 248:30–31, 1974.

[27] S. W Hawking. *Commun. Math. Phys.*, 43:199–220, 1975.

[28] E. Schödinger. *Physica*, 6:899, 1939.

[29] L. Parker. *Phys. Rev. Lett.*, 21:562–564, 1968.

[30] L. Parker. *Phys. Rev.*, 183:1057–1068, 1969.

[31] L. Parker. *Phys. Rev. D*, 3:346–356, 1971.

[32] L. Parker. *J. Phys. A - Math. Theor.*, 45:374023, 2012.

[33] Steven Corley and Ted Jacobson. *Phys. Rev. D*, 59:124011, 1999.

[34] L.P. Pitaevskii and S. Stringari. *Bose-einstein condensation*. Oxford University Press, Oxford, 2003.

[35] C. J. Pethick and H. Smith. *Bose-Einstein condensation in dilute gases*. Cambridge university press, Cambridge, 2004.

[36] F. Dalfovo, S. Giorgini, L.P. Pitaevskii, and S. Stringari. *Rev. Mod. Phys.*, 71:463–512, 1999.

[37] A.S. Parkins and D.F. Walls. *Phys. Rep.*, 303:1 – 80, 1998.

[38] M. Inguscio, S. Stringari, and C. E. Wieman. *Bose-Einstein Condensation in Atomic Gases - Proceedings of the International School of Physics Enrico Fermi, Course CXL, Varenna*. IOP Press, Amsterdam, 1999.

[39] S. N. Bose. *Z. Phys.*, 26:178, 1924.

[40] A. Einstein. In *itzungsberichte der Preussischen Akademie der Wissenschaften, Physikalisch-mathematische Klasse*, page 261 (1924); pages 3 (1925).

[41] E. A. Cornell and C. E. Wieman. *Rev. Mod. Phys.*, 74:875–893, 2002.

[42] M. H. Anderson, J. R. Ensher, M. R. Matthews, C. E. Wieman, and E. A. Cornell. *Science*, 269:198–201, 1995.

[43] K. B. Davis, M. O. Mewes, M. R. Andrews, N. J. van Druten, D. S. Durfee, D. M. Kurn, and W. Ketterle. *Phys. Rev. Lett.*, 75:3969–3973, 1995.

[44] C. C. Bradley, C. A. Sackett, J. J. Tollett, and R. G. Hulet. *Phys. Rev. Lett.*, 75:1687–1690, 1995.

[45] J. Weiner, V. S. Bagnato, S. Zilio, and P. S. Julienne. *Rev. Mod. Phys.*, 71:1–85, 1999.

[46] Alexander. L. Fetter. Theory of a dilute low-temperature trapped bose condensate. In M. Inguscio, S. Stringari, and C. E. Wieman, editors, *Proceedings of the International School of Physics Enrico Fermi, Course CXL, Varenna*, Amsterdam, 1999. IOP Press.

[47] Y. Castin. Bose-einstein condensates in atomic gases: Simple theoretical results. In R. Kaiser, C. Westbrook, and F. David, editors, *Coherent atomic matter waves: 27 July–27 August 1999*, pages 1–136. Springer Berlin Heidelberg, Berlin, Heidelberg, 2001.

[48] J. Dalibard. Collisional dynamics of ultra-cold atomic gases. In M. Inguscio, S. Stringari, and C. E. Wieman, editors, *Proceedings of the International School of Physics Enrico Fermi, Course CXL, Varenna*, Amsterdam, 1999. IOP Press.

[49] D. J. Heinzen. Ultracold atomic interactions. In M. Inguscio, S. Stringari, and C. E. Wieman, editors, *Proceedings of the International School of Physics Enrico Fermi, Course CXL, Varenna*, Amsterdam, 1999. IOP Press.

[50] L. D. Landau and E. M. Lifshitz. *Quantum mechanics: Non-relativistic theory (Vol. 3)*. Pergamon Press, Oxford, 1977.

[51] W. Ketterle, D. S. Durfee, and D.M. Stamper-Kurn. Making, probing and understanding bose-einstein condensates. In M. Inguscio, S. Stringari, and C. E. Wieman, editors, *Proceedings of the International School of Physics Enrico Fermi, Course CXL, Varenna*, Amsterdam, 1999. IOP Press.

[52] E. A. Cornell, J. R. Ensher, and Wieman C. E. Experiments in dilute atomic bose-einstein condensation. In M. Inguscio, S. Stringari, and C. E. Wieman, editors, *Proceedings of the International School of Physics Enrico Fermi, Course CXL, Varenna*, Amsterdam, 1999. IOP Press.

[53] N. Bogoliubov. *J. Phys. (USSR)*, 11:23, 1947.

[54] A. L. Fetter and J. D. Walecka. *Quantum Theory of Many-Particle Systems*. Dover, New York, 2003.

[55] L. P. Pitaevskii. *Zh. Eksp. Teor. Fys.*, 40:646, 1961.

[56] L. P. Pitaevskii. *JETP*, 13:451, 1961.

[57] E. P. Gross. *Nuovo Cimento*, 20:454, 1961.

[58] E. P. Gross. *J. Math. Phys*, 4:195, 1963.

[59] R. P. Feynman. *Progress in Low Temperature Physics*, 1:17 – 53, 1955.

[60] L. D. Landau and E. M. Lifshitz. *Fluid Mechanics*, volume 6. Pergamon Press, 1987.

[61] L. D. Landau. *J. Phys. (USSR)*, 5:71, 1941.

[62] E. M. Lifshitz and L. P. Pitaevskii. *Statistical Physics, Part 2: : Theory of the Condensed State (Vol. 9)*. Pergamon Press, Oxford, 1980.

[63] K. Huang. *Statistical Mechanics*. John Wiley & Sons, 1988.

[64] P. W. Anderson. *Rev. Mod. Phys.*, 38:298–310, 1966.

[65] Gordon Baym and C. J. Pethick. *Phys. Rev. Lett.*, 76:6–9, 1996.

[66] A. L. Fetter. *Ann. Phys.*, 70:67–101, 1972.

[67] A. Mostafazadeh. *Journal of Mathematical Physics*, 43:205–214, 2002.

[68] A. Mostafazadeh. *Journal of Mathematical Physics*, 43:2814–2816, 2002.

[69] A. Mostafazadeh. *Journal of Mathematical Physics*, 43:3944–3951, 2002.

[70] I. Stakgold and M. J. Holst. *Green's functions and boundary value problems*. John Wiley & Sons, New York, 1979.

[71] A. L. Fetter. *Rev. Mod. Phys.*, 81:647–691, 2009.

[72] K. Kasamatsu and M. Tsubota. *Prog. Low Temp. Phys.*, 16:351–403, 2008.

[73] M. Tsubota, K. Kasamatsu, and M. Kobayashi. Quantized vortices in superfluid helium and atomic bose-einstein condensates. In K. H. Bennemann and J. B. Ketterson, editors, *Novel Superfluids*, volume 1, pages 156–252. Oxford University Press, Oxford, 2013.

[74] A. Aftalion. *Vortices in Bose-Einstein Condensates*. Birkhäuser, Boston, 2006.

[75] L. Onsager. *Nuovo Cimento Suppl.*, 6:249, 1949.

[76] W. F. Vinen. *Proceedings of the Royal Society of London A: Mathematical, Physical and Engineering Sciences*, 240:114–127, 1957.

[77] W. F. Vinen. *Proceedings of the Royal Society of London A: Mathematical, Physical and Engineering Sciences*, 240:128–143, 1957.

[78] W. F. Vinen. *Proceedings of the Royal Society of London A: Mathematical, Physical and Engineering Sciences*, 242:493–515, 1957.

[79] H. E. Hall and W. F. Vinen. *Proceedings of the Royal Society of London A: Mathematical, Physical and Engineering Sciences*, 238:204–214, 1956.

[80] H. E. Hall and W. F. Vinen. *Proceedings of the Royal Society of London A: Mathematical, Physical and Engineering Sciences*, 238:215–234, 1956.

[81] W. F. Vinen. *Proceedings of the Royal Society of London A: Mathematical, Physical and Engineering Sciences*, 260:218–236, 1961.

[82] M. R. Matthews, B. P. Anderson, P. C. Haljan, D. S. Hall, M. J. Holland, J. E. Williams, C. E. Wieman, and E. A. Cornell. *Phys. Rev. Lett.*, 83:3358–3361, 1999.

[83] K. W. Madison, F. Chevy, W. Wohlleben, and J. Dalibard. *Phys. Rev. Lett.*, 84:806–809, 2000.

[84] J. Abo-Shaeer, C. Raman, J. M. Vogels, and W. Ketterle. *Science*, 292:476–9, 2001.

[85] G. B. Arfken and H. J. Weber. *Mathematical methods for physicists*. Academic press, Oxford, 2005.

[86] A. L. Fetter. In K. T. Mahanthappa and W. E. Britten, editors, *Lectures in Theoretical Physics*, volume XI-B, page 351. Gordon and Breach, New York, 1969.

[87] E. Lundh, C. J. Pethick, and H. Smith. *Phys. Rev. A*, 55:2126–2131, 1997.

[88] F. Dalfovo and S. Stringari. *Phys. Rev. A*, 53:2477–2485, 1996.

[89] A. A. Svidzinsky and A. L. Fetter. *Phys. Rev. Lett.*, 84:5919–5923, 2000.

[90] A. L. Fetter. *Rev. Mod. Phys.*, 81:647–691, 2009.

[91] P. O. Fedichev and G. V. Shlyapnikov. *Phys. Rev. A*, 60:R1779–R1782, 1999.

[92] L. D. Landau and E. M. Lifshitz. *Mechanics (Vol. 1)*. Butterworth-Heinemann, Oxford, 1976.

[93] Y. Aharonov and D. Bohm. *Phys. Rev.*, 115:485–491, 1959.

[94] Y. Aharonov and D. Bohm. *Phys. Rev.*, 123:1511–1524, 1961.

[95] M. V. Berry. *Proceedings of the Royal Society of London A: Mathematical, Physical and Engineering Sciences*, 392:45–57, 1984.

[96] R. Dum and M. Olshanii. *Phys. Rev. Lett.*, 76:1788–1791, 1996.

[97] P. M. Visser and G. Nienhuis. *Phys. Rev. A*, 57:4581–4591, 1998.

[98] G. Juzeliūnas and P. Öhberg. *Phys. Rev. Lett.*, 93:033602, 2004.

[99] G. Juzeliūnas, J. Ruseckas, P. Öhberg, and M. Fleischhauer. *Phys. Rev. A*, 73:025602, 2006.

[100] S.-L. Zhu, H. Fu, C.-J. Wu, S.-C. Zhang, and L.-M. Duan. *Phys. Rev. Lett.*, 97:240401, 2006.

[101] K. J. Günter, M. Cheneau, T. Yefsah, S. P. Rath, and J. Dalibard. *Phys. Rev. A*, 79:011604, 2009.

[102] I. B. Spielman. *Phys. Rev. A*, 79:063613, 2009.

[103] Y.-J. Lin, R. L. Compton, A. R. Perry, W. D. Phillips, J. V. Porto, and I. B. Spielman. *Phys. Rev. Lett.*, 102:130401, 2009.

[104] Y.-J. Lin, R. L. Compton, K. Jimenez-Garcia, J. V. Porto, and I. B. Spielman. *Nature*, 462:628–632, 2009.

[105] Y.-J. Lin, R. L. Compton, K. Jimenez-Garcia, W. D. Phillips, J. V. Porto, and I. B. Spielman. *Nat. Phys.*, 7:531–534, 20011.

[106] M. Aidelsburger, M. Atala, S. Nascimbène, S. Trotzky, Y.-A. Chen, and I. Bloch. *Phys. Rev. Lett.*, 107:255301, 2011.

[107] J. Dalibard. Introduction to the physics of artificial gauge fields. In M. Inguscio, W. Ketterle, S. Stringari, and G. Roati, editors, *Proceedings of the International School of Physics Enrico Fermi, Course CXCI, Varenna*, Amsterdam, 2014. IOP Press.

[108] A. Messiah. *Quantum Mechanics, (Vol. 2)*, volume 2. North-Holland, Amsterdam, 1962.

[109] R. Loudon. *The quantum theory of light*. Oxford University Press, Amsterdam, 2000.

[110] C. Cohen-Tannoudji, J. Dupont-Roc, G. Grynberg, and P. Thickstun. *Atom-photon interactions: basic processes and applications*. Wiley-VCH Verlag GmbH & Co. KGaA, Weinhem, 2004.

[111] C. Cohen-Tannoudji. Atomic motion in laser light. In J. Dalibard, J. M. Raimond, and J. Zinn-Justin, editors, *eds. Les Houches, Session LIII*. Elsevier Science Publisher, 1990.

[112] M. Cheneau, S. P. Rath, T. Yefsah, K. J. Günter, G. Juzeliūnas, and J. Dalibard. *EPL*, 83:60001, 2008.

[113] J. Ye, H. J. Kimble, and H. Katori. *Science*, 320:1734–1738, 2008.

[114] D. F. Walls and G. J. Milburn. *Quantum optics*. Springer Science & Business Media, 2007.

[115] G. Juzeliūnas, P. Öhberg, J. Ruseckas, and A. Klein. *Phys. Rev. A*, 71:053614, 2005.

[116] G. Juzeliūnas, J. Ruseckas, P. Öhberg, and M. Fleischhauer. *Phys. Rev. A*, 73:025602, 2006.

[117] D. R. Hofstadter. *Phys. Rev. B*, 14:2239, 1976.

[118] J. M. Luttinger. *Phys. Rev.*, 84:814, 1951.

[119] G. Nesciu. *Rev. Mod. Phys.*, 63:91, 1991.

[120] M. Lewenstein, A. Sanpera, B. Ahufinger, B. Damski, A. Sen(De), and U. Sen. *Advances in Physics*, 56:243–379, 2007.

[121] I. Bloch, J. Dalibard, and W. Zwerger. *Rev. Mod. Phys.*, 80:885–964, 2008.

[122] R. A. Williams, S. Al-Assam, and C. J. Foot. *Phys. Rev. Lett.*, 104:050404, 2010.

[123] J. H. Huckans, I. B. Spielman, B. Laburthe Tolra, W. D. Phillips, and J. V. Porto. *Phys. Rev. A*, 80:043609, 2009.

[124] S. Rahav, I. Gilary, and S. Fishman. *Phys. Rev. A*, 68:013820, 2003.

[125] N. Goldman and J. Dalibard. *Phys. Rev. X*, 4:031027, 2014.

[126] M. Bukov, L. DAlessio, and A. Polkovnikov. *Adv. Phys.*, 64:139–226, 2015.

[127] A. Eckardt, C. Weiss, and M. Holthaus. *Phys. Rev. Lett.*, 95:260404, 2005.

[128] J. Struck, C. Ölschläger, M. Weinberg, P. Hauke, J. Simonet, A. Eckardt, M. Lewenstein, K. Sengstock, and P. Windpassinger. *Phys. Rev. Lett.*, 108:225304, 2012.

[129] K. Jiménez-García, L. J. LeBlanc, R. A. Williams, M. C. Beeler, A. R. Perry, and I. B. Spielman. *Phys. Rev. Lett.*, 108:225303, 2012.

[130] F. D. M. Haldane. *Phys. Rev. Lett.*, 61:2015, 1988.

[131] G. Jotzu, M. Messer, R. Desbuquois, M. Lebrat, T. Uehlinger, D. Greif, and T. Esslinger. *Nature*, 515:237, 2014.

[132] J. Struck, M. Weinberg, C. Olschlager, P. Windpassinger, J. Simonet, K. Sengstock, R. Hoppner, P. Hauke, A. Eckardt, M. Lewenstein, and L. Mathey. *Nat. Phys.*, 9:738–743, 2013.

[133] M. Aidelsburger, M. Atala, M. Lohse, J. T. Barreiro, B. Paredes, and I. Bloch. *Phys. Rev. Lett.*, 111:185301, 2013.

[134] H. Miyake, G. A. Siviloglou, C. J. Kennedy, W. C. Burton, and W. Ketterle. *Phys. Rev. Lett.*, 111:185302, 2013.

[135] M. Aidelsburger, M. Atala, S. Nascimbène, S. Trotzky, Y.-A. Chen, and I. Bloch. *Applied Physics B*, 113:1–11, 2013.

[136] D. Jaksch and P. Zoller. *New J. Phys.*, 5:56, 2003.

[137] F. Gerbier and J. Dalibard. *New J. Phys.*, 12:033007, 2010.

[138] L. Dong, L. Zhou, B. Wu, B. Ramachandhran, and H. Pu. *Phys. Rev. A*, 89:011602, 2014.

[139] W. Zheng and N. R. Cooper. *Phys. Rev. Lett.*, 117:175302, 2016.

[140] K. E. Ballantine, B. L. Lev, and J. Keeling. *Phys. Rev. Lett.*, 118:045302, 2017.

[141] S. Greschner, G. Sun, D. Poletti, and L. Santos. *Phys. Rev. Lett.*, 113:215303, 2014.

[142] S. Greschner, D. Huerga, G. Sun, D. Poletti, and L. Santos. *Phys. Rev. B*, 92:115120, 2015.

[143] J.-H. Zheng, B. Xiong, G. Juzeliūnas, and D.-W. Wang. *Phys. Rev. A*, 92:013604, 2015.

[144] S. Butera, M. Valiente, and P. Öhberg. *J. Phys. B: At. Mol. Opt. Phys.*, 49:015304, 2016.

[145] A. L. Fetter and A. A. Svidzinsky. *J. Phys. Condens. Matter*, 13:R135, 2001.

[146] R. Fickler, R. Lapkiewicz, W. N. Plick, M. Krenn, C. Schaeff, S. Ramelow, and A. Zeilinger. *Science*, 338:640–643, 2012.

[147] G. Campbell, B. Hage, B. Buchler, and P. K. Lam. *Appl. Opt.*, 51:873–876, 2012.

[148] J. Courtial, K. Dholakia, L. Allen, and M. J. Padgett. *Opt. Commun.*, 144:210–213, 1997.

[149] U. Leonhardt and P. Öhberg. *Phys. Rev. A*, 67:053616, 2003.

[150] J.-M. Duan. *Phys. Rev. A*, 49:12381, 1994.

[151] R. M. Wald. *General relativity*. University of Chicago press, Chicago, 1984.

[152] C. W. Misner, K. S. Thorne, and J. A. Wheeler. *Gravitation*. W. H. Freeman and Company, San Francisco, 1973.

[153] C. Rovelli. *Proc. 9th Marcel Grossmann Meeting*, page 32, 2000.

[154] W. G. Unruh. *Phys. Rev. Lett.*, 46:1351–1353, 1981.

[155] M. Visser, C. Barceló, and S. Liberati. *Gen. Rel. Gravit.*, 34:1719–1734, 2002.

[156] S. I. Badulin, K. V. Pokazeev, and A. D. Rozenberg. *Izv. Atmos. Ocean. Phys.*, 19:1035, 1983.

[157] R. Schützhold and W. G. Unruh. *Phys. Rev. D*, 66:044019, 2002.

[158] G. Rousseaux, C. Mathis, P. Maïssa, T. G. Philbin, and U. Leonhardt. *New J. Phys.*, 10:053015, 2008.

[159] G. Rousseaux, P. Maïssa, C. Mathis, P. Coullet, T. G. Philbin, and U. Leonhardt. *New J. Phys.*, 12:095018, 2010.

[160] S. Weinfurtner, E. W. Tedford, M. C. J. Penrice, W. G. Unruh, and G. A. Lawrence. *Phys. Rev. Lett.*, 106:021302, 2011.

[161] U. Leonhardt and P. Piwnicki. *Phys. Rev. A*, 60:4301–4312, 1999.

[162] F. Baldovin, M. Novello, S. E. Perez Bergliaffa, and J. M. Salim. *Class. Quantum Grav.*, 17:3265, 2000.

[163] U. Leonhardt. *Phys. Rev. A*, 62:012111, 2000.

[164] U. Leonhardt and P. Piwnicki. *Phys. Rev. Lett.*, 84:822–825, 2000.

[165] M. Visser. *Phys. Rev. Lett.*, 85:5252, 2000.

[166] U. Leonhardt and P. Piwnicki. *Phys. Rev. Lett.*, 85:5253, 2000.

[167] B. Reznik. *Phys. Rev. D*, 62:044044, 2000.

[168] V. A. De Lorenci, R. Klippert, M. Novello, and J. M. Salim. *Phys. Lett. B*, 482:134–140, 2000.

[169] M. Novello, V. A. De Lorenci, J. M. Salim, and R. Klippert. *Phys. Rev. D*, 61:045001, 2000.

[170] M. Novello and J. M. Salim. *Phys. Rev. D*, 63:083511, 2001.

[171] I. Brevik and G. Halnes. *Phys. Rev. D*, 65:024005, 2001.

[172] J. Fiurášek, U. Leonhardt, and R. Parentani. *Phys. Rev. A*, 65:011802, 2001.

[173] U. Leonhardt. *Nature*, 415:406–409, 2002.

[174] U. Leonhardt. *Phys. Rev. A*, 65:043818, 2002.

[175] V. A. De Lorenci and R. Klippert. *Phys. Rev. D*, 65:064027, 2002.

[176] P. Piwnicki. *Int. J. Mod. Phys. A*, 17:1543, 2002.

[177] R. Schützhold, G. Plunien, and G. Soff. *Phys. Rev. Lett.*, 88:061101, 2002.

[178] U. Leonhardt. *Rep. Prog. Phys.*, 66:1207, 2003.

[179] M. Novello, S. Perez Bergliaffa, J. Salim, V. A. De Lorenci, and R. Klippert. *Class. Quantum Grav.*, 20:859, 2003.

[180] U. Leonhardt. *Rep. Prog. Phys.*, 66:1207, 2003.

[181] V. A. De Lorenci, R. Klippert, and Yu. N. Obukhov. *Phys. Rev. D*, 68:061502, 2003.

[182] W. G. Unruh and R. Schützhold. *Phys. Rev. D*, 68:024008, 2003.

[183] E. Bittencourt, V. A. De Lorenci, R. Klippert, M. Novello, and J. M. Salim. *Class. Quantum Grav.*, 31:145007, 2014.

[184] R. Schützhold, M. Uhlmann, L. Petersen, H. Schmitz, A. Friedenauer, and T. Schätz. *Phys. Rev. Lett.*, 99:201301, 2007.

[185] B. Horstmann, B. Reznik, S. Fagnocchi, and J. I. Cirac. *Phys. Rev. Lett.*, 104:250403, 2010.

[186] T. G. Philbin, C. Kuklewicz, S. Robertson, S. Hill, F. König, and U. Leonhardt. *Science*, 319:1367–1370, 2008.

[187] E. Rubino, F. Belgiorno, S. L. Cacciatori, M. Clerici, V. Gorini, G. Ortenzi, L. Rizzi, V. G. Sala, M. Kolesik, and D. Faccio. *New J. of Phys.*, 13:085005, 2011.

[188] F. Belgiorno, S. L. Cacciatori, M. Clerici, V. Gorini, G. Ortenzi, L. Rizzi, E. Rubino, V. G. Sala, and D. Faccio. *Phys. Rev. Lett.*, 105:203901, 2010.

[189] R. Schützhold and W. G. Unruh. *Phys. Rev. Lett.*, 107:149401, 2011.

[190] F. Belgiorno, S. L. Cacciatori, M. Clerici, V. Gorini, G. Ortenzi, L. Rizzi, E. Rubino, V. G. Sala, and D. Faccio. *Phys. Rev. Lett.*, 107:149402, 2011.

[191] S. Liberati, A. Prain, and M. Visser. *Phys. Rev. D*, 85:084014, 2012.

[192] I. Finazzi, S.and Carusotto. *EPJ Plus*, 127:78, 2012.

[193] W. G. Unruh and R. Schützhold. *Phys. Rev. D*, 86:064006, 2012.

[194] S. Giovanazzi. *Phys. Rev. Lett.*, 94:061302, 2005.

[195] R. Schützhold and W. G. Unruh. *Phys. Rev. Lett.*, 95:031301, 2005.

[196] P. D. Nation, M. P. Blencowe, A. J. Rimberg, and E. Buks. *Phys. Rev. Lett.*, 103:087004, 2009.

[197] D. Gerace and I. Carusotto. *Phys. Rev. B*, 86:144505, 2012.

[198] I. Carusotto and C. Ciuti. *Rev. Mod. Phys.*, 85:299–366, 2013.

[199] L. J. Garay, J. R. Anglin, J. I. Cirac, and P. Zoller. *Phys. Rev. Lett.*, 85:4643–4647, 2000.

[200] L. J. Garay, J. R. Anglin, J. I. Cirac, and P. Zoller. *Phys. Rev. A*, 63:023611, 2001.

[201] M. Visser and S. Weinfurtner. *Phys. Rev. D*, 72:044020, 2005.

[202] C. Barceló, A. Cano, L. J. Garay, and G. Jannes. *Phys. Rev. D*, 74:024008, 2006.

[203] C. Barceló, S. Liberati, and M. Visser. *Class. Quantum Grav.*, 18:1137, 2001.

[204] U. R. Fischer and M. Visser. *Ann. Phys.*, 304:22 – 39, 2003.

[205] C. Barceló, S. Liberati, S. Sonego, and M. Visser. *Class. Quantum Grav.*, 23:5341, 2006.

[206] M. Visser. *Class. Quantum Grav.*, 15:1767, 1998.

[207] U. Leonhardt, T. Kiss, and P. Öhberg. *J. Opt. B*, 5:S42, 2003.

[208] U. Leonhardt, T. Kiss, and P. Öhberg. *Phys. Rev. A*, 67:033602, 2003.

[209] J. Macher and R. Parentani. *Phys. Rev. A*, 80:043601, 2009.

[210] S. J. Robertson. *J. Phys. B*, 45:163001, 2012.

[211] I. Carusotto, S. Fagnocchi, A. Recati, R. Balbinot, and A. Fabbri. *New J. Phys.*, 10:103001, 2008.

[212] A. Recati, N. Pavloff, and I. Carusotto. *Phys. Rev. A*, 80:043603, 2009.

[213] P. É Larré, A. Recati, I. Carusotto, and N. Pavloff. *Phys. Rev. A*, 85:013621, 2012.

[214] R. Balbinot, I. Carusotto, A. Fabbri, C. Mayoral, and A. Recati. *Lecture Notes in Physics*, 870:181–219, 2013.

[215] S. Finazzi and I. Carusotto. *Phys. Rev. A*, 90:033607, 2014.

[216] P. Jain, S. Weinfurtner, M. Visser, and C. W. Gardiner. *Phys. Rev. A*, 76:033616, 2007.

[217] P. O. Fedichev and U. R. Fischer. *Phys. Rev. Lett.*, 91:240407, 2003.

[218] C. Barceló, S. Liberati, and M. Visser. *Int. J. Mod. Phys. D*, 12:1641, 2003.

[219] U. R. Fischer and R. Schützhold. *Phys. Rev. A*, 70:063615, 2004.

[220] P. O. Fedichev and U. R. Fischer. *Phys. Rev. A*, 69:033602, 2004.

[221] M. Uhlmann, Y. Xu, and R. Schützhold. *New J. Phys.*, 7:248, 2005.

[222] G. E. Volovik. *Phys. Rep.*, 351:195 – 348, 2001.

[223] O. Lahav, A. Itah, A. Blumkin, C. Gordon, S. Rinott, A. Zayats, and J. Steinhauer. *Phys. Rev. Lett.*, 105:240401, 2010.

[224] I. Shammass, S. Rinott, A. Berkovitz, R. Schley, and J. Steinhauer. *Phys. Rev. Lett.*, 109:195301, 2012.

[225] R. Schley, A. Berkovitz, S. Rinott, I. Shammass, A. Blumkin, and J. Steinhauer. *Phys. Rev. Lett.*, 111:055301, 2013.

[226] Y.-H. Wang, T. Jacobson, M. Edwards, and C. W. Clark. *Phys. Rev. A*, 96:023616, 2017.

[227] Y. H. Wang, T. Jacobson, M. Edwards, and C. W. Clark. *arXiv:1705.01907*, 2017.

[228] M. Tettamanti, S. L. Cacciatori, A. Parola, and I. Carusotto. *EPL*, 114:60011, 2016.

[229] I. Carusotto, S. X. Hu, L. A. Collins, and A. Smerzi. *Phys. Rev. Lett.*, 97:260403, 2006.

[230] J. Steinhauer. *Nat. Phys.*, 12:959965, 2016.

[231] I. Carusotto, R. Balbinot, A. Fabbri, and A. Recati. *The European Physical Journal D*, 56:391–404, 2010.

[232] J.-C. Jaskula, G. B. Partridge, M. Bonneau, R. Lopes, J. Ruaudel, D. Boiron, and C. I. Westbrook. *Phys. Rev. Lett.*, 109:220401, 2012.

[233] P. W. Milonni. *The quantum vacuum: an introduction to quantum electrodynamics*. Academic press, New York, 1994.

[234] N. Westerberg, C. Maitland, D. Faccio, K. Wilson, P. Öhberg, and E. M. Wright. *Phys. Rev. A*, 94:023805, 2016.

[235] P. Painlevè. *C.R. Hebd. Seances Acad. Sci.*, 173:677, 1921.

[236] A. Gullstrand. *Ark. Mat. Astron. Fys.*, 16:115, 1922.

[237] S. Corley and T. Jacobson. *Phys. Rev. D*, 59:124011, 1999.

[238] J. Macher and R. Parentani. *Phys. Rev. A*, 80:043601, 2009.

[239] S. Finazzi and R. Parentani. *New J. Phys.*, 12:095015, 2010.

[240] A. Coutant and R. Parentani. *Phys. Rev. D*, 81:084042, 2010.

[241] A. Coutant, R. Parentani, and S. Finazzi. *Phys. Rev. D*, 85:024021, 2012.

[242] W. G. Unruh. *Phys. Rev. D*, 51:2827–2838, 1995.

[243] W. Unruh and R. Schützhold. *Phys. Rev. D*, 71:024028, 2005.

[244] R. Brout, S. Massar, R. Parentani, and Ph. Spindel. *Phys. Rev. D*, 52:4559–4568, 1995.

[245] S. Corley and T. Jacobson. *Phys. Rev. D*, 54:1568–1586, 1996.

[246] J. Steinhauer. *Nat. Phys.*, 10:864–869, 2014.

[247] S. Corley. *Phys. Rev. D*, 57:6280–6291, 1998.

[248] H. Goldstein. *Classical Mechanics (2nd ed.)*. Addison-Wesley, 1980.

[249] M. Peskin and D. V. Shroeder. *An Introduction to Quantum Field Theory*. Perseus Books, Reading, Massachusetts, 1995.

[250] M. Abad and A. Recati. *Eur. Phys. J. D*, 67:148, 2013.

[251] E. Nicklas, W. Muessel, H. Strobel, P. G. Kevrekidis, and M. K. Oberthaler. *Phys. Rev. A*, 92:053614, 2015.

[252] S. W. Hawking. *Phys. Rev. D*, 14:2460–2473, 1976.